

Estimation of Wind Speed and Shear on Wind Turbines



E10 PROJECT

Gr 1030 Electronics & IT
Control and Automation
Aalborg University
06-06-2013

Title:

Estimation of Wind Speed and
Shear on Wind Turbines

Subject:

Master thesis

Project period:

February 4th - June 6th, 2013

Group:

Group 1030

Group members:

Mikkel Urban Kajgaard
Jesper Mogensen
Anders Wittendorff

Supervisors:

Rafael Wisniewski
Christoffer Sloth

Copies: 6

Page count: 123

Attachments: CD

Appendices: 4

Completion: June 6th 2013

Synopsis:

The goal for this project has been to develop a wind turbine model describing the deflections and displacements of the physical and mechanical parts as a function of incident wind for a 5 MW wind turbine. An estimator for estimating wind by terms of hub height wind speed and vertical shear should also be designed. An LPV model has been partly derived, in the means of stating the principles. However, not all of the terms necessary to express the model behaviour by means of system matrices describing mass, stiffness and damping, have been derived due to the time limitations of the project period. The model is instead tested and validated with system matrices from a rotor angle dependent linearisation, obtained from the NREL FAST toolbox for MATLAB. The model is validated against simulations using this toolbox as well. The derived model shows potential when simulated against the non-linear model from FAST, but deviates when the inputs deviates from the operating points. A linearised Kalman estimator has been designed, which estimates the two wind parameters subjected to process- and measurement noise with a mean deviation of respectively 1.22 % and 0.33 %.

Titel:

Estimering af Vindhastighed og Vindgradient på Vindmøller

Tema:

Speciale afhandling

Projekt periode:

4. februar - 6. juni, 2013

Gruppe:

Gruppe 1030

Gruppemedlemmer:

Mikkel Urban Kajgaard

Jesper Mogensen

Anders Wittendorff

Vejledere:

Rafael Wisniewski

Christoffer Sloth

Antal oplag: 6

Antal sider: 123

Bilag: CD

Appendikser: 4

Afsluttet: 6. juni, 2013

Synopsis:

Målet for dette projekt har været at udvikle en vindmøllemodel der beskriver bøjninger og forskydninger af de fysiske og mekaniske dele som funktion af den indfaldende vind for en 5 MW vindmølle. En estimator til at estimere vind i form af vindhastighed i navhøjde og vertikal gradient skulle også designes. En LPV model blev delvist udledt, i form af fastsættelse af principper for udledninger. Dog, blev ikke alle nødvendige udtryk til beskrivelse af modellens opførsel i form af systemmatricer for masse, stivhed og dæmpning udledt, grundet projektperiodens tidsbegrænsning. Modellen er istedet testet og valideret med systemmatricer fra en rotorvinkel-afhængig linearisering, udvundet fra NREL FAST værktøjet til MATLAB. Modellen er ligeledes valideret ved simuleringer med dette værktøj. Den udledte model viser potentiale når den simuleres mod den ulineære model i FAST, men afviger når styringssignalerne afviger fra arbejds punkterne. En lineariseret Kalman estimator er blevet designet, der udsat for processstøj estimerer de to vindparametre, med en gennemsnitlig afvigelse på henholdsvis 1.22% and 0.33%.

Preface

This report is the result of the 4th semester of the master programme in automation and control, produced by group 1030 in the spring 2013 at Aalborg University. As this is the master project, there is no main theme for this project.

This project deals with the subject of deriving a model and an estimation algorithm for modern multi megawatt wind turbines. This should, from usage of until today alternative sensors, estimate wind fields in terms of wind speed and shear. These parameters could be used to optimise the output electricity production, and to minimise structural loadings on the wind turbine. The project spawns from the fact that the technology currently used on wind turbines to determine wind field parameters, becomes out-dated and insufficient as the wind turbines increase in size, which is the result of the development upon these over the last decades.

The report is divided into main parts denoted by roman numbers. Each part is structured in chapters containing sections and in some cases even subsections depending on the specifics and detail on the subject. The chapters, sections and subsections are numbered in a manner, such that the numbering of chapter 1, section 2, subsection 3, is 1.2.3. In the back of the report, a collection of appendixes used throughout the project are to be found. References to these appendixes are done with capital letters in alphabetic order, appendix #1 being A, appendix #2 being B etc. In the back of the report at page 99, a list of the acronyms is found. When an acronym is used, it is defined such that the first time the term appears, the whole term is written and the acronym follows in brackets. From then on, only the acronym will appear unless there is a risk of giving rise to confusion. The Vancouver notation is used, when referring to literature, manuals and data sheets used throughout the project. These references are listed in the bibliography on page 102.

The report contains an enclosed CD. Specific files referred to on the CD appear as follows: `© /folder/filename.ext`. The enclosed CD contains the following:

- Relevant manuals and data sheets.
- The produced MatLab files (*.m) and the Simulink files (*.mdl and *.lib)
- A digital version of the report.

Mikkel Urban Kajgaard

Jesper Mogensen

Anders Wittendorff

Contents

1	Introduction	5
1.1	Project Outline	6
I	Preliminary Analysis	9
2	Wind Turbine System	11
2.1	Wind Turbines in General	11
2.2	Wind as Energy Source	14
2.3	Control of a Wind Turbine	16
3	Problem Description	21
3.1	Sensors	21
3.2	Reducing Asymmetric Loading	22
3.3	Conclusion	23
4	Requirement Specification	25
4.1	The Estimation Problem	25
5	Acceptance Test Description	27
II	Design and Implementation	29
6	Design Overview	31
7	Modelling a Wind Turbine	33
7.1	Coordinate system	34
7.2	Modelling	35
7.3	Tower Model	40
7.4	Drivetrain Model	43
7.5	Blade Model	45
7.6	Aerodynamics	49
7.7	Derivation Example	56
7.8	Parameter Distributions	61
7.9	State Space Formulation	62
8	Estimating Wind	65
8.1	Sensor Types	65
8.2	Sensor Setup	66
8.3	Kalman Estimator	67
9	Implementation Overview	71

9.1	Implmentation of the Model	71
9.2	Implementation of the Estimator	72
10	Acceptance Test	75
10.1	Model Validation	75
10.2	Test of Estimator	86
III	Conclusion and Perspectives	93
11	Conclusion	95
12	Perspectives	97
	Acronyms	99
	Bibliography	101
	Appendix	102
A	Parameter Distribution	105
B	System Matrices	111
C	Calculated Matrices	119
D	Simulation and Linearisation by usage of FAST	121

Nomenclature

R	Radial distance from blade tip to rotor axis
r	Radial distance from point on blade to rotor axis
H	Height from ground surface to the wind turbine hub
z	Height from ground surface to point on tower
$\beta(t)$	Blade pitch angle
q	Generalised coordinates
\dot{q}	Generalised velocities
\ddot{q}	Generalised Accelerations
q_1	Tower fore-aft displacement
q_2	Tower side-side displacement
q_3	Rotor azimuth angle
q_4	Angle of drivetrain torsion
q_5	Flapwise displacement of blade 1
q_6	Flapwise displacement of blade 2
q_7	Flapwise displacement of blade 3
q_8	Edgewise displacement of blade 1
q_9	Edgewise displacement of blade 2
q_{10}	Edgewise displacement of blade 3
θ_k	Azimuthal angle of k th blade
$T(t, q, \dot{q})$	Total kinetic energy of the system
$T_t(t, \dot{q})$	Kinetic energy of the tower
$T_{dt}(t, \dot{q})$	Kinetic energy of the drivetrain
$T_b(t, q, \dot{q})$	Kinetic energy of the blades
$V(t, q)$	Total potential energy of the system
$V_t(t, q)$	Potential energy of the tower
$V_{dt}(t, q)$	Potential energy of the drivetrain
$V_b(t, q)$	Potential energy of the blades
Q	Generalised external forces
M	Mass matrix
K	Stiffness matrix
K_s	Structural stiffness
K_g	Gravity induced stiffness
K_c	Centrifugal induced stiffness

C	Damping matrice
C_g	Damping contributions from gyroscopical loads
C_a	Aerodynamic damping
ζ	Damping factor
$F_{ak}(t, r, v_{xk}, v_{yk})$	Aerodynamic force on k th blade at radius r
$F_{Nk}(t, r, v_{xk})$	Force component normal to plane of rotation at radius r
$F_{Tk}(t, r, v_{yk})$	Force component tangential to plane of rotation at radius r
$v_{xk}(t, r)$	Relative wind along x -axis at radius r
$v_{yk}(t, r)$	Relative wind along y -axis at radius r
$x_{bk}(t, r)$	1st coordinate of k th blade at radius r
$y_{bk}(t, r)$	2nd coordinate of k th blade at radius r
$f_{yk}(r, \theta)$	Effect of gravity on the k th blade at radius r and angle θ
M_n	Mass of nacelle and rotor
$\mu_{tfa}(z)$	1st mode shape of tower fore-aft displacement
$\mu_{tss}(z)$	1st mode shape of tower side-side displacement
$m_t(z)$	Mass distribution of tower in height z
$m_b(r)$	Mass distribution of blade at r
$EI_{tfa}(z)$	flexural rigidity in tower fore-aft direction at height z
$EI_{tss}(z)$	flexural rigidity in tower side-side direction at height z
$EI_{bf}(r)$	flexural rigidity in blade flapwise direction at radius r
$EI_{be}(r)$	flexural rigidity in blade edgewise direction at radius r
δ_{tfa}	Slope of the mode shape μ_{tfa} at height H
δ_{tss}	Slope of the mode shape μ_{tss} at height H
θ_t	Torsional displacement of low speed shaft
θ_r	Absolute angular position of rotor
θ_g	Absolute angular position of generator
θ_{gls}	Angular position of rotor on low speed side
n	Gear ratio of drivetrain gear box
J_r	Moment of inertia of the rotor
J_g	Moment of inertia of the generator
$\tau_{aero}(t)$	Aerodynamic torque induced by wind
$\tau_l(t)$	Torque on gearbox at low speed side
$\tau_h(t)$	Torque on gearbox at high speed side
$\tau_g(t)$	Generator Torque
B_t	Viscous damping of low speed shaft
K_t	Stiffness of low speed shaft

$\varphi(r)$	Structural twist of blade at radius r
$\mu_{bf}(r)$	Flapwise mode shape of blade
$\mu_{be}(r)$	Edgewise mode shape of blade
$\mu_{bfop}(r)$	Flapwise out-of-plane blade mode shape
$\mu_{bfip}(r)$	Flapwise in-plane blade mode shape
$\mu_{beop}(r)$	Edgewise out-of-plane blade mode shape
$\mu_{beip}(r)$	Edgewise in-plane mode blade shape
$\phi(r)$	Wind inflow angle at radius r
$v_k(r)$	Wind normal to the plane of rotation on k th blade
$W_k(t, r, v_{xk}, v_{yk})$	Relative wind on the k th blade
Ω	Rotor speed
$\alpha(v_k)$	Angle of attack
$F_{Lk}(t, r, v_{xk}, v_{yk})$	Lift force on the k th blade at radius r
$F_{Dk}(t, r, v_{xk}, v_{yk})$	Drag force on the k th blade at radius r
$C_L(r)$	Lift coefficient at radius r
$C_D(r)$	Drag coefficient at radius r
$c(r)$	Chord length of blade cross section at radius r
$F_{Nk}(t, r, v_{xk}, v_{yk})$	Force normal to y -axis
$F_{Tk}(t, r, v_{xk}, v_{yk})$	Thrust force
$F_{Nv_{xk}}(r)$	Derivative of F_N w.r.t. v_{xk}
$F_{Nv_{yk}}(r)$	Derivative of F_N w.r.t. v_{yk}
$F_{Tv_{xk}}(r)$	Derivative of F_T w.r.t. v_{xk}
$F_{Tv_{yk}}(r)$	Derivative of F_T w.r.t. v_{yk}
$v_H(t)$	Mean wind in hub height (H)
$v_{wsk}(t)$	Wind shear wind component
$v_{tsk}(t)$	Tower shadow wind component

1 Introduction

One of the most discussed issues in the world today, is the increasing need for renewable energy sources. This is mainly because the fossil fuel sources are depleting, and because the requirements on CO₂ emissions tightens. One of the renewable energy sources is the wind turbine. For the wind turbine to replace today's coal- and oil power plants, the designs of the wind turbines have over the last decade of years undergone a significant development in order to exploit the wind energy optimally[1]. To make the individual turbines more efficient, the size of the wind turbines has increased, giving a greater wingspan, hence more wind energy can be exploited. However a greater wingspan leads to greater variations in the wind characteristics over the swept area. Furthermore, the flexibility of the turbines has as well increased as a trade-off from a light-weight design[1]. If the wind characteristics are not taken properly into account when designing a wind turbine controller it can cause an asymmetrical structural load on the blades and tower causing vibration and thereby the turbine to suffer unnecessary fatigue[1].

The most commonly used method for determining wind parameters is by usage of a wind vane and an anemometer placed on the top of the nacelle. From these two sensors measurements, an average wind speed and direction is calculated. The average wind speed is often either considered uniformly distributed across the entire disc shaped area swept by the blades[2], or used as a parameter in a wind model describing how the wind speed changes vertically and horizontally. The wind measurements from the anemometer are nowadays only used for the purpose of shutting the turbine down, if higher winds are detected, than the turbine is rated for. However, they are thought to be useful for optimizing wind energy production and minimise structural loading on the wind turbine if measured or estimated precise enough. The significance of the parameters increases as the size of the wind turbine increases. Therefore, the importance of the accuracy of the estimated parameters rises as well in order to provide optimal control inputs.

The speed of the wind rises as a function of the height above ground surface[3]. This difference is called the vertical wind shear. Furthermore the wind speed and direction is affected by turbulence stochastically occurring in any point of the rotor swept area. The greater the wingspan, the more fluctuations and variation of the wind field is experienced across the span, which results in an asymmetrical aerodynamic loading. Estimating the wind field based on the measurements from wind vane and anemometer is therefore insufficient due to the fact that it is an average measurement and generally not very informative in terms of estimating useful wind field characteristics describing how the wind changes across the whole rotor swept area[4][5].

Therefore it is desirable to explore alternative sensors for obtaining measurements. An alternative way of estimating the wind field could be by usage of sensors mounted in the blades and tower. This could be done by e.g. strain gauges measuring

the stretching/bending of the element, or by accelerometer measuring the different accelerations of the element on which it is mounted. Based on the information about the different elements on which the sensors are mounted the characteristics of the wind field could be determined.

From the statements above, the problem to be considered in this project is stated:

“How can wind shear and wind speed be estimated using measurement data from sensors mounted in the blades and tower of a wind turbine?”

1.1 Project Outline

As mentioned in the preface, this report is divided into chapters containing sections and subsections. This project outline is meant to give a more thorough overview on the structure of the report.

Chapter 2: Wind Turbine Systems

The purpose of this chapter is give an overview on the basics of how wind turbines are structured and functions. Furthermore, the different characteristics of wind fields and their effect on the wind turbines are described. The chapter finishes by a description on which actuators are used to control modern wind turbines, and how they are controlled.

Chapter 3: Problem Description

This chapter gives an overview of the sensors commonly used on modern wind turbines for determining wind fields. The chapter focuses on the drawbacks of these methods regarding optimizing power production while minimising structural loadings and finalises with a discussion on proposals for control strategies for reduction of asymmetric loadings on the turbines.

Chapter 4: Requirement Specification

This chapter specifies the estimation problem, and states the wanted outcome of this project. It outlines the specific requirements that are set by the project group for this project to answer the problem statement.

Chapter 5: Acceptance Test Description

This chapter specifies the tests needed to be carried out in order to determine whether the requirements specified in the requirement specification are met or not.

Chapter 6: Design Overview

This chapter defines the design strategy chosen regarding model and estimation scheme for this project.

Chapter 7: Modelling a Wind Turbine

This chapter puts focus on how the wind turbine is modelled in this work. The turbine is divided into smaller subsystems: *drivetrain*, *tower* and *blades* which are modelled individually. The aerodynamics are modelled and included to describe the interaction of this on the blades. The chosen wind model, containing the parameters wanted estimated, is presented. The chapter is concluded with some calculation examples on some of the entries for the system matrices describing the model.

Chapter 8: Estimating Wind

This chapter describes the design of the wind -speed and -direction estimation scheme for this project. First the different sensors considered applicable for the purpose are presented alongside with their pros and cons. The assumed sensor setup is following described. The chapter is concluded with a presentation of estimation strategies and the one used for this project is chosen.

Chapter 9: Implementation Overview

This chapter picks up from previous chapter, and covers the description of the implementation of the estimation scheme on the derived model.

Chapter 10: Acceptance Test

This chapter covers the description of how it is tested whether the work made in this project answers the problem statement and fulfils the requirement specification. First a description of the individual tests, followed by the results from the test and a discussion on these. First the model is validated by simulations against the NREL 5 MW turbine from the FAST toolbox in MATLAB. Afterwards, the estimation scheme is tested on the model for its capability of estimating vertical wind shear and wind speed.

Chapter 11: Conclusion

This chapter concludes whether the approach done in this work for estimating wind -shear and -direction is profitable regarding optimisation of power production and/or the asymmetrical loadings on the wind turbine

Chapter 12: Perspectives

This chapter describes further work that could be made on this project, assumed to improve the results obtained. Also ideas for further inclusions in the derived model are discussed.

Part I

Preliminary Analysis

2 Wind Turbine System

This chapter has the purpose of giving an overview of the structure and functionality of a wind turbines. First the wind turbines physical and mechanical construction is described to give an overview of the functionality. Afterwards the characteristics of a wind field and its effect on the wind turbine is described. Finally the means of controlling a wind turbine and the sensors used for control inputs are described.

2.1 Wind Turbines in General

A wind turbine is basically a construction, which converts the kinetic energy from the wind into electrical energy. The wind is caught by blades which makes the rotor rotate. The rotor is connected via a drivetrain to the generator which generates the electrical energy.

There are several types of wind turbines, having different advantages and disadvantages one over another. There are vertical axis wind turbines and Horizontal Axis Wind Turbines (HAWTs) (see Figure 2.1 and 2.2), from which the HAWT is the most common. Amongst HAWT there are as well 2 kinds: upwind and downwind, which basically means which way the rotor points relative to the wind as illustrated in Figure 2.3 and 2.4. The upwind turbine is the most preferable of these as the disturbances in the wind when passing by the tower are not as significant as for the downwind turbines. In this project, it is chosen to put focus on the pitch controlled upwind HAWT.

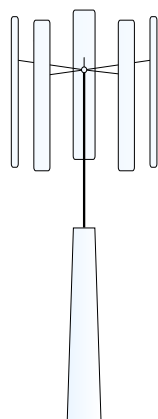


Figure 2.1. Vertical axis wind turbine.

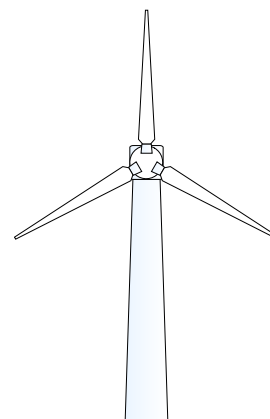


Figure 2.2. Horizontal axis wind turbine.

A HAWT is structured as illustrated in figure 2.5 on the following page. The wind turbine consists on the outside of the 4 parts: tower, nacelle, encapsulated rotor hub and rotor blades.

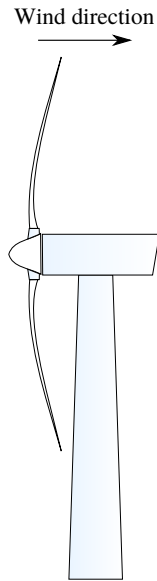


Figure 2.3. Upwind turbine.

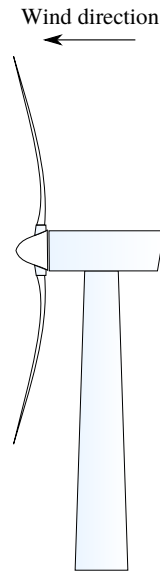


Figure 2.4. Downwind turbine.

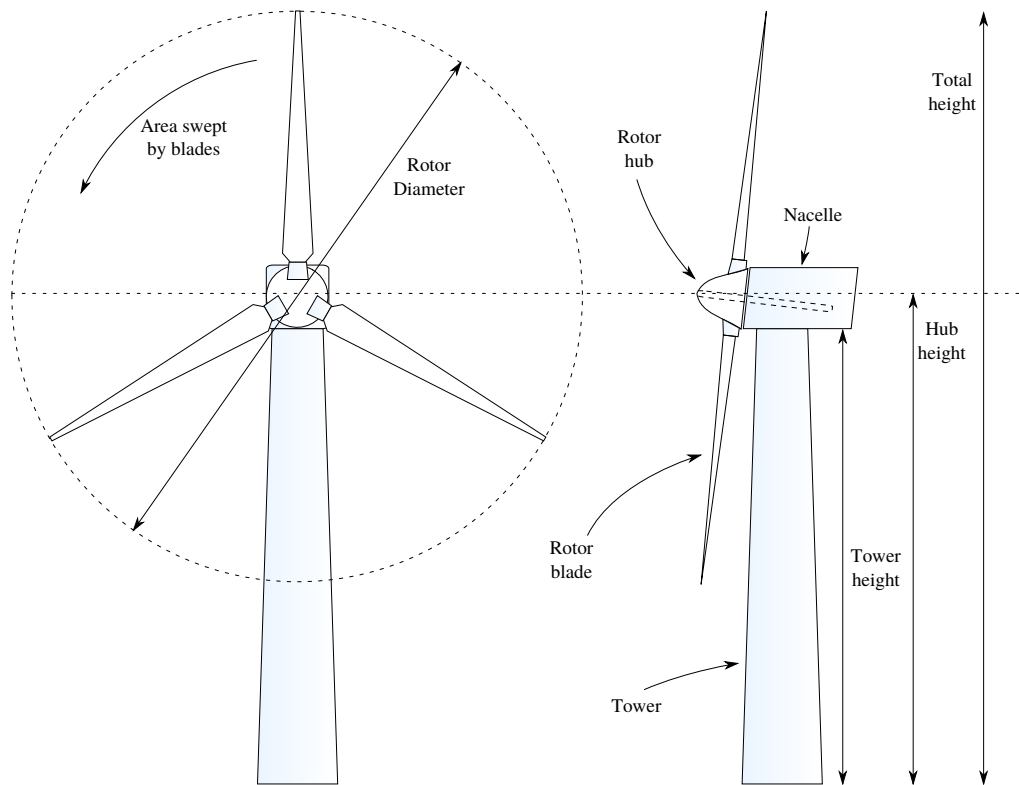


Figure 2.5. Wind turbine.

2.1.1 Tower

The turbine is fastened to the ground by the foot of the tower. The main purpose of the tower is to make sure that the blades do not collide with anything on the ground, why the tower is higher than the length of the blades. As the bottom of the tower is where the greatest stress is experienced, it is thickest here to ensure a solid stand. The tower decreases slightly conically in width towards the top.

2.1.2 Nacelle

At the top of the tower, the nacelle is fitted. Since the turbines have increased vastly in size over the last decades, the nacelle on many modern HAWTs contains the drivetrain and the whole mechanical-electrical energy conversion mechanism. A simplified illustration of the inside of the nacelle and rotor hub is seen in Figure 2.6[1]. The rotor hub is connected to a rotor shaft. The shaft is coupled through a gearbox and a brake to the generator, generating the electricity, which then is sent through a converter and onto the power grid. Furthermore, the nacelle contains the different cooling systems for oil and the generator, and all of the controllers are found here as well. The nacelle can turn 360° in order to operate in any wind direction.

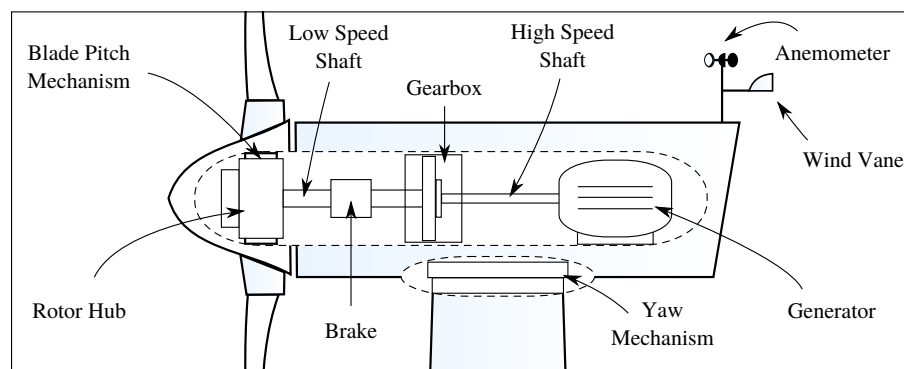


Figure 2.6. Inside of nacelle and rotor hub (Simplified).

2.1.3 Rotor Hub

On the front of the nacelle, the rotor hub is found. In the rotor hub, the blades are connected in a fitting connected to a motor which can pitch the blades from approximately 0° where most wind is captured by the blades and up to 90° where practically none is captured. The latter position is used when the turbine is wanted stopped. By pitching the blades within the $0^\circ - 90^\circ$ ensures that the wind turbine functions optimally within a certain spectrum of wind speeds. This spectrum is defined by the rating of the specific wind turbine which is further described in section 2.2.5. As illustrated in the Figure 2.5, the hub is often on especially larger turbines tilted in a certain angle upwards. This is called the rotor shaft tilting, and is done to ensure that the blades do not collide with the tower when in lower position.

2.1.4 Rotor Blades

The rotor blades are as mentioned above mounted in the rotor hub. The blades are aerofoil shaped, like the wings of an aeroplane. Furthermore, the blades are twisted throughout the length of the blades specifically for the individual types of turbines in accordance to exploit the wind energy as much as possible. The blades are as the tower thickest at the

bottom closest to the rotor hub, as this is where the greatest stress is seen. The blades are often, on especially larger wind turbines, precone which means that they are tilted slightly upwind to ensure that they do not collide with the tower when operating in high wind speeds.

The different mechanical parts of the wind turbine, which are to be modelled in this project, have been described with the naming conventions used throughout the rest of the report.

2.2 Wind as Energy Source

The behaviour of wind in general in an area is mainly dependent on the climate and the topography in the given area. The wind field experienced by a wind turbine is therefore variable in both time and space, affected by different parameters also including the wind turbine itself[3]. It is relevant for wind turbine designs to have information on the wind direction and the wind speed across the rotor swept area in order to account for these, when trying to maximise energy capture and minimise structural loading. In order to describe these changes across the rotor swept area, the wind field characteristics are described by several factors. The differences in wind speed and direction over the swept area are mainly caused by the factors: wind shear, turbulence, tower shadow, and wake, which are briefly described in the following.

2.2.1 Wind Shear

Wind shear refers to the change in wind speed over an area and occurs in three dimensions where horizontally and vertically shear are most relevant for wind turbines. Vertical shear is the most dominant shear effect on a wind turbine due to the ground slowing down the wind leading to the fact that the wind speed increases as a function of the height. The effect of shear is often described by using a mean wind speed which changes with the elevation above the ground. The mean wind speed and shear is typically considered as a low frequent variation which depends on the time of the day and the topography in the surrounding area and is to some extent predictable[3, p. 7]. The vertical wind shear can be modelled in several ways and in different variety of detail depending on the topography in the area. The model used in this project is described in chapter 7 section 7.6.3.

2.2.2 Turbulence

The effect of turbulence refers to changes in wind speed which occurs stochastically in periods of minutes and down to seconds[1, p. 10]. The effect of turbulence has a minor effect on the overall energy capture obtained by the wind turbine, whereas the low frequent variations in the wind are more relevant. However the blades are affected by the stochastic changes in the wind speed, which if the wind turbine is yawwise misaligned relative to the

wind direction causes asymmetrical loadings on the blades. These loadings propagate from the blades to the drivetrain and tower. The quality of the power from the wind is also affected by turbulence, since it can cause fluctuations in the angular velocity of the rotor and thereby on the generator resulting in fluctuations in the power extracted, which is not preferable when the turbine is connected to the electrical power grid.

2.2.3 Tower Shadow

Tower shadow occurs due to the presence of the tower blocking the wind, which needs to flow around the tower. This causes a drop in the wind speed, which leads to difference in aerodynamic loading on the blades when they move past the tower.[1, p. 219][3, p. 25]. As well as for the wind shear, the tower shadow can be modelled in several ways. The model used in this project is described furtherer in chapter 7 section 7.6.4

2.2.4 Wake

The effect of wake refers to the fact that the wind speed and direction respectively decreases and changes as the wind passes through the rotor swept area. This is due to the blades extracting kinetic energy from the wind, causing the rotor to rotate and results in a drop in wind speed in the area on the backside of the rotor swept area. The wake induced changes in wind direction occurs since the rotating blades has an impact on the wind field. The effect of wake is most relevant when considering wind farms where the wake effect of one turbine could affect neighbouring wind turbines[1, p. 33].

2.2.5 Power Extraction

The theoretically maximum available energy from the wind can according to [6] be described by

$$\begin{aligned} P &= \frac{1}{2} \dot{m} V_0^2 \\ &= \frac{1}{2} \rho A V_0^3 \end{aligned} \tag{2.1}$$

where

P is the available energy	[W]
\dot{m} is the mass flow rate	[kg/s]
V_0 is the wind speed	[m/s]
ρ is the density of the air	[kg/m ³]
A is the rotor swept area	[m ²]

However, this is only theoretically and requires the wind speed to be fully reduced to zero, meaning that in the case of a wind turbine, the wind speed should be 0 after passing through the blades span in order to obtain the amount of energy that the formula 2.1

states. As this is not practically possible, a coefficient C_p is used to scale to find the actual power obtained. This coefficient has an upper limit called the Betz limit, $C_{P_{\max}}$ of $16/27 \approx 0.593$, which defines the actual maximum possible obtainable power. Modern wind turbines come close to this maximum by around 0.5[6].

In Figure 2.7 the ideal power curve for a pitch controlled wind turbine is illustrated.

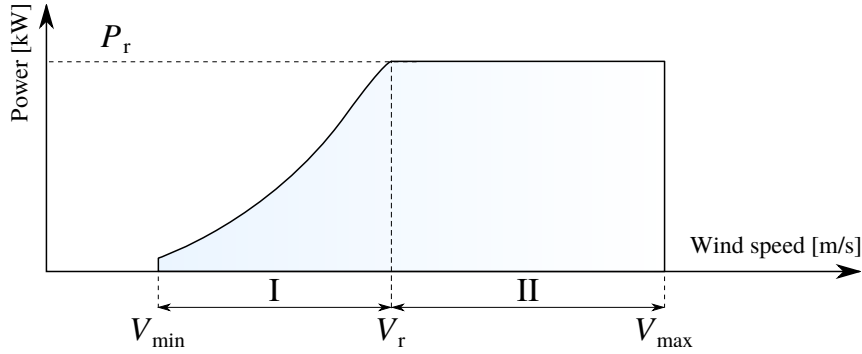


Figure 2.7. Ideal Power Curve.

where

P_r is the rated power of the wind turbine	[W]
V_{\min} is the below rated wind speed limit	[m/s]
V_{\max} is the above rated wind speed limit	[m/s]
V_r is the rated wind speed	[m/s]
I is the region with below rated power production	[-]
II is the region with rated power production	[-]

The rated power of the wind turbine P_r varies from one wind turbine to another. It defines the power output, that the wind turbine is designed to produce. The wind speed limits respectively V_{\min} and V_{\max} defines the interval of wind speeds, where the wind turbine can operate within. The two regions of operation, region **I** and region **II** are more thoroughly described in section 2.3.4.

It has been described how the wind effects the turbine, and how the wind turbine utilises the kinetic energy in the wind to produce electrical energy. Also the relevant wind characteristics describing a wind field has been presented. Following is described how the wind turbines are controlled to optimise the energy extraction from the wind.

2.3 Control of a Wind Turbine

The current way of controlling a wind turbine, can be separated into several controllers for different purposes. The actuators used for control purpose of a wind turbine are mainly pitch actuators, electrical generator used as torque actuator, and an electrical motor used as yaw actuator. A Wind turbine controller has different operational states

including, amongst others, standby, start-up, power production, shut-down or stopped due to failure. The active state is dependent on the turbine type and wind condition. In this project the only operational state considered is “power production”, why pitch-, torque- and yaw actuator are the only relevant actuators.

The inputs for the controller, in terms of measurements from different sensors installed in the wind turbine, could be anemometer, wind vane, rotor speed sensor, electrical power sensor, pitch position sensors, accelerometers and load sensors where the latter two are placed in the blades, tower and the drivetrain. Based on these sensor inputs, outputs for the mentioned actuators can be calculated by a control algorithm. The relevant actuators are described in the following.[1]

2.3.1 Pitch Actuator

The pitch control is used to control how much power is generated from the aerodynamic load caused by the wind. When the wind speed is below the rated speed for a turbine, the turbine should extract as much power as possible from the wind, why there is no need for pitching the blades. However for above rated wind speed, pitch control can be used to vary the power extracted from the aerodynamic loading. Pitching of the blades can be done either by using an individual or collective blade pitch approach.[3]

2.3.2 Torque Actuator

The torque control is done in different ways dependent on whether variable- or fixed-speed operation is wanted. The type of generator used in both operation modes is an asynchronous induction generator. The torque developed in such a generator is developed as a result of slip speed between the rotor and the stator. When the rotor runs slower than the stator the generator acts as a motor and the slip is positive, for generator operation the rotor runs faster than the stator and a negative slip is obtained giving a power output.

In a fixed-speed wind turbine the generator is connected to the electrical grid. Dependent on the grid frequency and number of magnetic poles in the generator a synchronous speed will be obtained. As the wind field varies the torque supplied by the rotor will vary accordingly and thereby the generator torque will change to match the torque supplied by the rotor, meaning the torque is not directly controllable.

In a variable-speed wind turbine different modifications can be done in order to obtain the possibility of adjusting the generator speed. As an example a frequency converter is used to change the frequency experienced by the generator, making it possible to change the synchronous generator speed[1].

2.3.3 Yaw Actuator

The yaw control is used in order to point the wind turbine directly into the wind. This is done in order to maximise the power output and to avoid asymmetric structural loading on the wind turbine. An electric motor is used as actuator to turn the nacelle such that it points into the wind. This is usually done based on sensor measurement from the wind vane. The wind vane is for upwind turbines mounted on the top of the nacelle and is therefore subject to disturbances from the rotor. The measurements from the wind vane is therefore averaged and if yaw misalignment reaches a certain level the yaw motor is used to correct for the error.[1].

2.3.4 Power Production Controller

An example of a control scheme for power production used in modern wind turbines is seen in Figure 2.8, where the objective is to upkeep a given reference generator speed. The figure is inspired by [7] and [8] and illustrates the usage of a pitch controller and a variable speed torque actuator based on two regions of operation. The reference for the controller is the angular speed of the generator $\omega_{g,\text{ref}}$. Following is a description on the controller behaviour when in the two regions respectively, region **I** and region **II** (see Figure 2.7 on page 16).

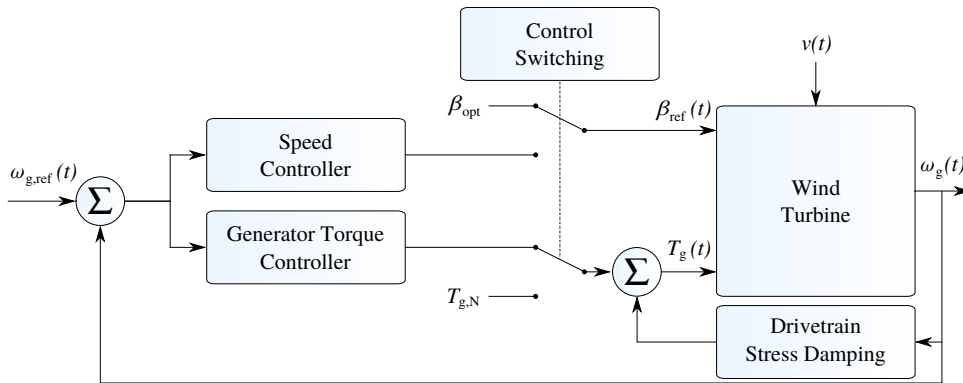


Figure 2.8. Block diagram showing example of currently used control strategy.

In **region I** (partial load operation) the wind turbine produces power below its rating, and pitching is seldom used at these wind speeds, hence the pitch $\beta_{\text{ref}}(t)$ is kept constant. In this region, the power production is maximised by the *Generator Torque Controller*, adjusting the generator torque, $T_g(t)$, in accordance to optimizing the ratio between blade tip speed and the wind speed[3]. At wind speeds below the minimum rated wind speed for the wind turbine, the available energy in the wind is insufficient for the turbine to produce surplus power why the turbine at these wind speeds is shut down.

In **region II**, the aerodynamic torque caused by the wind makes the power output from the turbine exceed its limit why the power output must be kept constant at the rated

power. This constant output is kept by using the *Speed Controller* to control the pitch angle of the blades. The higher wind speeds, the greater pitch angle. At wind speeds above the maximum rated wind speed for the wind turbine, the blades can be pitched no further and the wind turbine is shut down, as operation in this area could cause structural overload on the turbine[3].

The drivetrain stress damper is active at all time and has the purpose of limiting torque oscillations in the gearbox. This is usually done by adding a rippled signal to the torque input, where the ripple frequency should be at the frequency of the torque oscillations.[8]

In this chapter, the structure and functions of modern wind turbines have been described. Also the characteristics of a wind field have been outlined, and the relevance of knowing these from a control point of view.

3 Problem Description

This chapter provides an overview of the currently typical usage of wind sensors for estimating the wind field on wind turbines, and which drawbacks it causes in terms of optimising the power production and minimising the loadings on tower, blades and drivetrain. Afterwards the possibility of using alternative sensors to estimate wind field parameters is discussed, followed by a description on possible usages of it in a controller, which reduces the before mentioned asymmetrical loadings by usage of individual pitch control.

Variations in the the wind field occur, as mentioned in chapter 2.2 on page 14, due to the effect of wind shear, turbulence, tower shadow, and wake. The increase in size of the wind turbines means that the area swept by the rotor blades becomes larger; hence the changes in the wind field become more significant as well, causing asymmetrical loading on the wind turbine. Therefore a detailed wind field estimation for preparation of a controller compensating for asymmetrical aerodynamic loading would be beneficial.

3.1 Sensors

The most commonly used sensors in modern wind turbines to determine characteristics of the wind field, are a wind vane and an anemometer mounted on the top of the nacelle[3] as shown in Figure 2.6 on page 13. These sensors are used to determine an average wind speed and average wind direction. The sensors are affected by the wake of the wind turbine which can cause noisy and unreliable measurements and thereby cause errors in the determined wind speed and direction. Furthermore the sensors have dynamics in terms of the inertia in the mechanical sensor construction which should be accounted for by modelling the dynamics of it, which can cause further errors in the measurement[9].

Since the wind direction is used as input on the yaw controller in order to point the wind turbine directly into the wind, an error in determining the wind direction will cause yaw misalignment. The effects of this is that the energy in the wind is not fully utilized and an asymmetrical load on the blades and tower occurs. The wind speed measured from the anemometer is only used to determine cut-in and cut-out speeds[4] for the wind turbine, which are respectively the wind speeds at which the wind turbine is beneficial to turn on and the wind at which the turbine suffers overload; hence if the wind speed exceeds a certain level the wind turbine is shut down.

The quality and reliability of the wind speed and direction measurements makes it insufficient for determination of the wind field experienced by the entire rotor, hence it is not applicable for control purposes. Therefore additional sensors must be used if wanting

to estimate useful parameters of the wind. An approach could be to use sensors mounted in the blades and tower measuring loads and accelerations. In [1, p. 497] it is for instance suggested to use load sensors in the blades. Another approach suggested by both Risø and National Renewable Energy Laboratory (NREL) is the usage of lidar placed in the rotating hub, to detect the upwind inflow[10]. However a consequence of this method is that the lidar makes use of the bending of a laser beam, which detects the wind speed at a certain distance ahead from the hub, which means that in case of turbulence, these data might not be reliable to base a wind field estimation on[11, p. 7].

The usage of additional sensors could make it possible to obtain measurements on deflection and vibrations caused by asymmetrical loading on the wind turbine structure. This asymmetrical loading could via modelling of wind disturbances be traced back to parameters used for control purpose.

In [5], it is attempted to calculate the effective wind speed, based on estimations of rotor speed and aerodynamic torque by use of a combined state and input observer. In [12] it is suggested to use a set of strain gauges in combination with accelerometers, in a cascade coupling of Kalman filters estimating wind field parameters, where a combination of accelerometer and strain gauge yields deflection of blades and towers. In [5] the wind speed was calculated and [12]is still under development regarding estimation of the wind field parameters.

3.2 Reducing Asymmetric Loading

The pitching of the blades is usually done collectively, meaning that the same pitch is applied to all blades at once. The collective blade pitch results in the asymmetrical aerodynamic loading due to wind shear, tower shadow and turbulence not being taken properly into account. This leads to increased structural fatigue and thereby shortens the lifetime of a wind turbine.

Therefore the possibility of using individual pitch control could be considered, since usage of such would make it possible to adjust the blade pitch based on the azimuthal angle of it. Measuring the load and vibration in the individual blades would make it possible to predict the aerodynamic force experienced by a blade and accounting for it by usage of the individual pitch actuators.

The effect of vertical wind shear causes vibrations in the blades which propagates to the tower, due to the blades experiencing different aerodynamic loading dependent of angle position. The effect of shear is usually present and with very low frequent in changes, hence it can be considered constant and should be possible to detect and account for by individual pitching.

Every time a blade passes the tower, tower shadow causes vibration in the blades as well. It is therefore deterministic and could also be taken into account by usage of individual pitching.

Turbulence is stochastically occurring and therefore the asymmetrical loading caused

by it might not be possible to account for. The possibility of accounting for it depends on the length of the period in which the turbulence is occurring, and if any correlation is detectable.

3.3 Conclusion

The possibility of compensating for the asymmetrical loading caused by the wind should be possible by usage of azimuth dependent individual pitch control instead of collective. By considering the wind shear height dependent, and knowing that the tower shadow occurs in a specific area of the rotor swept area, the pitching could be done cyclic. In order to implement a controller which pitches the blades individually additional sensors alongside with wind field estimation should be used.

4 Requirement Specification

The previous chapter concluded that individual pitching, based on usage of anemometer and wind vane measurements, is insufficient due to the non-deterministic effect of turbulence and errors in the measurements. This chapter will map out the requirements for an estimation of the wind field characteristics based on adding additional sensors to a wind turbine.

4.1 The Estimation Problem

The usage of anemometer and wind vane is insufficient for control purpose and therefore usage of other sensors is required. Alternatively sensors used could be in terms of accelerometers and load sensors as e.g. strain gauges mounted in the tower and blades, which could yield information about deflection and vibrations presumably caused by asymmetrical loading from the wind field.

The main usage could be to utilise the possibility of using individual pitch control in order to compensate for asymmetrical loading caused by difference in wind fields across the wingspan. This project is confined to include only the effects of wind shear and wind speed for estimation, based on usage of load sensors and accelerometers. This means, that the model does not account for yaw error, turbulence and wake. Therefore the following requirements are set.

r.1 Derive a model describing blade and tower deflections and vibrations caused by wind perturbation.

A model for usage in estimation of the wind field parameters must be designed in order to see the effects of wind field characteristics on the blade and tower vibrations and deflections.

r.2 Estimate wind parameters based on loading measurements.

An estimation scheme must be designed in order to determine wind field characteristics in terms of vertical shear and wind speed.

5 Acceptance Test Description

This chapter describes how the outlined requirement will be tested.

Requirement **r.1** will be tested in the following way: The derived model will be adopted in **MATLAB** for validation. It is then chosen to use the NREL **FAST** toolbox[13], as a benchmark for the validation, since this software is known and acknowledged for its performance[13]. The used turbine model will be the NREL 5MW Onshore wind turbine[14]. The requirement is met if the derived model's response to control inputs and wind disturbances corresponds to the output from **FAST**. This is e.g. assessed based on the eigen-frequencies of the output.

Requirement **r.2** will be tested in the following way: A simulation will be carried out in **FAST** where the wind field will be specified by given values for shear, wind speed and yaw error. The estimation scheme will then be tested by comparing the estimated wind field parameters to the ones specified in the wind simulation. The requirement will be considered met if there is agreement between the simulated and estimated wind field parameters.

Part II

Design and Implementation

6 Design Overview

This chapter provides an overview on the design strategy for fulfilling the requirements regarding the estimation problem described in chapter 4.

The overall design structure of the wind field estimator is illustrated in the block diagram 6.1. The strategy is based on usage of sensors, a model describing relevant dynamics alongside with the effects of wind perturbation, and an estimation scheme for determining wind field parameters based on the sensor data.

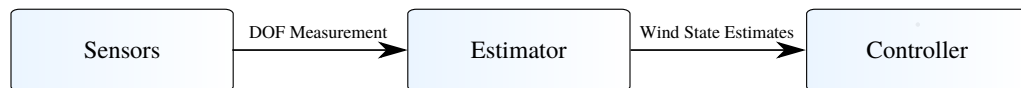


Figure 6.1. Block diagram of the wind estimation strategy.

The idea is that the sensors measure relevant information about the degrees of freedom which will be included as states in the model to be used in the estimator. The states will describe deflection and vibration on the mechanical and physical structure of the wind turbine. The vibrations and deflections will be measured in blades, tower and drivetrain since these are the parts of the turbine in which structural fatigue occur. The asymmetrical loading on the rotor blades caused by wind perturbation propagates through these parts of the wind turbine, which makes it relevant to estimate and compensate for by means of control.

The main idea is therefore to utilise the possibility of obtaining parameters describing the wind by usage of an estimator. This should make it possible to make intelligent control in order to compensate for the asymmetrical loading by providing appropriate actuator inputs.

In order to obtain sensors measurement of the Degree of Freedoms (DOFs), which will be used in the model to describe the structural loading on the wind turbine, a turbine simulator is used. In order to obtain structural data for developing a model to use in the filter, a predefined turbine is used. As mentioned, this is the NREL 5 MW onshore Turbine. The structural parameters of the wind turbine are defined in [14] and in order to simulate the presence of measurements, the turbine will be simulated using FAST[15]. The wind field experienced by the wind turbine will be simulated by usage of `Aerodyn`[16].

The following chapters describe the development of a model and the estimator. The model is derived and computed based on the necessary parameters taken from the specifications of the NREL 5 MW turbine. Afterwards an estimator for the wind field characteristics will be designed.

7 Modelling a Wind Turbine

This chapter describes considerations and assumptions done with regard to modelling the wind turbine in this work. The turbine is divided in three mechanical subsystems, being the drivetrain, a flexible tower and flexible blades. Finally the aerodynamics is included as a subsystem in the model to describe the interaction between the wind and the turbine blades.

The purpose of this chapter is to derive a non-linear model and an LPV model like the one proposed in [7]. It is chosen to derive both types of models to allow for different estimation schemes to be tested. In this work, tower and blades are regarded as flexible structures and therefore have distributed parameters, yielding them an infinite number of modes. However, this can not be implemented, and it is therefore assumed that the tower and blades only possess a finite, and low number of modes. This model simplification method is known as the Assumed Modes Method[17]. Other alternatives such as Finite Element Method can be used to approximate a system with distributed parameters. However this is computational heavy[18], and is therefore not considered furtherer. In this work it is chosen only to use the first mode shape of each of the flexible structures. This assumption is made to keep the number of states in the filter low, in order to reduce computation. To simplify derivations, the precone of the blades, the shaft tilt and the rotor overhang are neglected. These effects are however included in the wind turbine model of the simulation tool FAST, which the model of this work is intended to be validated against. Parameters such as mode shapes, mass distributions, flexural rigidity distributions, ect. are obtained from the FAST input files for the NREL 5 MW wind turbine, which is used for the validation[15]. The derivation procedure done in this work is done in accordance to the following steps:

- Obtain data from FAST.
- Approximate mass distribution, stiffness distribution, etc. from data.
- Apply Lagrangian Mechanics to derive generalised Mass, Stiffness and Damping.
- Generalise the aero-dynamical force.
- Include gravity load as additional stiffness.

7.1 Coordinate system

The chosen 10 DOFs, for modelling the wind turbine's flexible structure, are illustrated in Figure 7.1 and listed below the figure. The coordinate system and direction of the blade rotation is illustrated as well.

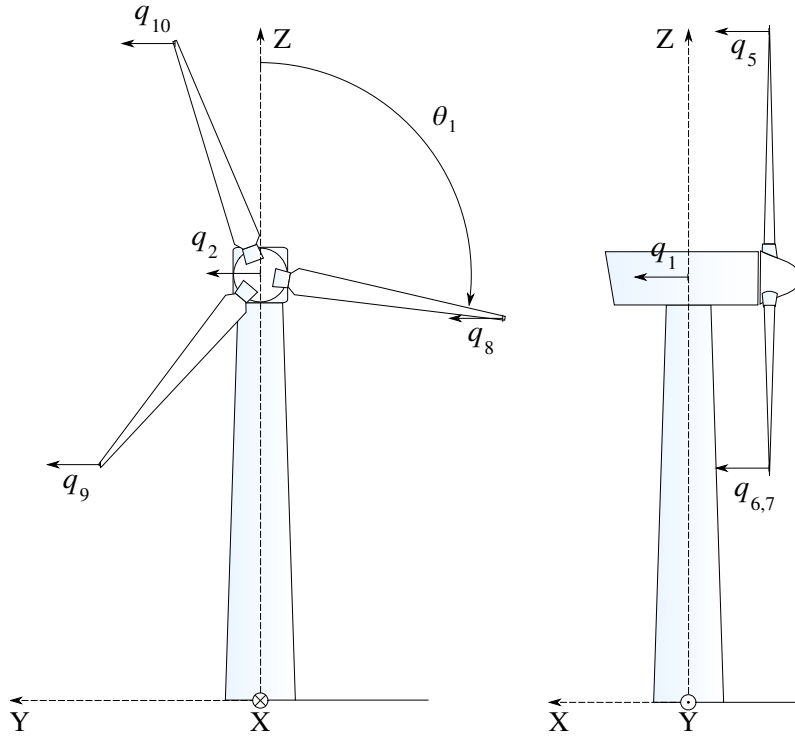


Figure 7.1. Model of the wind turbine.

where

$q_1 \in \mathbb{R}$	is the tower fore-aft displacement	[m]
$q_2 \in \mathbb{R}$	is the tower side-side displacement	[m]
$q_3 \in \mathbb{R}$	is the angular displacement of the generator (low speed side)	[rad]
$q_4 \in \mathbb{R}$	is the torsion of the low speed shaft in the drivetrain	[rad]
$q_5 \in \mathbb{R}$	is the flap-wise displacement of blade 1	[m]
$q_6 \in \mathbb{R}$	is the flap-wise displacement of blade 2	[m]
$q_7 \in \mathbb{R}$	is the flap-wise displacement of blade 3	[m]
$q_8 \in \mathbb{R}$	is the edge-wise displacement of blade 1	[m]
$q_9 \in \mathbb{R}$	is the edge-wise displacement of blade 2	[m]
$q_{10} \in \mathbb{R}$	is the edge-wise displacement of blade 3	[m]
$\theta_1 \in \mathbb{R}$	is the angular position of blade 1	[rad]

7.2 Modelling

To derive a model that describes the dynamics of a wind turbine, Lagrangian mechanics is used [19, p. 21].

Consider the Lagrangian

$$L(t, q, \dot{q}) = T(t, q, \dot{q}) - V(t, q), \quad [\text{J}] \quad (7.1)$$

where

$$\begin{aligned} q \in \mathbb{R}^n & \quad \text{are the generalised coordinates,} \\ \dot{q} \in \mathbb{R}^n & \quad \text{are the generalised velocities,} \\ L \in \mathbb{R} & \quad \text{is the Lagrangian,} \quad [\text{J}] \\ T \in \mathbb{R} & \quad \text{is the kinetic energy of the system,} \quad [\text{J}] \\ V \in \mathbb{R} & \quad \text{is the potential energy of the system.} \quad [\text{J}] \end{aligned}$$

The considered system has 10 DOFs i.e. $n = 10$. For the wind turbine, it should be noted that the kinetic energy is not only a function of time and generalised coordinates, but also the generalised velocities. This is due to the rotation of the blades, which will introduce gyroscopic and centrifugal loads. The kinetic and potential energy of the system are sums of several energy contributions. These contributions are from the tower, the drivetrain and the blades. Hence, the kinetic energy is

$$T(t, q, \dot{q}) = T_t(t, \dot{q}) + T_{dt}(t, \dot{q}) + T_b(t, q, \dot{q}), \quad [\text{J}] \quad (7.2)$$

and the potential energy is

$$V(t, q) = V_t(t, q) + V_{dt}(t, q) + V_b(t, q), \quad [\text{J}] \quad (7.3)$$

The Euler-Lagrange equation for a system subject to external forces is

$$0 = \frac{d}{dt} \left(\frac{\partial L(t, q, \dot{q})}{\partial \dot{q}} \right) - \frac{\partial L(t, q, \dot{q})}{\partial q} + \frac{\partial \mathcal{F}(t, \dot{q})}{\partial \dot{q}} - Q(t), \quad (7.4)$$

where

$$\begin{aligned} \mathcal{F} \in \mathbb{R} & \quad \text{is Rayleigh's dissipation function,} \quad [\text{W}] \\ Q \in \mathbb{R}^n & \quad \text{is the generalised, external forces.} \end{aligned}$$

In the considered system there are several external forces, interacting with the wind turbine. They consist of both conservative and non-conservative forces. The external forces are the following

$$Q = Q_\tau \tau(t) + Q_g + Q_a \quad (7.5)$$

where

$Q_\tau \in \mathbb{R}^{10}$	is the gain of the torque applied by the generator,
$Q_g \in \mathbb{R}^{10}$	is the generalised force induced by gravity,
$Q_a \in \mathbb{R}^{10}$	is the generalised force induced by the aerodynamics,
$\tau \in \mathbb{R}$	is the applied generator torque.

The considered system is subject to two non-conservative forces, which are friction and aerodynamics. Both of these forces contribute to the damping of the system, which are respectively denoted as structural- and aerodynamic damping. A third contribution to the damping is caused by gyroscopic loading due to blade rotation, which is seen later in a derivation example.

The Euler-Lagrange equation (eq. 7.4) has four terms in this case. The first two relate to respectively mass and structural stiffness of the system. The third is the structural friction in the wind turbine. The generalised forces introduce the aerodynamic damping, a gravity induced stiffness[7] and the last term is considered a controlled input. A third term contributing to the stiffness of the system arises from centrifugal loads on the blades. This stiffness term can not readily be seen from the Euler-Lagrange equation, but will be more obvious from the derivation example presented in section 7.7 on page 56. Consider the Euler-Lagrange equation and all the mentioned stiffness and damping terms, then the non-linear system dynamics of the wind turbine has the following form

$$Q_\tau \tau(t) + Q_a(t) = M\ddot{q}(t) + (C_s + C_g)\dot{q}(t) + (K_s + K_g + K_c)q(t), \quad (7.6)$$

where

$\ddot{q} \in \mathbb{R}^{10}$	is the generalised acceleration,
$M \in \mathbb{R}^{10 \times 10}$	is the mass matrix,
$C_s \in \mathbb{R}^{10 \times 10}$	is the structural damping,
$C_g \in \mathbb{R}^{10 \times 10}$	is the damping due to gyroscopic loads,
$K_s \in \mathbb{R}^{10 \times 10}$	is the structural stiffness,
$K_g \in \mathbb{R}^{10 \times 10}$	is the stiffness induced by gravity,
$K_c \in \mathbb{R}^{10 \times 10}$	is the stiffness due centrifugal loads.

The eq. 7.6 describes the wind turbine system. It is however non-linear due to the aerodynamic forces $Q_a(t)$. The following subsection explains how to linearise the aerodynamics in order to obtain an LPV model.

7.2.1 Generalised Aerodynamic Force

The aerodynamic force arises from the interaction between the wind and each of the blades. This force depends on position of the blade, i.e. the radius r , which is the distance from

the centre of the rotor to a given point on the blade. Therefore the k th blade is subject to the aerodynamic force (see Figure 7.2)

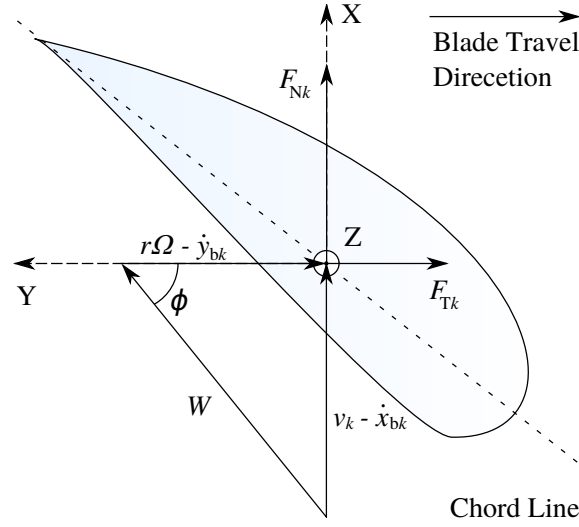


Figure 7.2. Cross section of k th blade illustrating F_{Nk} and F_{Tk} .

$$F_{ak}(t, r, v_{xk}, v_{yk}) = \begin{bmatrix} F_{Nk}(t, r, v_{xk}) & F_{Tk}(t, r, v_{yk}) \end{bmatrix}^T \quad [\text{N}] \quad (7.7)$$

where

$$\begin{aligned} F_{Nk} &\in \mathbb{R} && \text{is the force component normal to the plane of rotation,} && [\text{N}] \\ F_{Tk} &\in \mathbb{R} && \text{is the force component tangential to the plane of rotation,} && [\text{N}] \\ v_{xk} &\in \mathbb{R} && \text{is the relative wind along the } x\text{-axis,} && [\text{m/s}] \\ v_{yk} &\in \mathbb{R} && \text{is the relative wind along the } y\text{-axis.} && [\text{m/s}] \end{aligned}$$

The relative winds are the winds from which the aerodynamics arises. In this work they are defined respectively as the difference between the incident wind and the structural motion of the blade along the x -axis, i.e.

$$v_{xk}(t, r) \stackrel{\text{def}}{=} v_k(r) - \dot{x}_{bk}(t, r) \quad [\text{m/s}] \quad (7.8)$$

and the difference between rotor speed and the blade motion along the y -axis

$$v_{yk}(t, r) \stackrel{\text{def}}{=} r\Omega - \dot{y}_{bk}(t, r) \quad [\text{m/s}] \quad (7.9)$$

The force F_{ak} is expressed in Cartesian coordinates and must be transformed to generalised coordinates in order to be included in the Euler-Lagrange equation. Generalising the aerodynamics and including all three blades yields

$$Q_a(t) = \sum_{k=1}^3 \int_0^R \frac{\partial x_{bk}(t, r)}{\partial q} F_{Nk}(t, r, v_{xk}) + \frac{\partial y_{bk}(t, r)}{\partial q} F_{Tk}(t, r, v_{yk}) dr \quad (7.10)$$

where

$$\begin{aligned} x_{bk} &\in \mathbb{R} && \text{is the 1st coordinate of the } k\text{th blade,} && [\text{m}] \\ y_{bk} &\in \mathbb{R} && \text{is the 2nd coordinate of the } k\text{th blade.} && [\text{m}] \end{aligned}$$

The aerodynamics is non-linear w.r.t. the generalised velocity \dot{q} , the pitch control input β and the speed of the incident wind v_k . Therefore the aerodynamic force is linearised w.r.t. each of those variables to derive the LPV model. The linearisation splits the generalised aerodynamics into the three terms

$$\tilde{Q}_a = \frac{\partial Q_a}{\partial \dot{q}} \dot{q}(t) + \frac{\partial Q_a}{\partial \beta} \beta(t) + \frac{\partial Q_a}{\partial v_k} v_k(t) \quad (7.11)$$

$$\tilde{Q}_a = C_a \dot{q}(t) + Q_\beta \beta(t) + Q_v v_k(t) \quad (7.12)$$

where

$\tilde{Q}_a \in \mathbb{R}^{10}$ is the perturbations in the generalised force from its operating point,

$C_a \in \mathbb{R}^{10 \times 10}$ is the aerodynamic damping,

$Q_\beta \in \mathbb{R}^{3 \times 10}$ is the gain for perturbations of the pitch angle,

$Q_v \in \mathbb{R}^{3 \times 10}$ is the gain for perturbations of the incident wind's speed.

The first term of \tilde{Q}_a depends on the generalised velocity, $\dot{q}(t)$, and can therefore be treated as additional damping in the system. This damping is referred to as aerodynamic damping. The two other terms depend respectively on input and disturbance and are therefore treated as forcing functions of the system. The linearised system is

$$Q_\tau \tau(t) + Q_\beta \beta(t) + Q_v v_k(t) = M \ddot{q}(t) + (C_s + C_g - C_a) \dot{q}(t) + (K_s + K_g + K_c) q(t), \quad (7.13)$$

The system in equation 7.13 is linear, however still azimuth dependent, so the matrices must be evaluated for each time step, when used for control or estimation. It is noticeable that the aerodynamic damping matrix has a negative sign, however each entry of the matrix will also have negative sign. The aerodynamic therefore contribute with a positive damping as expected.

The gains for the forcing vectors are found by combining eq. 7.10 and eq. 7.11, giving the aerodynamic damping as

$$c_{ija} = \sum_{k=1}^3 \int_0^R \frac{\partial x_{bk}}{\partial q_i} \left[\frac{\partial F_{Nk}}{\partial v_{xk}} \frac{\partial v_{xk}}{\partial \dot{q}_j} + \frac{\partial F_{Nk}}{\partial v_{yk}} \frac{\partial v_{yk}}{\partial \dot{q}_j} \right] + \frac{\partial y_{bk}}{\partial q_i} \left[\frac{\partial F_{Tk}}{\partial v_{xk}} \frac{\partial v_{xk}}{\partial \dot{q}_j} + \frac{\partial F_{Tk}}{\partial v_{yk}} \frac{\partial v_{yk}}{\partial \dot{q}_j} \right] dr, \quad (7.14)$$

and the gain coefficients of the pitch input are

$$Q_{\beta ij} = \sum_{k=1}^3 \int_0^R \frac{\partial x_{bk}}{\partial q_i} \frac{\partial F_{Nk}}{\partial \beta_j} + \frac{\partial y_{bk}}{\partial q_i} \frac{\partial F_{Tk}}{\partial \beta_j} dr, \quad (7.15)$$

and the gain coefficients of the incident wind disturbance are

$$Q_{vij} = \sum_{k=1}^3 \int_0^R \frac{\partial x_{bk}}{\partial q_i} \frac{\partial F_{Nk}}{\partial v_j} + \frac{\partial y_{bk}}{\partial q_i} \frac{\partial F_{Tk}}{\partial v_j} dr, \quad (7.16)$$

This concludes the description of the aerodynamics. The other external forces in this system are explained in the following subsections. The force applied from the generator is described in connection with drivetrain model.

7.2.2 Gravity

The wind turbine experience loads from gravity, which should be included as an external force in the Euler-Lagrange equation in a similar manner as the aerodynamics. However due to limited time, gravity is included in a more ad-hoc manner like proposed in [7]. Consider Figure 7.3

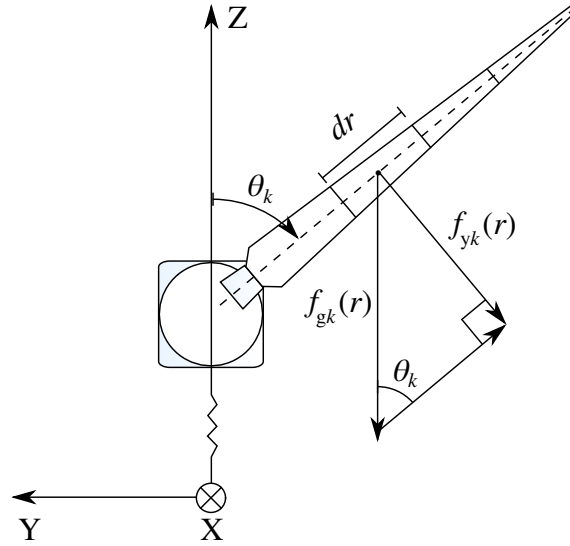


Figure 7.3. Illustration of gravity's effect on a element of the blade at radius r .

Gravity component of gravity normal to the blade, is computed

$$f_{yk}(r, \theta_k) = \int_0^R m_b(r) dr g \sin(\theta_k) \quad (7.17)$$

The stiffness arises from a change in the force due a change in the generalised coordinate[7]. In the case of the generator displacement this is then computed as

$$\frac{\partial f_{yk}(r)}{\partial q_3} = \int_0^R m_b(r) dr g \cos(\theta_k) \quad (7.18)$$

The related stiffness coefficients are found using the mode shapes. The flapwise stiffness for the first blade is

$$k_{53g} = \int_0^R m_b(r) \mu_{bfip}(r) dr g \cos(\theta_1) \quad (7.19)$$

and edgewise stiffness is

$$k_{83g} = \int_0^R m_b(r) \mu_{beip}(r) dr g \cos(\theta_1) \quad (7.20)$$

7.2.3 Structural Damping

The structural damping of the wind turbine is found by considering the non-conservative force of friction. The friction is included using Rayleigh's dissipation function [19, p. 24]

$$\mathcal{F}(t, \dot{q}) = \frac{1}{2} \dot{q}(t)^T C_s \dot{q}(t). \quad [\text{W}] \quad (7.21)$$

Here C_s is a diagonal matrix, which contains the structural (viscous) damping coefficients in the diagonal entries. These coefficients are given as

$$c_{iis} = 2\zeta_i \sqrt{k_{ii} m_{ii}}, \quad [\text{Ns/m}] \quad (7.22)$$

where

$C_s \in \mathbb{R}^{10 \times 10}$	is the structural damping,	
$c_{iis} \in \mathbb{R}$	is the i th structural damping coefficient,	
$\zeta_i \in \mathbb{R}$	is the i th damping factor.	[-]
$k_{ii} \in \mathbb{R}$	is the i th stiffness coefficient.	
$m_{ii} \in \mathbb{R}$	is the i th mass coefficient.	

7.3 Tower Model

The tower of the wind turbine is modelled as a clamped-free-end beam with the nacelle as a lumped mass, attached to the free end of the beam. This is shown in Figure 7.4 along with parameters, describing the tower and nacelle.

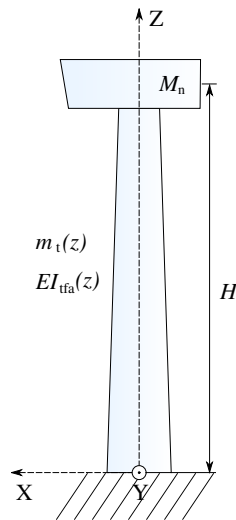


Figure 7.4. Model of the wind turbine tower.

A system with distributed parameters have infinitely many orthogonal modes and therefore some approximations are required to reduce the number of states. In this work the first mode shape for the side-side motion and the fore-aft motion is used to model the dynamics of the flexible tower. These mode shapes are shown in Figure 7.5 and Figure 7.6. The

fore-aft mode shape is given as

$$\begin{aligned} \mu_{\text{tfa}}(z) = & 0.7004 \left(\frac{z}{H}\right)^2 + 2.1963 \left(\frac{z}{H}\right)^3 - 5.6202 \left(\frac{z}{H}\right)^4 \\ & + 6.2275 \left(\frac{z}{H}\right)^5 - 2.5040 \left(\frac{z}{H}\right)^6 \end{aligned} \quad [-] \quad (7.23)$$

and side-side mode shape is

$$\begin{aligned} \mu_{\text{tss}}(z) = & 1.3850 \left(\frac{z}{H}\right)^2 - 1.7684 \left(\frac{z}{H}\right)^3 + 3.0871 \left(\frac{z}{H}\right)^4 \\ & - 2.2395 \left(\frac{z}{H}\right)^5 + 0.5357 \left(\frac{z}{H}\right)^6 \end{aligned} \quad [-] \quad (7.24)$$

The mode shapes are obtained from the FAST input file for the NREL 5 MW turbine [/FAST_data/NRELOffshrbSline5MW_Tower_Onshore.dat](#). They are normalised w.r.t. the tower height H , such that $\mu_{\text{tfa}}(H) = 1$. They are 6th order polynomials, where the first coefficient is zero due to a boundary condition of being clamped. To be able to compute some motions of the system, the slope of the mode shapes at height H is required. These are denoted as

$$\delta_{\text{tfa}} = \left. \frac{\partial \mu_{\text{tfa}}(z)}{\partial z} \right|_{z=H} \quad [\text{m}^{-1}] \quad (7.25)$$

and

$$\delta_{\text{tss}} = \left. \frac{\partial \mu_{\text{tss}}(z)}{\partial z} \right|_{z=H} \quad [\text{m}^{-1}] \quad (7.26)$$

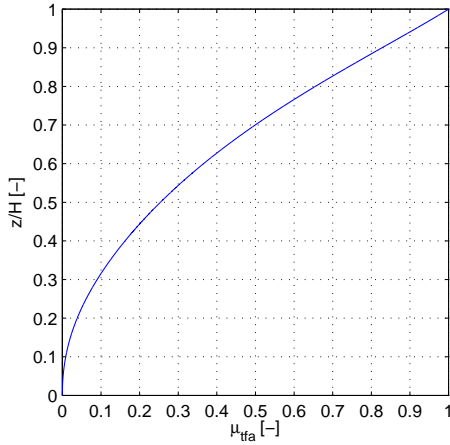


Figure 7.5. 1st tower fore-aft mode shape.

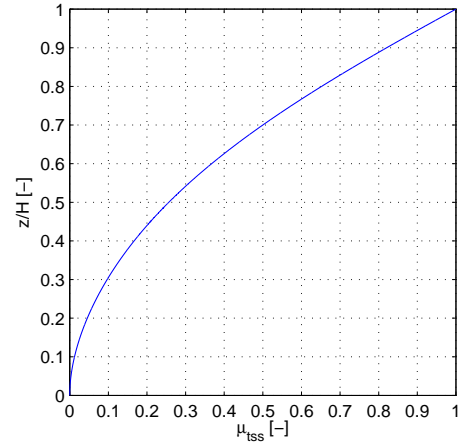


Figure 7.6. 1st tower side-side mode shape.

The kinetic energy of the wind turbine tower and nacelle is described using the time derivative of $\mu_{\text{tfa}}(z)q_1(t)$, which is the velocity for every point of the tower. The kinetic energy of the wind turbine tower and nacelle is the due to fore-aft and side-side motion is

$$\begin{aligned} T_t(t, \dot{q}) = & \frac{1}{2} \int_0^H m_t(z) \left[\frac{\partial \mu_{\text{tfa}}(z)q_1(t)}{\partial t} \right]^2 dz + \frac{1}{2} M_n \left[\frac{\partial \mu_{\text{tfa}}(H)q_1(t)}{\partial t} \right]^2 \\ & + \frac{1}{2} \int_0^H m_t(z) \left[\frac{\partial \mu_{\text{tss}}(z)q_2(t)}{\partial t} \right]^2 dz + \frac{1}{2} M_n \left[\frac{\partial \mu_{\text{tss}}(H)q_2(t)}{\partial t} \right]^2 \end{aligned} \quad [\text{J}] \quad (7.27)$$

where

$H \in \mathbb{R}$	is the height of the tower,	[m]
$m_t \in \mathbb{R}$	is the mass distribution of the tower,	[kg/m]
$M_n \in \mathbb{R}$	is mass of the nacelle and rotor,	[kg]
$\mu_{\text{tfa}} \in \mathbb{R}$	is the 1st mode shape of the tower fore-aft displacement,	[-]
$\mu_{\text{tss}} \in \mathbb{R}$	is the 1st mode shape of the tower side-side displacement.	[-]

The first two terms describe the kinetic energy for respectively the tower and nacelle due to fore-aft motion. The last two terms relate to the side-side motion. Next, the facts that $\mu_{\text{tfa}}(H) = 1$ and that the mode shapes are time-invariant are applied. Rewriting in terms of generalised velocities, the kinetic energy is then expressed as

$$\begin{aligned}
 T_t(t, \dot{q}) &= \frac{1}{2} \left(\int_0^H m_t(z) \mu_{\text{tfa}}(z)^2 dz + M_n \right) \dot{q}_1(t)^2 \\
 &+ \frac{1}{2} \left(\int_0^H m_t(z) \mu_{\text{tss}}(z)^2 dz + M_n \right) \dot{q}_2(t)^2
 \end{aligned} \quad [\text{J}] \quad (7.28)$$

Because of the elasticity of the flexible tower, the potential energy is stored and is computed as [18, p. 387]

$$\begin{aligned}
 V_t(t, q) &= \frac{1}{2} \int_0^H EI_{\text{tfa}}(z) \left[\frac{\partial^2 \mu_{\text{tfa}}(z) q_1(t)}{\partial z^2} \right]^2 dz \\
 &+ \frac{1}{2} \int_0^H EI_{\text{tss}}(z) \left[\frac{\partial^2 \mu_{\text{tss}}(z) q_2(t)}{\partial z^2} \right]^2 dz
 \end{aligned} \quad [\text{J}] \quad (7.29)$$

Knowing that the generalised coordinates are independent of r , equation 7.29 is rewritten to

$$\begin{aligned}
 V_t(t, q) &= \frac{1}{2} \left(\int_0^H EI_{\text{tfa}}(z) \left[\frac{\partial^2 \mu_{\text{tfa}}(z)}{\partial z^2} \right]^2 dz \right) q_1(t)^2 \\
 &+ \frac{1}{2} \left(\int_0^H EI_{\text{tss}}(z) \left[\frac{\partial^2 \mu_{\text{tss}}(z)}{\partial z^2} \right]^2 dz \right) q_2(t)^2
 \end{aligned} \quad [\text{J}] \quad (7.30)$$

where

$EI_{\text{tfa}} \in \mathbb{R}$	is the flexural rigidity in the sideways direction,	[Nm ²]
$EI_{\text{tss}} \in \mathbb{R}$	is the flexural rigidity in the fore-aft direction.	[Nm ²]

The flexural rigidity $EI(z)$ is the product of the modulus of elasticity E and the cross sectional area moment of inertia $I(z)$. Throughout the report, the flexural rigidity is used since data for these are available. Now the energy in tower and nacelle is accounted for, then mass, stiffness and damping coefficients can be derived. These derivations are presented in section 7.7 on page 56.

7.4 Drivetrain Model

The drivetrain is modelled as a lumped system with two rotating bodies, being the rotor and the generator. These bodies are interconnected through a gearbox as shown on Figure 7.7. The rotor is connected to gearbox through a flexible low speed shaft. On the high speed side of the gearbox, a non-flexible shaft is connected to the generator. This is a relative simple system and therefore Lagrangian mechanics is not used in the following derivations. The flexible shaft of the drivetrain could be modelled as a system with distributed parameters, however only data for a lumped system is available for NREL turbine used in this work. Also, data for stiffness and damping of the generator and the rotor are not available, so it is omitted in the model.

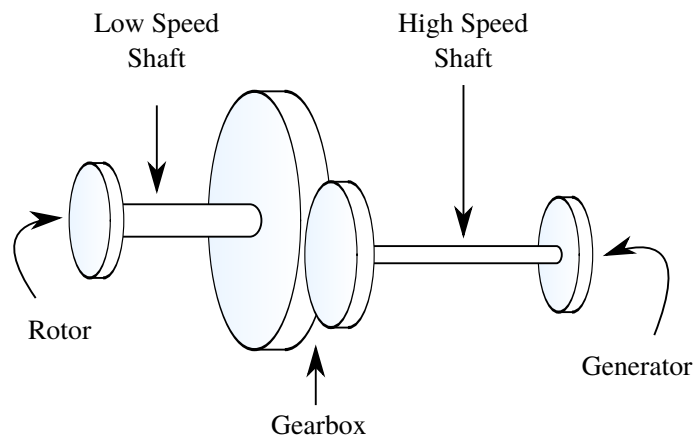


Figure 7.7. Model of the wind turbine's drivetrain.

As the low speed shaft is flexible, it is subject to the torsional displacement

$$\theta_t(t) = \theta_r(t) - \frac{1}{n}\theta_g(t) = \theta_r(t) - \theta_{gls}(t) \quad [\text{rad}] \quad (7.31)$$

where:

$\theta_t \in \mathbb{R}$	is the torsional displacement of the low speed shaft	[rad]
$\theta_r \in \mathbb{R}$	is the absolute angular position of the rotor	[rad]
$\theta_g \in \mathbb{R}$	is the absolute angular position of the generator	[rad]
$\theta_{gls} \in \mathbb{R}$	is the angular position of the generator on the low speed side	[rad]
$n \in \mathbb{R}$	is the gear ratio of the gearbox	[-]

Figure 7.8 shows a diagram of the rotating elements in the drivetrain, and illustrates the torques applied to them.

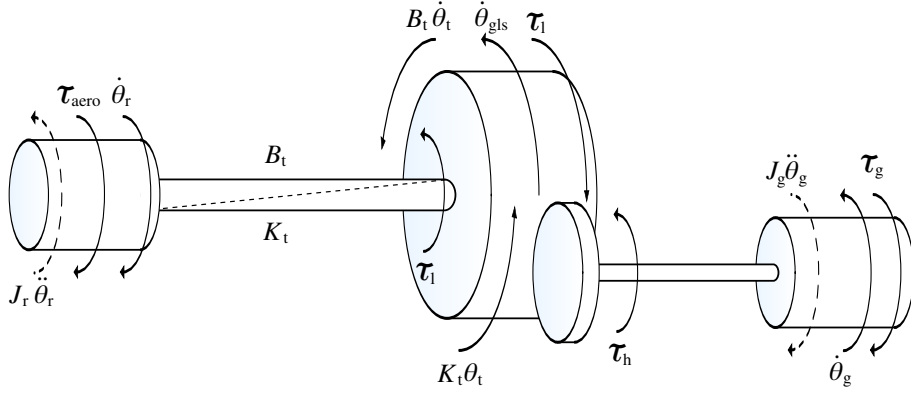


Figure 7.8. Diagram illustrating the parameters of the wind turbine's drivetrain. The dashed line illustrates the torsion of the shaft from rotor to gearbox on the low speed side

The moment equation for the rotor is

$$J_r \ddot{\theta}_r(t) = \tau_{\text{aero}}(t) - \tau_1(t), \quad [\text{Nm}] \quad (7.32)$$

and the torque loading the gearbox on the low speed side is

$$\tau_1 = n\tau_h = B_t \dot{\theta}_t + K_t \theta_t, \quad [\text{Nm}] \quad (7.33)$$

where

$J_r \in \mathbb{R}$	is the moment of inertia of the rotor,	$[\text{kgm}^2]$
$\tau_{\text{aero}} \in \mathbb{R}$	is the aerodynamic torque induced by the wind,	$[\text{Nm}]$
$\tau_1 \in \mathbb{R}$	is the torque on the gearbox on the low speed side,	$[\text{Nm}]$
$\tau_h \in \mathbb{R}$	is the torque on the gearbox on the high speed side,	$[\text{Nm}]$
$B_t \in \mathbb{R}$	is the viscous damping of the low speed shaft,	$[\text{Nms/rad}]$
$K_t \in \mathbb{R}$	is the stiffness of the low speed shaft.	$[\text{Nm/rad}]$

Inserting eq. 7.31 and eq. 7.33 in eq. 7.32, then the moment of the rotor is expressed as

$$J_r \ddot{\theta}_{\text{gls}}(t) + J_r \ddot{\theta}_t(t) = \tau_{\text{aero}}(t) - \tau_1(t) \Rightarrow \quad [\text{Nm}] \quad (7.34)$$

$$J_r \ddot{\theta}_{\text{gls}}(t) + J_r \ddot{\theta}_t(t) = \tau_{\text{aero}}(t) - B_t \dot{\theta}_t - K_t \theta_t \quad [\text{Nm}] \quad (7.35)$$

The moment equation for the generator, on the high speed side, is

$$J_g \ddot{\theta}_g(t) = \tau_h(t) - \tau_g(t) \Rightarrow \quad [\text{Nm}] \quad (7.36)$$

$$J_g \ddot{\theta}_g(t) = \frac{\tau_1(t)}{n} - \tau_g(t) \Rightarrow \quad [\text{Nm}] \quad (7.37)$$

$$n J_g \ddot{\theta}_{\text{gls}}(t) = \frac{\tau_1(t)}{n} - \tau_g(t) \Rightarrow \quad [\text{Nm}] \quad (7.38)$$

$$n^2 J_g \ddot{\theta}_{\text{gls}}(t) = \tau_1(t) - n\tau_g(t) \quad [\text{Nm}] \quad (7.39)$$

where

$J_g \in \mathbb{R}$	is the moment of inertia of the generator	$[\text{kgm}^2]$
$\tau_g \in \mathbb{R}$	is the generator torque	$[\text{Nm}]$

Adding eq. 7.34 to eq. 7.39 the moment equation of the generator reduces to

$$(J_r + n^2 J_g) \ddot{\theta}_{\text{gls}} + J_r \ddot{\theta}_t = \tau_{\text{aero}} - n\tau_g \quad [\text{Nm}] \quad (7.40)$$

Using eq. 7.40 and eq. 7.35, then the dynamics of the drivetrain are expressed, in matrix form, as

$$\begin{bmatrix} J_r + n^2 J_g & J_r \\ J_r & J_r \end{bmatrix} \begin{bmatrix} \ddot{\theta}_{\text{gls}}(t) \\ \ddot{\theta}_t(t) \end{bmatrix} + \begin{bmatrix} 0 & 0 \\ 0 & B_t \end{bmatrix} \begin{bmatrix} \dot{\theta}_{\text{gls}}(t) \\ \dot{\theta}_t(t) \end{bmatrix} + \begin{bmatrix} 0 & 0 \\ 0 & K_t \end{bmatrix} \begin{bmatrix} \theta_{\text{gls}}(t) \\ \theta_t(t) \end{bmatrix} = \begin{bmatrix} \tau_{\text{aero}}(t) \\ \tau_{\text{aero}}(t) \end{bmatrix} + \begin{bmatrix} -n \\ 0 \end{bmatrix} \tau_g(t) \quad (7.41)$$

The states of the derived drivetrain model are already in terms of generalised coordinate, which means the forces are also generalised. The matrix equation can therefore be rewritten to

$$\begin{bmatrix} J_r + n^2 J_g & J_r \\ J_r & J_r \end{bmatrix} \begin{bmatrix} \ddot{q}_3(t) \\ \ddot{q}_4(t) \end{bmatrix} + \begin{bmatrix} 0 & 0 \\ 0 & B_t \end{bmatrix} \begin{bmatrix} \dot{q}_3(t) \\ \dot{q}_4(t) \end{bmatrix} + \begin{bmatrix} 0 & 0 \\ 0 & K_t \end{bmatrix} \begin{bmatrix} q_3(t) \\ q_4(t) \end{bmatrix} = \begin{bmatrix} \tilde{Q}_3 \\ \tilde{Q}_4 \end{bmatrix} + \begin{bmatrix} Q_{\tau 3} \\ Q_{\tau 4} \end{bmatrix} \tau(t) \quad (7.42)$$

It should be noted that $Q_{\tau i} = 0$, except for $i = 3$. The parameters of the drivetrain are obtained from the FAST input file

Ⓢ [/FAST_data/NRELOffshrBslne5MW_Onshore.fst](#) and are presented in Table 7.1. The value of J_r is the sum of the moments of inertia for the rotor and 3 blades.

Parameter	Value	Unit
J_r	38,830,000	kgm ²
J_g	534.116	kgm ²
K_t	867,637,000	N/rad
B_t	6,215,000	Ns/rad
n	97	-

Table 7.1. Drivetrain parameter obtain from the NREL 5 MW wind turbine.

7.5 Blade Model

The blades of the wind turbine are modelled similar to the tower as a flexible beam with a clamped end and a free end. The motion of the blades is, however more complex because of the rotation of the blades. Figure 7.9 illustrates the blade model and the parameters related to it.

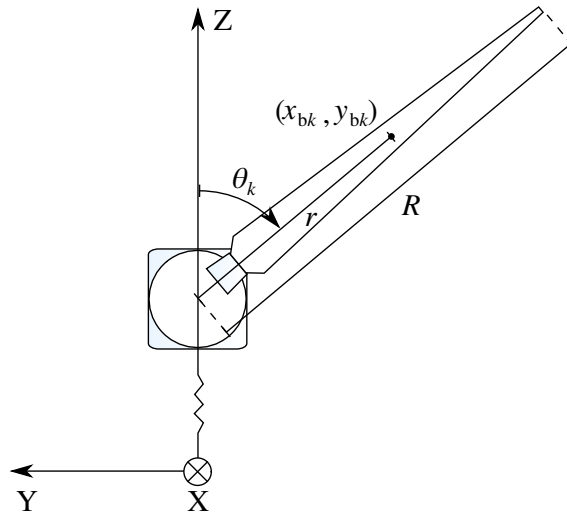


Figure 7.9. Front view of a blade.

As in the case of the tower, only the first mode shape is used to model respectively the flap- and edgewise motion of each blade. The mode shapes are obtained from the FAST input file for the NREL 5 MW turbine [/FAST_data/NRELOffshrBslne5MW_Blade.dat](#), and are normalised w.r.t. the blade radius R . The mode shapes are shown in Figure 7.10 and Figure 7.11. The flapwise mode shape is

$$\begin{aligned} \mu_{bf}(r) = & 0.0622 \left(\frac{r}{R}\right)^2 + 1.7254 \left(\frac{r}{R}\right)^3 - 3.2452 \left(\frac{r}{R}\right)^4 \\ & + 4.7131 \left(\frac{r}{R}\right)^5 - 2.2555 \left(\frac{r}{R}\right)^6 \end{aligned} \quad [-] \quad (7.43)$$

and the edgewise mode shape is

$$\begin{aligned} \mu_{be}(r) = & 0.3627 \left(\frac{r}{R}\right)^2 + 2.5337 \left(\frac{r}{R}\right)^3 - 3.5772 \left(\frac{r}{R}\right)^4 \\ & + 2.3760 \left(\frac{r}{R}\right)^5 - 0.6952 \left(\frac{r}{R}\right)^6 \end{aligned} \quad [-] \quad (7.44)$$

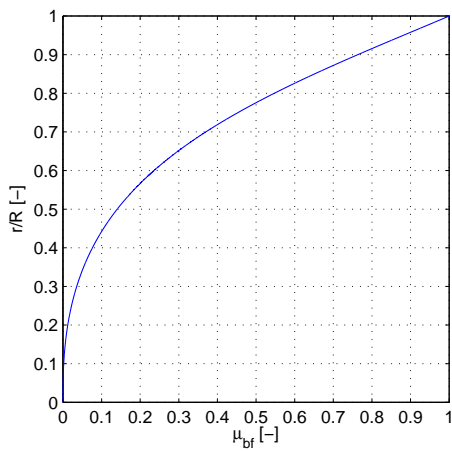


Figure 7.10. 1st blade flapwise mode shape.

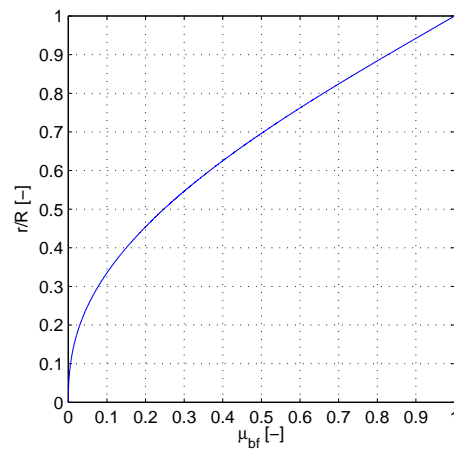


Figure 7.11. 1st blade edgewise mode shape.

In order to compute some of the motions, the components for these modes w.r.t. x -axis and y -axis are required. Components along the x -axis are denoted as 'Out-of-Plane' mode shapes and components along the y -axis are 'In-Plane' mode shapes. The naming refers to the plane of rotation for the blades. Figure 7.12 shows these mode shapes. The angle that the mode shapes is rotated w.r.t. the axis is due to structural twist and blade pitch. The structural twist is time independent and varies as a function of the radius. The blade pitch angle changes in full load operation.

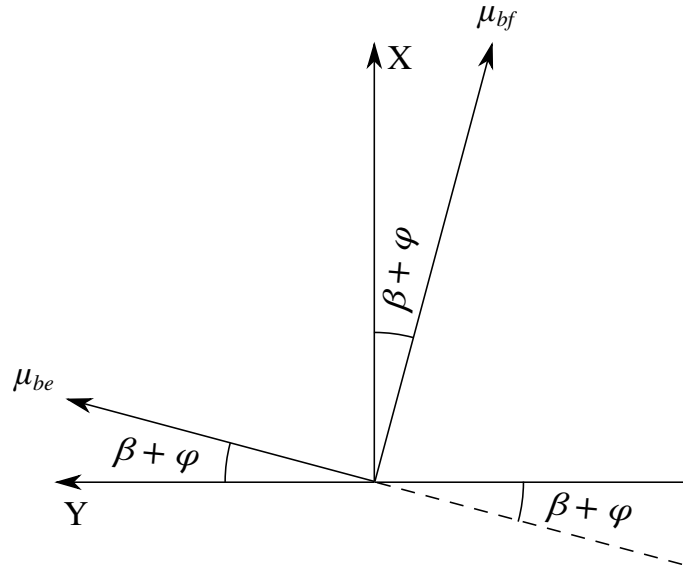


Figure 7.12. Blade mode shapes with respect to in plane and out of plane.

Resolving the mode shapes in in-plane and out-of-plane directions, yield the expressions stated below. Note that the in-plane component $\mu_{bfip}(r)$ is negative, due to its direction on the y -axis.

$$\mu_{bfop}(r) = \mu_{bf}(r) \cos(\beta + \varphi(r)) \quad [-] \quad (7.45)$$

$$\mu_{bfip}(r) = -\mu_{bf}(r) \sin(\beta + \varphi(r)) \quad [-] \quad (7.46)$$

$$\mu_{beop}(r) = \mu_{be}(r) \sin(\beta + \varphi(r)) \quad [-] \quad (7.47)$$

$$\mu_{beip}(r) = \mu_{be}(r) \cos(\beta + \varphi(r)) \quad [-] \quad (7.48)$$

where

β	is blade pitch angle	[rad]
φ	is the structural twist of the blade	[rad]
μ_{bfop}	is the flapwise, out of plane blade mode shape,	[-]
μ_{bfip}	is the flapwise, in plane blade mode shape,	[-]
μ_{beop}	is the edgewise, out of plane blade mode shape,	[-]
μ_{beip}	is the edgewise, in plane blade mode shape.	[-]

The position of a blade depends on several other states, since the tower- and drivetrain motion affects the motion of the blade. The x -position of the k th blade is

$$x_{bk}(t, r) = (1 + r \cos(\theta_k(t))\delta_{\text{tfa}})q_1(t) + \mu_{\text{bfop}}(r)q_{k+4}(t) + \mu_{\text{beop}}(r)q_{k+7}(t), \quad [\text{m}] \quad (7.49)$$

Note that in eq. 7.49 the rotor overhang is neglected as mentioned earlier. The first term is the motion of a flexible tower with a rigid blade. This is shown in Figure 7.13. Including the last two terms accounts for the flexibility of the blade. Combined the three terms describe the motion of a flexible blade mounted on a flexible tower. It should be noted that if the structural twists of the blades are removed and they are not pitched, there will be no term from the edgewise motion, $q_{k+7}(t)$, contributing.

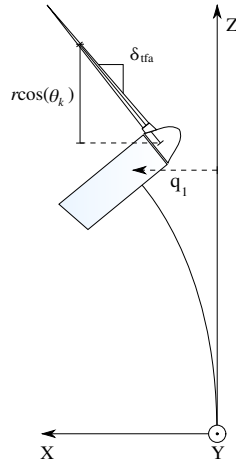


Figure 7.13. A rigid blade mounted on a flexible tower.

The corresponding velocity is

$$\begin{aligned} \dot{x}_{bk}(t, r) &= (1 + r \cos(\theta_k(t))\delta_{\text{tfa}})\dot{q}_1(t) + \mu_{\text{bfop}}(r)\dot{q}_{k+4}(t) + \mu_{\text{beop}}(r)\dot{q}_{k+7}(t) \\ &\quad - \Omega\delta_{\text{tfa}}r \sin(\theta_k(t))q_1(t), \end{aligned} \quad [\text{m/s}] \quad (7.50)$$

The y -position of the k th blade is found, in a similar manner, to be

$$y_{bk}(t, r) = (1 + r \cos(\theta_k)\delta_{\text{tss}})q_2(t) + r \sin(\theta_k) + \mu_{\text{bfip}}(r)q_{k+4}(t) + \mu_{\text{beip}}(r)q_{k+7}(t), \quad [\text{m}] \quad (7.51)$$

The first term describes the displacement of the tower's sideways motion. The next term is the displacement due to the rotation of the rotor, which is the sum of $q_3(t)$ and $q_4(t)$. The last terms introduce the flexibility of the blades. The corresponding velocity is

$$\dot{y}_{bk}(t, r) = (1 + r \cos(\theta_k)\delta_{\text{tss}})\dot{q}_2(t) + \mu_{\text{bfip}}(r)\dot{q}_{k+4}(t) + \mu_{\text{beip}}(r)\dot{q}_{k+7}(t) \quad (7.52)$$

$$- \Omega\delta_{\text{tss}}r \sin(\theta_k(t))q_2(t) + r\Omega \cos(\theta_k), \quad [\text{m/s}] \quad (7.53)$$

where

θ_k	is the azimuthal angle of the k th blade,	[rad]
μ_{tfa}	is the 1st mode shape of the tower fore-aft displacement,	[-]
\dot{q}_{k+4}	is generalised flapwise velocity of the k th blade,	[m/s]
\dot{q}_{k+7}	is generalised edgewise velocity of the k th blade.	[m/s]

The kinetic energy of the three blades is

$$T_b(t, \dot{q}, q) = \frac{1}{2} \sum_{k=1}^3 \int_0^R m_b(r) [\dot{x}_{bk}(t, r)]^2 dr + \frac{1}{2} \sum_{k=1}^3 \int_0^R m_b(r) [\dot{y}_{bk}(t, r)]^2 dr, \quad [\text{J}] \quad (7.54)$$

and the potential energy is

$$V_b(t, q) = \frac{1}{2} \sum_{k=1}^3 \int_0^R EI_{\text{bf}}(r) \left[\frac{\partial^2 \mu_{\text{bf}}(r) q_{k+4}(t)}{\partial r^2} \right]^2 dz + \frac{1}{2} \sum_{k=1}^3 \int_0^R EI_{\text{be}}(r) \left[\frac{\partial^2 \mu_{\text{be}}(r) q_{k+7}(t)}{\partial r^2} \right]^2 dr, \quad [\text{J}] \quad (7.55)$$

where

$R \in \mathbb{R}$	is the radius of the blade from hub to tip,	[m]
$H \in \mathbb{R}$	is the height of the tower,	[m]
$m_b \in \mathbb{R}$	is the mass distribution of the blade,	[kg/m]
$EI_{\text{bf}} \in \mathbb{R}$	is the flexural rigidity in the flapwise direction of the blade,	[Nm ²]
$EI_{\text{be}} \in \mathbb{R}$	is the flexural rigidity in the edgewise direction of the blade,	[Nm ²]
$\mu_{\text{bf}} \in \mathbb{R}$	is 1st assumed mode for the blade flapwise motion,	[-]
$\mu_{\text{be}} \in \mathbb{R}$	is 1st assumed mode for the blade edgewise motion.	[-]

7.6 Aerodynamics

7.6.1 Aerodynamic Loads

This section introduces the wind model, which is used to describe the interaction between blade and the wind. To keep computation low it is chosen to use a model based on Blade Element Momentum Theory (BEM Theory)[6, p. 48][1, p. 57], which is a simple model compared to e.g. Computational Fluid Dynamics (CFD)[1, p. 190]. The simplicity of this model is preferable, since the filter should carry out the computation in real-time. To derive this model, consider Figure 7.14, which shows a cross-section of a wind turbine blade at an azimuth angle of 0 rad. The incident wind speed, $v_k(t)$, is normal to the y -axis. The yz -plane is also referred to as the plane of rotation.

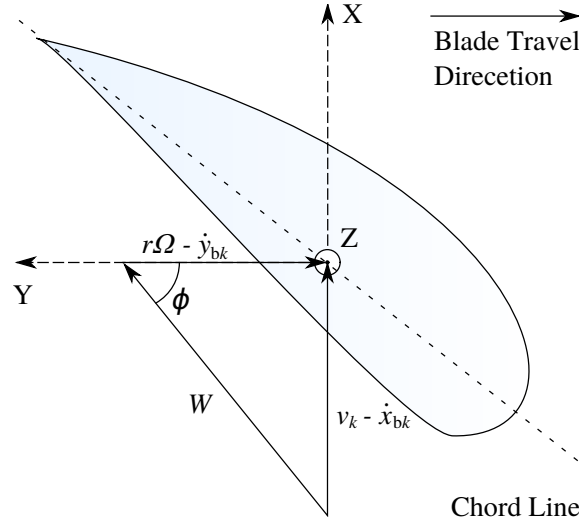


Figure 7.14. cross section of a blade, with wind inflow at an azimuthal angle of 0 rad

Due to the incident wind and the rotation of the blade, the k th blade is subject to the relative wind W_k , which is given as the difference between wind and structural motion, i.e.

$$W_k(t, r) = \sqrt{(v_k(r) - \dot{x}_{bk}(t, r))^2 + (r\Omega - \dot{y}_{bk}(t, r))^2} \quad [\text{m/s}] \quad (7.56)$$

$$W_k(t, r, v_{xk}, v_{yk}) = \sqrt{v_{xk}^2(t, r) + v_{yk}^2(t, r)} \quad [\text{m/s}] \quad (7.57)$$

where

ϕ	is the wind inflow angle	[rad]
v_k	is the wind normal to the plane of rotation on the k th blade	[m/s]
W_k	is the relative wind on the k th blade	[m/s]
Ω	is the rotor speed	[rad/s]
r	is radius to the cross-section	[m]

The wind inflow angle, $\phi(r)$, is the angle between the relative wind, W_k , and the plane of rotation (see Figure 7.15) and is computed as

$$\phi(r) = \alpha(v_k) + \beta + \varphi(r) \quad [\text{rad}] \quad (7.58)$$

where

α	is the angle of attack	[rad]
β	is blade pitch angle	[rad]
φ	is the structural twist of the blade	[rad]

The wind induces 2 forces respectively called the lift - and drag force, which respectively have directions normal and tangential to the chord line of the cross-section. These are illustrated in Figure 7.15.

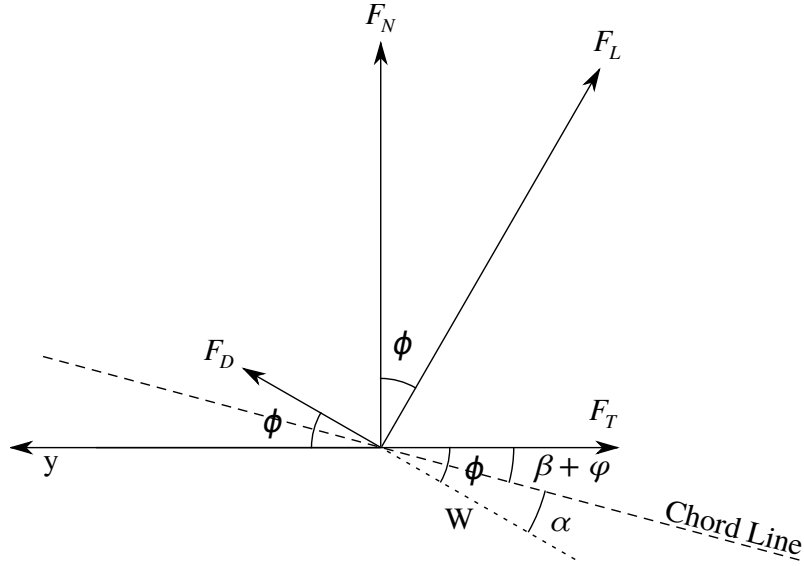


Figure 7.15. Forces acting at a blade cross-section at radius r .

The lift force is given as [7][6, p. 48]

$$F_{Lk}(t, r, v_{xk}, v_{yk}) = \frac{1}{2} \rho(r) c(r) W_k(t, r, v_{xk}, v_{yk})^2 C_L(\alpha(v_k), r) dr \quad [\text{N/m}] \quad (7.59)$$

and the drag force is [7][6, p. 48]

$$F_{Dk}(t, r, v_{xk}, v_{yk}) = \frac{1}{2} \rho(r) c(r) W_k(t, r, v_{xk}, v_{yk})^2 C_D(\alpha(v_k), r) dr \quad [\text{N/m}] \quad (7.60)$$

where

F_{Lk}	is the lift force on the k th blade at radius r	[F/m]
F_{Dk}	is the drag force on the k th blade at radius r	[F/m]
C_L	is the lift coefficient at radius r	[-]
C_D	is the drag coefficient at radius r	[-]
c	is the chord length of the cross-section at radius r	[m]

These two forces can be resolved into forces in normal and tangential to the plane of rotation. The tangential force is also referred to as the thrust force, since it is responsible for the rotation of the blade. The force normal to the y -axis is

$$F_{Nk}(t, r, v_{xk}, v_{yk}) = F_{Lk}(t, r, v_{xk}, v_{yk}) \cos(\beta + \varphi(r)) + F_{Dk}(t, r, v_{xk}, v_{yk}) \sin(\beta + \varphi(r)) \quad [\text{N/m}] \quad (7.61)$$

and the thrust force

$$F_{Tk}(t, r, v_{xk}, v_{yk}) = F_{Lk}(t, r, v_{xk}, v_{yk}) \sin(\beta + \varphi(r)) - F_{Dk}(t, r, v_{xk}, v_{yk}) \cos(\beta + \varphi(r)) \quad [\text{N/m}] \quad (7.62)$$

which are rewritten to

$$F_{Nk}(t, r, v_{xk}, v_{yk}) = \frac{1}{2} \rho(r) c(r) (v_{xk}(t, r)^2 + v_{yk}(t, r)^2) [C_L(\alpha(v_k), r) \cos(\beta + \varphi(r)) + C_D(\alpha(v_k), r) \sin(\beta + \varphi(r))] dr \quad [\text{N/m}] \quad (7.63)$$

and

$$F_{Tk}(t, r, v_{xk}, v_{yk}) = \frac{1}{2} \rho(r) c(r) (v_{xk}(t, r)^2 + v_{yk}(t, r)^2) [C_L(\alpha(v_k), r) \sin(\beta + \varphi(r)) - C_D(\alpha(v_k), r) \cos(\beta + \varphi(r))] dr \quad [\text{N/m}] \quad (7.64)$$

The derivatives w.r.t. the winds v_{xk} and v_{yk} and the pitch β are required for the linearisation of the aerodynamic. The derivative of F_N w.r.t. v_{xk} is

$$\begin{aligned} f_{Nv_{xk}}(r) &= \frac{\partial F_{Nk}}{\partial v_{xk}} \\ &= \frac{1}{2} \rho(r) c(r) [2v_k C_L(\alpha(v_k), r) \cos(\beta + \varphi(r)) + C_D(\alpha(v_k), r) \sin(\beta + \varphi(r))] \\ &\quad + r\Omega \left(\frac{\partial C_L(\alpha(v_k), r)}{\partial \alpha(v_k)} + C_D(\alpha(v_k), r) \right) \cos(\beta + \varphi(r)) \\ &\quad + r\Omega \left(\frac{\partial C_D(\alpha(v_k), r)}{\partial \alpha(v_k)} - C_L(\alpha(v_k), r) \right) \sin(\beta + \varphi(r)) dr \quad [\text{Ns/m}] \end{aligned} \quad (7.65)$$

The derivative in equation eq. 7.65 have been simplified using the assumption that $W \approx \Omega r$ and $\frac{\partial \phi}{\partial v} \approx \frac{1}{\Omega r}$, which are justified in [1, p. 225]. The remaining partial derivatives are found in [20, p. 57].

7.6.2 Wind Model

The wind needs to be modelled, such that it is possible to estimate it by different terms in the estimation scheme. It is chosen to describe the wind by the 3 terms of contribution being; mean wind speed in hub height, the vertical wind shear and the contribution from tower shadow. Thereby the wind is modelled as

$$v_k(t) = v_H(t) + v_{wsk}(t) + v_{tsk}(t) \quad [\text{m/s}] \quad (7.66)$$

where

v_k	is the total wind experienced by k th blade	[m/s]
v_H	is the wind speed at hub height	[m/s]
v_{wsk}	is the wind shear component	[m/s]
v_{tsk}	is the tower shadow component	[m/s]

The components of wind shear, and tower shadow are modelled individually in the following

7.6.3 Wind Shear Model

For the vertical wind shear to be taken into account a model for this is needed. This shear can be modelled in many ways, varying in complexity, dependent on e.g. the topography

in the particular area where the shear should be calculated. A commonly used model for the vertical wind shear is seen in equation 7.67[16].

$$v(z) = v_H \left(\frac{z}{H} \right)^\sigma, \quad [\text{m/s}] \quad (7.67)$$

where

z	is the height,	[m]
H	is the hub height,	[m]
$v(z)$	is the wind speed at the height z ,	[m/s]
v_H	is the wind speed at the hub height,	[m/s]
σ	is the wind shear coefficient.	[-]

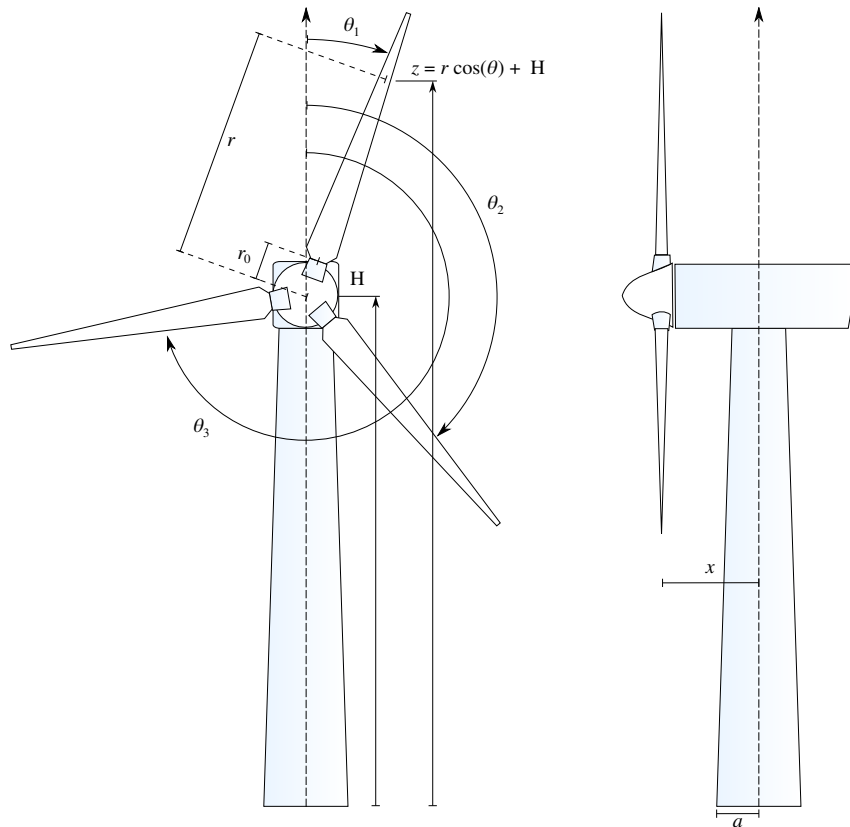


Figure 7.16. Definitions on the parameters used in the wind model.

From figure 7.16 some of the dimensions and variables used onwards are illustratively defined. Then the formula 7.67 can be rewritten as 7.69.

$$v(r, \theta_k) = v_H \left(\frac{r \cos(\theta_k) + H}{H} \right)^\sigma \quad [\text{m/s}] \quad (7.68)$$

$$= v_H \left(1 + \frac{r \cos(\theta_k)}{H} \right)^\sigma \quad [\text{m/s}] \quad (7.69)$$

Figure 7.17 illustrates the effect of the wind shear at the tip of a blade ($r = 63\text{ m}$) as a function of the azimuthal angle of the k th blade θ_k as described by equation 7.69 under the conditions stated in table 7.2. The values are inspired by the FAST documentation [/FAST_documentation/Definition of a 5-MW Reference Wind Turbine for Offshore System Development.pdf](#), and the value for the wind shear coefficient from [16]. The reason for setting $r = R$ is to observe the total change in wind speed from the blade being in top position to being in lowest position.

Parameter	Value	Unit	Description
r	63	[m]	radial distance on blade from rotor axis
R	63	[m]	total length of blade
r_0	1.5	[m]	radial distance from rotor axis to blade root
H	90	[m]	hub height
v_H	10	[m/s]	wind speed at hub height
σ	0.14	[-]	wind shear coefficient
x	5.02	[m]	distance from blade to tower midline
a	2.74	[m]	tower radius in height $H - R$

Table 7.2. Conditions set for illustration of wind shear and tower shadow.

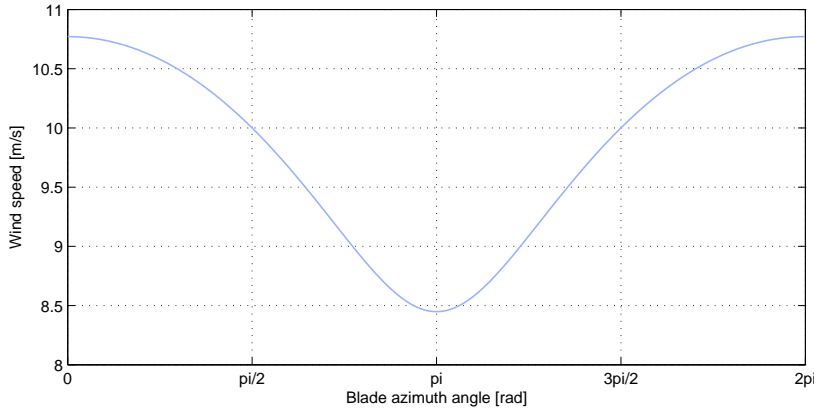


Figure 7.17. Wind shear illustration.

This expression is nonlinear and as the model is linear, this particular model can not be readily implemented. In [21] by Dolan and Lehn, this model can be expressed as a 3rd order Taylor expansion. The used model for the wind shear is this derived model (equation 7.70), which sums up the integration of the wind speed components over the radius of all 3 blades.

$$\begin{aligned}
 v_{ws} &= \frac{2v_H}{3sR^2} \sum_{k=1}^3 \int_{r_0}^R \left[\frac{r^2\sigma}{H} \cos \theta_k + \frac{r^3\sigma(\sigma-1)}{2H^2} \cos^2 \theta_k + \frac{r^4\sigma(\sigma-1)(\sigma-2)}{6H^3} \cos^3 \theta_k \right] dr, \quad [\text{m/s}] \\
 &= \frac{2v_H}{3sR^2} \sum_{k=1}^3 \left[\left(\frac{R^3\sigma}{3H} \cos \theta_k + \frac{R^4\sigma(\sigma-1)}{8H^2} \cos^2 \theta_k + \frac{R^5\sigma(\sigma-1)(\sigma-2)}{30H^3} \cos^3 \theta_k \right) \right. \\
 &\quad \left. - \left(\frac{r_0^3\sigma}{3H} \cos \theta_k + \frac{r_0^4\sigma(\sigma-1)}{8H^2} \cos^2 \theta_k + \frac{r_0^5\sigma(\sigma-1)(\sigma-2)}{30H^3} \cos^3 \theta_k \right) \right] \quad (7.70)
 \end{aligned}$$

with

$$s \triangleq 1 - \left(\frac{r_0}{R}\right)^2$$

where

v_H	is the wind speed at the hub height,	[m/s]
H	is the hub height,	[m]
σ	is the wind shear coefficient,	[-]
θ_k	is the angle of the k th blade,	[rad]
r_0	is the distance at which the blade profile begins,	[m]
r	is radial distance from rotor axis,	[m]
R	is the total length of the blade.	[m]

7.6.4 Tower Shadow

The tower shadow contributes to the wind model as well, and the model used in this project is, as well as the wind shear model, borrowed from the model derived in [21] and is formulated as in equation 7.71. As there is no tower above the nacelle, the model is only valid in the interval $\theta_k \in [\frac{\pi}{2}, \frac{3\pi}{2}]$.

$$v_{ts} = \frac{2mV_H}{3sR^2} \sum_{k=1}^3 \left[\frac{a^2 \ln(R^2 \sin^2 \theta_k + x^2)}{2 \sin^2 \theta_k} - \frac{a^2 \ln(r_0^2 \sin^2 \theta_k + x^2)}{2 \sin^2 \theta_k} + \frac{a^2 x^2}{\sin^2 \theta_k (R^2 \sin^2 \theta_k + x^2)} - \frac{a^2 x^2}{\sin^2 \theta_k (r_0^2 \sin^2 \theta_k + x^2)} \right] \quad [\text{m/s}] \quad (7.71)$$

with

$$m \triangleq 1 + \frac{\sigma(\sigma - 1)R^2}{8H^2}$$

where

a is the radius of the tower [m]

x is the distance from tower midline to the blade (overhang) [m]

Figure 7.18 illustrates the contribution to the wind model from the tower shadow for the k th blade, under the conditions listed in table 7.2.

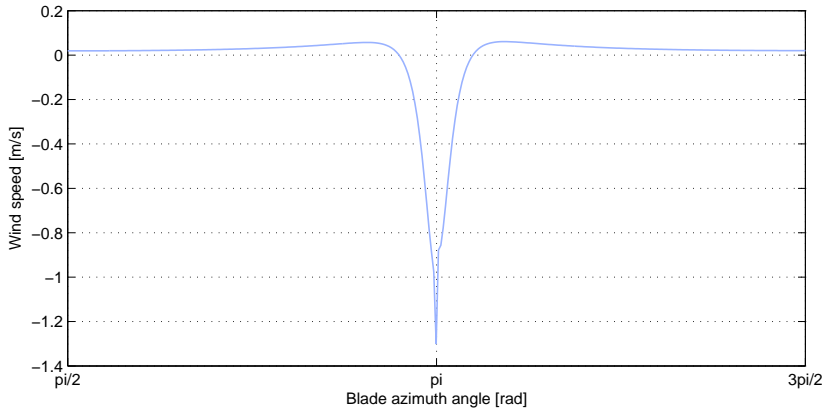


Figure 7.18. Tower shadow illustration

7.7 Derivation Example

The four subsystems of the wind turbine have now been described. An example of the derivations of mass, stiffness, etc. done in this project, is now presented. This example is intended to make the derivation procedure more obvious and also to show the extent of the derivations done in this work, since a large amount of the project time was invested in the derivations of the model.

In this example only the tower fore-aft displacement, $q_1(t)$, is considered, which yields the entries of the first row in the mass, stiffness and damping matrices. Consider the Euler-Lagrange equation from eq. 7.4, now only with partial derivatives w.r.t. the tower fore-aft displacement, yielding

$$0 = \frac{d}{dt} \left(\frac{\partial L(t, q, \dot{q})}{\partial \dot{q}_1} \right) - \frac{\partial L(t, q, \dot{q})}{\partial q_1} + \frac{\partial \mathcal{F}(t, \dot{q})}{\partial \dot{q}_1} - \tilde{Q}_1(t) \quad [\text{N}] \quad (7.72)$$

Equation 7.72 represents the first of 10 equations, which describe the wind turbine model. The structural stiffness related to the fore-aft motion is derived by considering the second term on the right hand side.

7.7.1 Structural Stiffness

The second term of eq. 7.72 is split into the following terms

$$- \frac{\partial L(t, q, \dot{q})}{\partial q_1} = - \frac{\partial T(t, q, \dot{q})}{\partial q_1} + \frac{\partial V(t, q)}{\partial q_1} \quad [\text{N}] \quad (7.73)$$

It should be noted that $T(t)$ and $V(t)$ are all the kinetic and potential energies in the system, not only for the tower. The structural stiffness is then found by taking the partial derivative of $V(t, q)$ w.r.t. $q_1(t)$. Since only equation 7.30 (on prefeq:tower_pot_energy2) depends on $q_1(t)$, it is only necessary to derive w.r.t. this energy contribution, which yields

$$\frac{\partial V(t, q)}{\partial q_1} = \left(\int_0^H EI_{\text{tfa}}(z) \left[\frac{\partial^2 \mu_{\text{tfa}}(z)}{\partial z^2} \right]^2 dz \right) q_1(t) \quad [\text{N}] \quad (7.74)$$

from which the structural stiffness is found to be

$$k_{11s} = \int_0^H EI_{\text{tfa}}(z) \left[\frac{\partial^2 \mu_{\text{tfa}}(z)}{\partial z^2} \right]^2 dz \quad [\text{N/m}] \quad (7.75)$$

The only kinetic energy that depends on $q_1(t)$ is the kinetic energy of the blade 7.54 (on page 49). Hence the derivative w.r.t. q_1 is

$$\frac{\partial T(t, q, \dot{q})}{\partial q_1} = -\Omega^2 \delta_{\text{tfa}}^2 \sum_{k=1}^3 \left(\int_0^R m_b(r) r^2 \sin(\theta_k(t))^2 dr \right) q_1(t) \quad (7.76)$$

$$+ \Omega \delta_{\text{tfa}} \sum_{k=1}^3 \left(\int_0^R m_b(r) [1 + r \cos(\theta_k(t)) \delta_{\text{tfa}}] r \sin(\theta_k(t)) dr \right) \dot{q}_1(t) \quad (7.77)$$

$$+ \Omega \delta_{\text{tfa}} \sum_{k=1}^3 \left(\int_0^R m_b(r) \mu_{\text{bfop}}(r) r \sin(\theta_k(t)) dr \right) \dot{q}_{k+4}(t) \quad (7.78)$$

$$+ \Omega \delta_{\text{tfa}} \sum_{k=1}^3 \left(\int_0^R m_b(r) \mu_{\text{beop}}(r) r \sin(\theta_k(t)) dr \right) \dot{q}_{k+7}(t) \quad [\text{N}] \quad (7.79)$$

All of these terms from the kinetic energy are however cancelled out when considering the first term of eq. 7.72.

7.7.2 Mass and Gyroscopic Damping

The potential energy does not depend on the generalised velocity, so the first term of 7.72 is reduced to

$$\frac{d}{dt} \left(\frac{\partial L(t, q, \dot{q})}{\partial \dot{q}_1} \right) = \frac{d}{dt} \left(\frac{\partial T(t, q, \dot{q})}{\partial \dot{q}_1} \right) \quad [\text{N}] \quad (7.80)$$

In this example, the total kinetic energy has two contributions depending on $\dot{q}_1(t)$. That is the kinetic energy of the tower and the nacelle and the kinetic energy of the blades. These are respectively eq. 7.28 on page 42 and eq. 7.54 on page 49. The term related to $\dot{y}_{bk}(t, r)$, in eq. 7.54, is independent on the fore-aft motion and is therefore left out in this

example. The derivative w.r.t. $\dot{q}_1(t)$ is

$$\frac{d}{dt} \left(\frac{\partial T(t, q, \dot{q})}{\partial \dot{q}_1} \right) = \left(\int_0^H m_t(z) \mu_{\text{tfa}}(z)^2 dz + M_n \right) \ddot{q}_1(t) \quad (7.81)$$

$$+ \sum_{k=1}^3 \left(\int_0^R m_b(r) [1 + r \cos(\theta_k(t)) \delta_{\text{tfa}}]^2 dr \right) \ddot{q}_1(t) \quad (7.82)$$

$$+ \sum_{k=1}^3 \left(\int_0^R m_b(r) [1 + r \cos(\theta_k(t)) \delta_{\text{tfa}}] \mu_{\text{bfop}}(r) dr \right) \ddot{q}_{k+4}(t) \quad (7.83)$$

$$+ \sum_{k=1}^3 \left(\int_0^R m_b(r) [1 + r \cos(\theta_k(t)) \delta_{\text{tfa}}] \mu_{\text{beop}}(r) dr \right) \ddot{q}_{k+7}(t) \quad (7.84)$$

$$- 2\Omega \delta_{\text{tfa}} \sum_{k=1}^3 \left(\int_0^R m_b(r) [1 + r \cos(\theta_k(t)) \delta_{\text{tfa}}] r \sin(\theta_k(t)) dr \right) \dot{q}_1(t) \quad (7.85)$$

$$- \Omega^2 \delta_{\text{tfa}} \sum_{k=1}^3 \left(\int_0^R m_b(r) [1 + r \cos(\theta_k(t)) \delta_{\text{tfa}}] r \cos(\theta_k(t)) dr \right) q_1(t) \quad (7.86)$$

$$+ \Omega^2 \delta_{\text{tfa}}^2 \sum_{k=1}^3 \left(\int_0^R m_b(r) r^2 \sin(\theta_k(t))^2 dr \right) q_1(t) \quad (7.87)$$

$$- \Omega \delta_{\text{tfa}} \sum_{k=1}^3 \left(\int_0^R m_b(r) [1 + r \cos(\theta_k(t)) \delta_{\text{tfa}}] r \sin(\theta_k(t)) dr \right) \dot{q}_1(t) \quad (7.88)$$

$$- \Omega \delta_{\text{tfa}} \sum_{k=1}^3 \left(\int_0^R m_b(r) \mu_{\text{bfop}}(r) r \sin(\theta_k(t)) dr \right) \dot{q}_{k+4}(t) \quad (7.89)$$

$$- \Omega \delta_{\text{tfa}} \sum_{k=1}^3 \left(\int_0^R m_b(r) \mu_{\text{beop}}(r) r \sin(\theta_k(t)) dr \right) \dot{q}_{k+7}(t) \quad (7.90)$$

The first term stems from the kinetic energy of the tower, while the remaining terms are from the kinetic energy of the blades. The last 4 terms, 7.87 to 7.90, cancel out with the 4 terms 7.76 to 7.79 from $\frac{\partial T(t, q, \dot{q})}{\partial q_1}$. The terms 7.81 to 7.84 are entries of the mass matrix and are expressed as

$$m_{11} = \int_0^H m_t(z) \mu_{\text{tfa}}(z)^2 dz + M_n + \sum_{k=1}^3 \int_0^R m_b(r) [1 + r \cos(\theta_k(t)) \delta_{\text{tfa}}]^2 dr. \quad [\text{kg}] \quad (7.91)$$

In the case where $k = 1$, i.e. for the first blade, the term 7.83 yields the mass coefficient

$$m_{15} = \int_0^R m_b(r) [1 + r \cos(\theta_1(t)) \delta_{\text{tfa}}] \mu_{\text{bfop}}(r) dr, \quad [\text{kg}] \quad (7.92)$$

and for $k = 1$ term 7.84 yields the coefficient

$$m_{18} = \int_0^R m_b(r) [1 + r \cos(\theta_1(t)) \delta_{\text{tfa}}] \mu_{\text{beop}}(r) dr. \quad [\text{kg}] \quad (7.93)$$

Term 7.85 depends on the generalised velocity of the tower and is regarded as damping due to gyroscopic loads. This damping is denoted as

$$c_{11g} = -2\Omega \delta_{\text{tfa}} \sum_{k=1}^3 \int_0^R m_b(r) [1 + r \cos(\theta_k(t)) \delta_{\text{tfa}}] r \sin(\theta_k(t)) dr. \quad [\text{Ns/m}] \quad (7.94)$$

The damping of the wind turbine therefore consists of structural-, aerodynamic- and gyroscopic damping, i.e.

$$c_{ij} = c_{ijs} + c_{ija} + c_{ijg}. \quad [\text{Ns/m}] \quad (7.95)$$

Term 7.86 depends on the generalised coordinate of the tower and is regarded as additional stiffness due to centrifugal loading on the blades. This stiffness is denoted as

$$k_{11c} = -\Omega^2 \delta_{\text{tfa}} \sum_{k=1}^3 \int_0^R m_b(r) [1 + r \cos(\theta_k(t)) \delta_{\text{tfa}}] r \cos(\theta_k(t)) dr. \quad [\text{N/m}] \quad (7.96)$$

The total stiffness of the wind turbine therefore consists of structural-, gravity induced- and centrifugal stiffness, i.e.

$$k_{ij} = k_{ijs} + k_{ijg} + c_{ijc}. \quad [\text{N/m}] \quad (7.97)$$

7.7.3 Aerodynamic Damping

As shown in the introduction of this chapter, the ij th entry of the aerodynamic damping is given as

$$c_{ija} = \sum_{k=1}^3 \int_0^R \frac{\partial x_{bk}}{\partial q_i} \left[\frac{\partial F_{Nk}}{\partial v_{xk}} \frac{\partial v_{xk}}{\partial \dot{q}_j} + \frac{\partial F_{Nk}}{\partial v_{yk}} \frac{\partial v_{yk}}{\partial \dot{q}_j} \right] + \frac{\partial y_{bk}}{\partial q_i} \left[\frac{\partial F_{Tk}}{\partial v_{xk}} \frac{\partial v_{xk}}{\partial \dot{q}_j} + \frac{\partial F_{Tk}}{\partial v_{yk}} \frac{\partial v_{yk}}{\partial \dot{q}_j} \right] dr \quad [-] \quad (7.98)$$

Remembering that the equations for the k th blade's motion are

$$x_{bk}(t, r) = (1 + r \cos(\theta_k(t)) \delta_{\text{tfa}}) q_1(t) + \mu_{\text{bfop}}(r) q_{k+4}(t) + \mu_{\text{beop}}(r) q_{k+7}(t), \quad [\text{m}] \quad (7.99)$$

$$\begin{aligned} \dot{x}_{bk}(t, r) &= (1 + r \cos(\theta_k(t)) \delta_{\text{tfa}}) \dot{q}_1(t) + \mu_{\text{bfop}}(r) \dot{q}_{k+4}(t) + \mu_{\text{beop}}(r) \dot{q}_{k+7}(t) & (7.100) \\ &- \Omega \delta_{\text{tfa}} r \sin(\theta_k(t)) q_1(t), & [\text{m/s}] \\ & & (7.101) \end{aligned}$$

and

$$y_{bk}(t, r) = (1 + r \cos(\theta_k) \delta_{\text{tss}}) q_2(t) + r \sin(\theta_k) + \mu_{\text{bfip}}(r) q_{k+4}(t) + \mu_{\text{beip}}(r) q_{k+7}(t), \quad [\text{m}] \quad (7.102)$$

$$\begin{aligned} \dot{y}_{bk}(t, r) &= (1 + r \cos(\theta_k) \delta_{\text{tss}}) \dot{q}_2(t) + \mu_{\text{bfip}}(r) \dot{q}_{k+4}(t) + \mu_{\text{beip}}(r) \dot{q}_{k+7}(t) & (7.103) \\ &- \Omega \delta_{\text{tss}} r \sin(\theta_k(t)) q_2(t) + r \Omega \cos(\theta_k), & [\text{m/s}] \\ & & (7.104) \end{aligned}$$

The wind normal to the plane of rotation is given as

$$v_{xk} = v_k - \dot{x}_{bk}(t, r), \quad [\text{m/s}] \quad (7.105)$$

and the wind parallel to plane of rotation is

$$v_{yk} = r\Omega - \dot{y}_{bk}(t, r), \quad [\text{m/s}] \quad (7.106)$$

The aerodynamic damping is now computed using the former 6 equations. The derivations for the first 2 aerodynamic damping coefficients are now presented.

$$\begin{aligned} \frac{\partial x_{bk}}{\partial q_1} &= 1 + r \cos(\theta_k) \delta_{\text{tfa}} & \frac{\partial y_{bk}}{\partial q_1} &= 0 \\ \frac{\partial F_{Nk}}{\partial v_{xk}} &= f_{Nvxk}(r) & \frac{\partial F_{Nk}}{\partial v_{yk}} &= f_{Nvyk}(r) \\ \frac{\partial v_{xk}}{\partial \dot{q}_1} &= -(1 + r \cos(\theta_k) \delta_{\text{tfa}}) & \frac{\partial v_{yk}}{\partial \dot{q}_1} &= 0 \end{aligned}$$

Combining the derivatives yields

$$c_{11a} = - \sum_{k=1}^3 \int_0^R (1 + r \cos(\theta_k) \delta_{\text{tfa}})^2 f_{Nvxk}(r) dr \quad [\text{Ns/m}]$$

The derivatives for the next coefficient are

$$\begin{aligned} \frac{\partial x_{bk}}{\partial q_1} &= 1 + r \cos(\theta_k) \delta_{\text{tfa}} & \frac{\partial y_{bk}}{\partial q_1} &= 0 \\ \frac{\partial F_{Nk}}{\partial v_{xk}} &= f_{Nvxk}(r) & \frac{\partial F_{Nk}}{\partial v_{yk}} &= f_{Nvyk}(r) \\ \frac{\partial v_{xk}}{\partial \dot{q}_2} &= 0 & \frac{\partial v_{yk}}{\partial \dot{q}_2} &= -\delta_{\text{tss}} r \end{aligned}$$

which yields

$$c_{12a} = - \sum_{k=1}^3 \int_0^R (1 + r \cos(\theta_k) \delta_{\text{tfa}}) f_{Nvyk}(r) \delta_{\text{tss}} r dr \quad [\text{Ns/m}]$$

This is an example of how to derive 2 of the entries of the aerodynamic damping matrix. This matrix is not symmetric and therefore consists of almost 100 equations to define all the entries. The negative sign on the entries are cancelled by the negative sign on the aerodynamic damping matrix, so this phenomenon adds more damping to the system.

Remark 1 *The formula used is the same as in the used source[20]. However the results obtained here are not the same as in the used literature. Therefore all the 100 entries for the aerodynamic damping matrix C has been derived in appendix B.3*

7.7.4 Structural Damping

The derivative of the dissipation function is considered to derive the structural damping.

$$\frac{\partial \mathcal{F}(t, \dot{q})}{\partial \dot{q}_1} = c_{11s} \dot{q}_1(t) = 2\zeta_1 \sqrt{k_{11} m_{11}} \dot{q}_1(t) \quad [\text{N}] \quad (7.107)$$

and the structural damping is therefore

$$c_{11s} = 2\zeta_1 \sqrt{k_{11}m_{11}}, \quad [\text{Ns/m}] \quad (7.108)$$

The mass and stiffness coefficient are compute and the damping factor $\zeta_1 = 0.01$ are from the FAST input file `/FAST_data/NRELOffshrBsline5MW_Tower_Onshore.dat`.

The derivation of the total model is quite big. The presented example represents approximately 1/10th of the total number of equations, which forms the final model of the wind turbine. However, since the approach now should be more obvious, then the remaining equations are placed in an appendix. They are found in Appendix B.1 on page 111.

7.8 Parameter Distributions

The parameters for usage in the developed model are for the tower and blades given in terms of distributed parameters.

For computation of the model, it is convenient to have a function describing the behaviour of these parameters as a function of height and radius for respectively the tower and the blades. Therefore the parameters are interpolated in MATLAB, using 1st order splines between each point from the input file to obtain a first order linear function.

An example is the mass distribution for the tower. In the Figure 7.19 the data from the FAST input file is plotted as the black dots, and the interpolated function is plotted alongside being the blue curve.

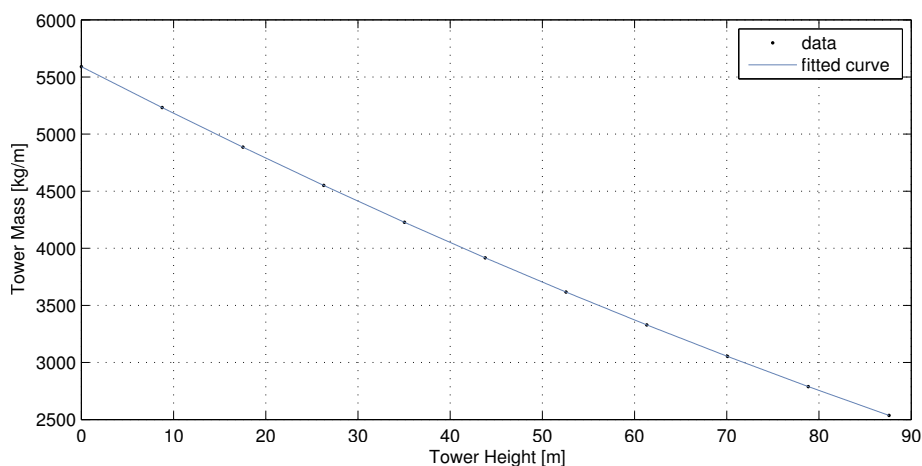


Figure 7.19. Mass distribution of the tower.

In 7.109 the mass distribution is listed as a function of the height z .

$$m_t(z) = \begin{cases} 5590.870000 - 40.91780822 z & z < 8.76 \\ 5579.100000 - 39.57420091 z & z < 17.52 \\ 5555.540000 - 38.22945205 z & z < 26.28 \\ 5520.230000 - 36.88584475 z & z < 35.04 \\ 5473.110000 - 35.54109589 z & z < 43.80 \\ 5414.310000 - 34.19863014 z & z < 52.56 \\ 5343.630000 - 32.85388128 z & z < 61.32 \\ 5261.170000 - 31.50913242 z & z < 70.08 \\ 5167.090000 - 30.16666667 z & z < 78.84 \\ 5061.070000 - 28.82191781 z & \text{otherwise} \end{cases} \quad [\text{kg/m}] \quad (7.109)$$

The used input data file is found on the enclosed CD [/FAST_data/](#). The distributed parameters describing mass and stiffness of the tower are obtained from [/FAST_data/NRELOffshrBslne5MW_Tower_Onshore.dat](#). The distributed parameters describing mass, flexural rigidity, structural twist of the blades are obtained from [/FAST_data/NRELOffshrBslne5MW_Blade.dat](#). All the used distributed structural parameters are treated likewise, and the results are found in appendix A

Aerodynamic data in terms of the Lift and Drag coefficients alongside with inflow angle are obtained from [/FAST_data/NRELOffshrBslne5MW_AeroDyn.ipt](#). The inflow angle, Lift and drag coefficients alongside with derivatives w.r.t. angle of attack are described in appendix A.3, where a calculation example is given.

7.9 State Space Formulation

The equations, which describes the dynamics of the wind turbine as an LPV system are given in matrix form as

$$M(\theta)\ddot{q}(t) + C(\theta)\dot{q}(t) + K(\theta)q(t) = Q_\beta\beta(t) + Q_\tau\tau(t) + Q_vv(t), \quad (7.110)$$

which leads to

$$\ddot{q}(t) = M(\theta)^{-1} (-C(\theta)\dot{q}(t) - K(\theta)q(t) + Q_\beta(\theta)\beta(t) + Q_\tau\tau(t) + Q_v(\theta)v(t)) \quad (7.111)$$

The matrix equation, 7.111, for the generalised accelerations is used to formulate the system in state space form, which is

$$\begin{bmatrix} \dot{q}(t) \\ \ddot{q}(t) \end{bmatrix} = \begin{bmatrix} 0 & I \\ -M(\theta)^{-1}K(\theta) & -M(\theta)^{-1}C(\theta) \end{bmatrix} \begin{bmatrix} q(t) \\ \dot{q}(t) \end{bmatrix} + \begin{bmatrix} 0 & 0 \\ M(\theta)^{-1}Q_\beta(\theta) & M(\theta)^{-1}Q_\tau \end{bmatrix} \begin{bmatrix} \beta(t) \\ \tau(t) \end{bmatrix} + \begin{bmatrix} 0 \\ M(\theta)^{-1}Q_v(\theta) \end{bmatrix} v(t). \quad (7.112)$$

In a shorter notation the state space system is

$$\dot{x}(t) = A(\theta)x(t) + B(\theta)u(t) + E(\theta)d(t) \quad (7.113)$$

where

$A \in \mathbb{R}^{20 \times 20}$	is the state transition matrix	[-]
$B \in \mathbb{R}^{20 \times 4}$	is the gain of the control inputs	[-]
$E \in \mathbb{R}^{20 \times 3}$	is the gain of the wind disturbance	[-]

The state vector $x(t)$ is

$$x(t) = \begin{bmatrix} q(t) \\ \dot{q}(t) \end{bmatrix}, \quad \dot{x}(t) = \begin{bmatrix} \dot{q}(t) \\ \ddot{q}(t) \end{bmatrix}$$

The input vector $u(t)$ contains the blade pitch on each blade, $\beta_i(t)$, for $i = 1, 2, 3$, and the applied generator torque, $\tau(t)$

$$u(t) = \begin{bmatrix} \beta_1(t) & \beta_2(t) & \beta_3(t) & \tau(t) \end{bmatrix}^T, \quad (7.114)$$

The disturbance $d(t)$ is the wind speed on each blade

$$d(t) = \begin{bmatrix} v_1(t) & v_2(t) & v_3(t) \end{bmatrix}^T. \quad (7.115)$$

For simulation purpose, the continuous-time system eq. 7.113 is discretised using a zero-order-hold transformation. The discrete-time system is denoted as

$$x_s(k+1) = \Phi_s(\theta)x_s(k) + \Gamma_s(\theta)u(k) + \Gamma_d(\theta)d(k) \quad (7.116)$$

This discrete model is used when simulating the model and for implementing in the estimator. However a modification to the model is carried out in order to avoid computational problems. The state describing the angular displacement of the generator, $q_3(t)$, is excluded, since it is constantly increasing i.e. an unstable mode.

8 Estimating Wind

This chapter is meant to give an overview of the various considerations made, when designing the estimation scheme for wind speed and wind shear. First a brief outline of the different sensor types and their pros and cons in the specific setup alongside with a justification, why these sensors specifically have been chosen to consider. Finally, the estimation strategy is presented and the implementation of this on the model derived in the previous chapter is undergone.

8.1 Sensor Types

There are different types of sensors considerable for measurements that can be used for estimating the wind fields. The sensors considered in this project are briefly described below. It should be noted that this project does not focus on the full derivation from measurements to deflection data used in the estimation scheme, hence only the idea of which sensors could be used for the purpose with no further development, is presented

8.1.1 Strain Gauges

A strain gauge is a stretchable sensor which, dependent on the strain it is subject to, gives a corresponding output. The sensor often consist of a very thin metal wire, which due to its thickness is stretchable within a certain range. As the length of the wire is increased, the resistance in the wire increases as well, and vice versa for a decrease in length. In the matter of this project, this means that one or several sensors would be attached on each blade and on the tower. In this way, it is possible to measure the bending of the blades and the tower, and thereby determine the wind force on each of these elements. Using strain gauges on blades and tower is already a configuration in some wind turbines [12].

One of the advantages of using strain gauges is that they are easily implementable on the wind turbine.

Another advantage of using strain gauges is that the output is fairly easy to convert to force applied from the wind if the mode shapes of the blade is known. However, as the practical implementation of this conversion is not part of this master project, this is not furtherer considered.

A disadvantage of the strain gauge is that the voltage output is very low (measures in mV). In combination with high amplitude vibrations, which are known to occur on the wind turbine, especially on the wings, the reliability and accuracy of the sensor output

decreases.

Another disadvantage of the strain gauge is that due to its thickness, it is very sensitive to temperature changes. On modern multi megawatt wind turbines, the temperature is not the same in top position as it is in bottom position. The temperature experienced varies as well as a function of rotation speeds, why this makes this sensor type unsuitable for the purpose.

The strain gauge comes in a great span of variants though, and some of these can withstand the before mentioned disadvantages. However, as the performance goes up, so does the price[22].

8.1.2 Accelerometers

Accelerometers could be placed along the tower and the blades in cooperation with the strain gauges. From the accelerations measured and the assumed mode shapes for the wind turbine's tower and blades respectively, alongside with a start position measured from the strain gauge, the deflection of the tower can be determined from integrating over the accelerometer data. From this, the wind force on the different parts can be determined, and thereby wind speed and -direction.

One of the advantages of using the accelerometers, is that many wind turbines already contains at least one accelerometer in the tower and one in each blade as well[12], why the implementation would be simple in comparison to installing new sensors on each wind turbine.

A disadvantage of using accelerometers is that if it is not sufficient with only one accelerometer on the tower and one on each blade, the implementation of more is not as simple a task as for the strain gauges, since accelerometers most often must be calibrated for the specific setup. These calibrations includes biasing, drifting etc.

8.2 Sensor Setup

More sensors, such as flowmeters have been considered, however as the disadvantages of using such are so dominant in comparison to the two above described it is chosen to only consider these sensors for usage in the estimation scheme for this project. The is assumed to be the usage of the already implemented accelerometers. This is chosen primarily because the practical implementation of these is already done, meaning that the approach made throughout this project can be implemented with close to no further hardware changes on the wind turbine. It is chosen to assume that measurements are obtained from only one accelerometer on each blade and one on the tower, as this is the configuration known to already exist on modern wind turbines[12]. The strain gauges however need to be implemented. An idea for this implementation, would be to install

them on the inside of the blades and tower, as this will expose them for the least fatigue from surroundings and the weather.

8.3 Kalman Estimator

Chapter 7 on page 33 proposed a model for the wind turbine as well as a model for the wind, and how it interacts with the wind turbine. This section describes an approach to estimate the wind speed and the parameters related to the wind shear. Consider the discrete version of the non-linear dynamics of the wind turbine system formulated in a short notation as:

$$x_s(k) = f_1(x_s(k-1), u(k-1)). \quad (8.1)$$

The model for the wind speed, which includes shear and tower shadow as described in chapter 7.6.3 on page 52, is denoted in short as

$$v(k) = f_2(v_{zH}(k-1), \sigma(k-1)). \quad (8.2)$$

The two parameters describing the wind shear, which are the hub height wind speed and the power coefficient, are modelled as constants

$$v_{zH}(k) = v_{zH}(k-1) \quad (8.3)$$

$$\sigma(k) = \sigma(k-1). \quad (8.4)$$

The system equations are augmented with the model for the wind speed and the shear parameter, such that the augmented state vector becomes

$$x(k) = \begin{bmatrix} x_s(k)^T & v(k)^T & v_{zH}(k) & \sigma(k) \end{bmatrix}^T \quad (8.5)$$

where

$x_s \in \mathbb{R}^{20}$	is the state vector,
$v \in \mathbb{R}^3$	is wind speed on the blades,
$v_{zH} \in \mathbb{R}$	is the wind speed at hub height,
$\sigma \in \mathbb{R}$	is the wind shear coefficient,
$x \in \mathbb{R}^{25}$	is the augmented state vector.

From this point on the notation of time is denoted as a subscript. This is done to have a more convenient way of formulating the filter equations. By this, the current state is denoted x_k and the previous state x_{k-1} . The set of non-linear equations, which describe the dynamics of the augmented system are

$$x_k = f(x_{k-1}, u_{k-1}) + w_{k-1}, \quad w_k \sim \mathcal{N}(0, Q_k) \quad (8.6)$$

and with the sensor dynamics

$$z_k = h(x_k) + v_k, \quad v_k \sim \mathcal{N}(0, R_k). \quad (8.7)$$

The model is assumed to be subject to the additive, zero-mean, white noise, being the process noise w and the sensor noise v . Also the process and sensor noise are assumed to be uncorrelated, so the covariance is

$$\mathbb{E}\left\{ \begin{bmatrix} w_k \\ v_k \end{bmatrix} \begin{bmatrix} w_k^T & v_k^T \end{bmatrix} \right\} = \begin{bmatrix} Q_k & 0 \\ 0 & R_k \end{bmatrix} \quad (8.8)$$

The estimation error is defined as the difference between the states and the state estimates.

$$e_k = x_k - \hat{x}_{k|k}, \quad (8.9)$$

with the covariance of the error denoted as

$$P_k = \mathbb{E}\{e_k e_k^T\} \quad (8.10)$$

Several estimation methods exist for non-linear systems, e.g. linearised Kalman filter, Extended Kalman Filter (EKF), Unscented Kalman Filter (UKF)[23]. The latter two are more suitable for this estimation problem due to the non-linearities in the aerodynamics (7.63 and 7.64 on page 52). In these equations, it is seen, that the input of β occur in sine- and cosine functions. Also, the relative winds are squared, resulting in non-linearity in the incident wind and generalised velocities. The linearised Kalman filter will deviate, if states and inputs change too much w.r.t. the operating points. The algorithm for the Extended Kalman Filter (EKF)[23, p. 310] is written below. The notation $\hat{x}_{k|k-1}$ is used to denote the k th predicted state given the previous estimate, while $\hat{x}_{k|k}$ denotes the state estimate found by correcting the predicted state with the measurement.

Prediction Step:

Predict the current state by using previous state estimates and previous inputs in the non-linear system equations.

$$\hat{x}_{k|k-1} = f(\hat{x}_{k-1|k-1}, u_{k-1}) \quad (8.11)$$

Linearise the system, in the current state prediction, with the Jacobians

$$\Phi_k = \left. \frac{\partial f(x_k, u_k)}{\partial x_k} \right|_{\hat{x}_{k|k-1}, u_k} \quad (8.12)$$

$$H_k = \left. \frac{\partial h(x_k)}{\partial x_k} \right|_{\hat{x}_{k|k-1}} \quad (8.13)$$

Predict the error covariance by propagating a previous estimate through the linearised system and also using statistics of process noise, i.e. the covariance.

$$P_{k|k-1} = \Phi_k P_{k-1|k-1} \Phi_k^T + Q_{k-1} \quad (8.14)$$

Update Step:

Compute the current Kalman gain

$$K_k = P_{k|k-1} H_k^T (H_k P_{k|k-1} H_k^T + R_{k-1})^{-1} \quad (8.15)$$

Estimate states by correcting the prediction with measurements

$$\hat{x}_{k|k} = \hat{x}_{k|k-1} + K_k (z_k - h(\hat{x}_{k|k-1})) \quad (8.16)$$

Estimate the error covariance

$$P_{k|k} = (I - K_k H_k) P_{k|k-1} \quad (8.17)$$

The EKF has the advantage, compared to the linearised Kalman filter, that it handles changes in e.g. azimuth angle ($\theta(t) = q_3(t) + q_4(t)$), which varies from 0 to 2π . A disadvantage of EKF is the linearisation procedure. For the proposed wind turbine model, the expressions for the Jacobians become very large. Especially the linearisation of the aerodynamics gives rise to some problems, i.e. it requires some partial derivatives w.r.t. angle of attack and the pitch angle, which are not known. Some assumptions like those in [7] (see section 7.6.1 on page 49) are made to reduce the expressions e.g. $W \approx \Omega r$ etc. Likewise, some approximations, need to be calculated e.g. the derivatives of the lift and drag coefficients with respect to the angle of attack. The approximations made on these in this project are found in A.3. This occurs even for a uniform wind and by extending with the effects of wind shear, tower shadow etc., the derivations get even more complicated. These problems could be avoided by using a UKF instead, where stochastic linearisation is used instead of Jacobians. The disadvantage of the UKF is that it requires more computation than EKF.

It is assumed, that the UKF is the better filter of the 3 for the estimation purpose of this project, since the approximations required for calculating the Jacobians are avoided. However in this work, it would be preferable to try out both UKF and EKF in order to compare the performance of those. If the UKF is not significantly better than the EKF, it would be preferable to use EKF to keep computation complexity low.

9 Implementation Overview

This chapter covers the implementation of the developed wind turbine model and the designed linearised Kalman filter. Due to time limitations, the model was not fully derived and validated, why it was not suitable for usage in the wind estimator. However the model developed is, as mentioned in the previously, tested with the linearised azimuth dependent LPV system matrices from FAST, to determine whether or not the model derived acts correspondingly to the FAST model. Afterwards, the linearised Kalman filter is implemented on this model and tested to determine if it is capable of estimating the wind field parameters, hub height speed and wind shear coefficient

9.1 Implmentation of the Model

The developed model, described in chapter 7, was intended to be validated by simulation against the National Renewable Energy Laboratory (NREL) 5 MW non-linear wind turbine simulator used as benchmark. Afterwards, the output of the turbine simulator, given a set of inputs, would have been compared to the output from the developed model, utilised by simulation of the derived non-linear equitations. However such a model is not derived and it is therefore chosen to test the model with the matrices from the FAST linearisation around operating points for rotor speed, hub height wind speed and wind shear. The matrices are obtained in accordance to the description in appendix D.

The parameters described in chapter 7.8 are used to compute the linearised mass, stiffness, damping and forcing matrices described in chapter 7, where the following operating points are used for linearisation. Rotor speed of 12.1 rpm, collective blade pitch angle of 0 rad and a uniform wind field with a wind speed of 10 m/s. Wind shear and pitch angle are neglected to keep the computation complexity low. The computations of the matrices are done by usage of **Maple** in which the equations described in appendix B are computed. The **Maple** worksheet used for calculating the matrices is found on the CD [/model_matrices/model.mw](#). Note that since the model was not fully developed the parts which was not developed is taken from [20].

In order to obtain a set of linearised matrices from FAST a linearisation is performed based on the same parameters and operating points used when calculating the developed model[15]. An example of the FAST matrices is given in appendix C alongside with the corresponding matrices obtained by evaluating the developed model. They are all evaluated at a rotor angle position of 0 rad.

In order to compare the matrices from FAST against the ones from the model, the Euclidean norm is used since it calculates the most dominant singular value in a matrix. The Euclidean norm is described by equation 9.1[24].

The Euclidean norm is calculated for matrices evaluated at 0 rad and compared in percentage deviation from the fast model. The percentage comparison is done by usage of equation 9.2.

$$\|A\|_2 = \sqrt{\lambda_{\max}(A^*A)} = \sigma_{\max}(A) \quad (9.1)$$

$$P_A = \frac{\|A_{\text{model}} - A_{\text{fast}}\|_2}{\|A_{\text{fast}}\|_2} \quad (9.2)$$

Where:

A	is a given square Matrix
A_{model}	is a matrix calculated from the derived model
A_{fast}	is a matrix obtained by linearisation in FAST
λ_{\max}	is the largest eigenvalue
σ_{\max}	is the largest singular value
P_A	is the percentage that A_{model} deviates from A_{fast}

The percentage deviation for the calculated matrices are the following:

- Mass Matrix at 0 degree: $P_M = 0.18\%$
- Stiffness Matrix at 0 degree: $P_K = 0.019\%$
- Damping Matrix at 0 degree $P_C = 151\%$

The Mass and Stiffness matrices seem to match the corresponding matrices from FAST, while the damping matrix shows large deviations. In order to have a model for usage in the estimator it is therefore chosen to use the linearised matrices from FAST onwards in the project. The way in which the linearised matrices are obtained and used for simulation and comparison with the benchmark NREL 5 MW turbine, is described in appendix D. As is the structure of the linearised model.

9.2 Implementation of the Estimator

In order to implement a UKF and EKF as described in section 8.3 a non-linear model would be needed, however due to time limits a linear model was developed. The usage of a Kalman filter for estimation of the wind speed and vertical wind shear power exponent is approached by a linear Kalman filter. The equations for this filter are presented in the following. The linearised state space system used is described in appendix D.

The system and disturbance dynamics are described by equation 9.3 and 9.4.

$$x_s(k+1) = \Phi_s(\theta)x_s(k) + \Gamma_s(\theta)u(k) + \Gamma_d(\theta)d(k) \quad (9.3)$$

$$x_d(k+1) = \Phi_d x_d(k) \quad (9.4)$$

$$d(k) = H_d x_d(k) \quad (9.5)$$

where

$x_s(k) \in \mathbb{R}^{19}$	is the system state vector
$x_d(k) \in \mathbb{R}^2$	is the disturbance state vector
$u(k) \in \mathbb{R}^4$	is the control input vector
$d(k) \in \mathbb{R}^2$	is the disturbance vector
$\Phi_s(\theta) \in \mathbb{R}^{19 \times 19}$	is the system state transition matrix
$\Phi_d(\theta) \in \mathbb{R}^{2 \times 2}$	is the disturbance state transition matrix
$\Gamma_s(\theta) \in \mathbb{R}^{19 \times 4}$	is gain of the control inputs
$\Gamma_d(\theta) \in \mathbb{R}^{2 \times 2}$	is gain of the disturbances
$H_d \in \mathbb{R}^{2 \times 2}$	is the output disturbance matrix

The discretised system can now be augmented as follows:

$$\begin{bmatrix} x_s(k+1) \\ x_d(k+1) \end{bmatrix} = \begin{bmatrix} \Phi_s(\theta) & \Gamma_d(\theta)H_d \\ 0 & \Phi_d \end{bmatrix} \begin{bmatrix} x_s(k) \\ x_d(k) \end{bmatrix} + \begin{bmatrix} \Gamma_s(\theta) \\ 0 \end{bmatrix} u(k),$$


$$x(k+1) = \Phi(\theta)x(k) + \Gamma(\theta)u(k)$$

$$y(k) = Hx(k)$$

$$y(k) = \begin{bmatrix} H_s & 0_{19 \times 2} \end{bmatrix} x(k)$$

Where:

$x(k) \in \mathbb{R}^{21}$	is the augmented state vector
$\Phi(\theta) \in \mathbb{R}^{21 \times 21}$	is the augmented system state transition matrix
$\Gamma(\theta) \in \mathbb{R}^{21 \times 4}$	is gain of the control inputs
$H \in \mathbb{R}^{19 \times 21}$	is the augmented output matrix
$H_s \in \mathbb{R}^{19 \times 19}$	is the system output vector

The wind disturbances is chosen to be modelled as a step, hence $\Phi_d(\theta)$ is an identity matrix. The Kalman filter equations in terms of prediction and update step is, in chapter 8.3, described for the Extended Kalman Filter (EKF). These equations also apply to the linear Kalman filter with the modification that the system is not linearised in every iteration. Hence the linearisation carried out in the prediction step of the filter, see equation 8.11, 8.12 and 8.13 on page 68 is not carried out. This means, that in this case, the same **FAST** linearised matrices are used in every prediction step. The **MATLAB** files in which the Kalman filter is implemented is attached on the enclosed cd  [/estimator](#).

10 Acceptance Test

This chapter covers the acceptance test, described on chapter 5, of the requirements specified in chapter 4. Following are the results of the tests, and a discussion on these regarding whether the requirements set in the requirement specification are met. First the model are tested and afterwards the filter is tested.

10.1 Model Validation

The validation of the model is carried out at wind speeds below the rated wind speed for the 5 MW turbine. This is done such that the blade pitch angle is kept at 0° , which is the operating point, that the model matrices are linearised about. For the validation of the used model, 3 differently configured models are tested against each other where model #1 is the FAST non-linear turbine model while model #2 and #3 are two different linearised models obtained from FAST linearisation, as described in appendix D. The properties and inclusions for these 3 different models are listed in table 10.1.

Model	Blade precone	Shaft tilt	Rotor overhang	Non-linear model
#1	✓	✓	✓	✓
#2	÷	÷	÷	÷
#3	✓	✓	✓	÷

Table 10.1. The three models used for validation.

Model #1 is the benchmark model from FAST, being a non-linear model which takes both blade precone, rotor shaft tilting, and rotor overhang into account.

Model #2 is a FAST linearised model comparable to the model attempted derived in this project, which excludes blade precone, rotor shaft tilting, and rotor overhang.

Model #3 is a FAST linearised model that includes blade precone, rotor shaft tilting and rotor overhang. The reason for constructing and examining this model is to investigate the the impact of including or excluding the mentioned parameters.

More models could have been made by the means of including respectively blade preconing, rotor shaft tilting and rotor overhang one at a time, to determine the impact of excluding only some of the dynamics compared to excluding all 3 at the same time. However, it is a time consuming process, why only these 3 models have been made and tested.

The validation is carried out in accordance to the description in appendixD with operation points set for the linearisation in terms of rotor speed, $\bar{\Omega}$, of 1.2671 rad/s, hub height wind speed, \bar{v} , of 10 m/s and a vertical shear with a power exponent of 0.1.

In order to examine the linearised models' response, when deviations from the

operating point is imposed, the wind speed is stepped from 10 m/s to 11 m/s after 60 s. In Figure 10.1(a) the wind speed during the simulation is shown alongside with the vertical shear exponent in Figure 10.1(b). The presence of shear causes the operation point value for the wind speed of 10 m/s being changed to 9.995 m/s. The NREL 5 MW turbine non-linear simulator, represented by model #1, is run for 120 seconds generating a series of input and output data. This input and output data is used for simulating model #2 and #3 and comparing them to model #1.

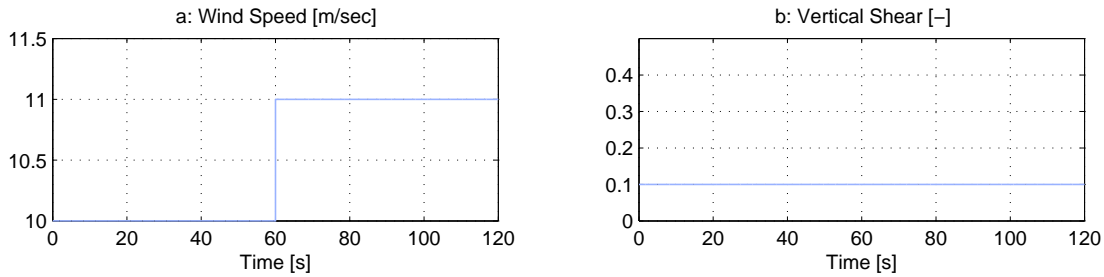


Figure 10.1. Input wind data.

10.1.1 Model #1 vs. Model #2

First Model #2 is validated up against #1. Figure 10.2 shows the tower displacements and the tower displacement velocities for model #1 and model #2. It is seen in the Figure 10.2(a) that the fore-aft displacement has an offset of approximately 0.075 m. It is as well seen in Figure 10.3 which is a close up of the Figure 10.2(b), at around 60 s, where the step on the wind speed from 10 m/s to 11 m/s occur, the model #2 starts deviating more from the benchmark, both in amplitude, and an increase in delay seems to occur as well. The deviation in amplitude is explained from the fact that the system matrices used for model #2 are linearised around operation points, hence the increase in deviation when leaving the operation point. The delay is assumed to be caused by some of the excluded dynamics, in terms of the neglected blade precone, rotor shaft tilting and rotor overhang.

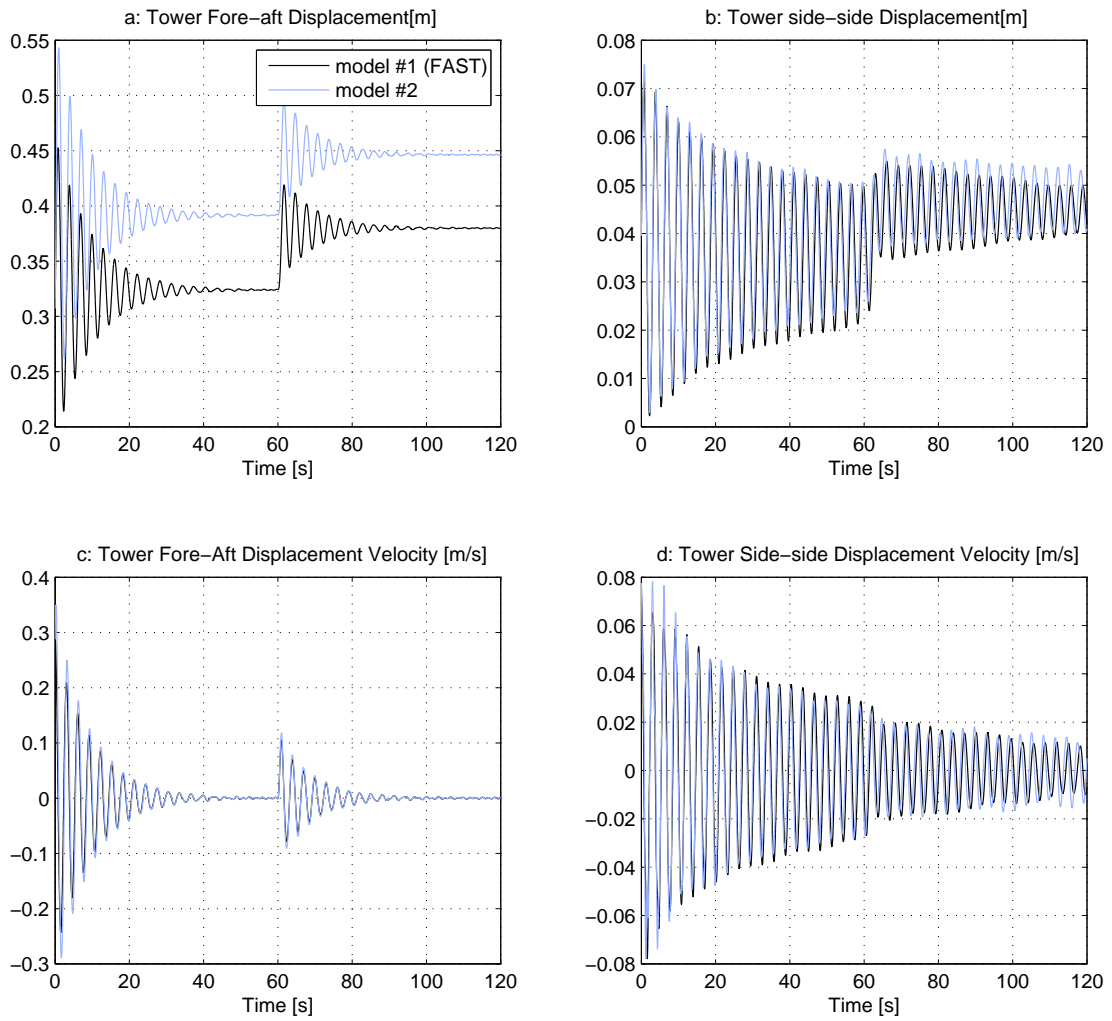


Figure 10.2. Tower displacements (#1 vs. #2).

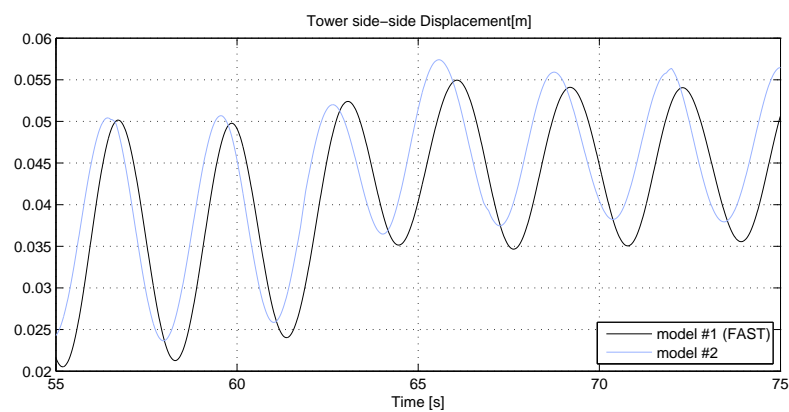


Figure 10.3. Tower displacement side-side (#1 vs. #2) close-up.

Figure 10.4(b) shows that regarding the generator speed, model #2 does not track the benchmark model, neither before nor after the step. The deviation after the step is expected, as the wind deviates from its operating point. However as the model #2 also here deviates from model #1, before the step, the excluded dynamics seem to have an impact here as well.

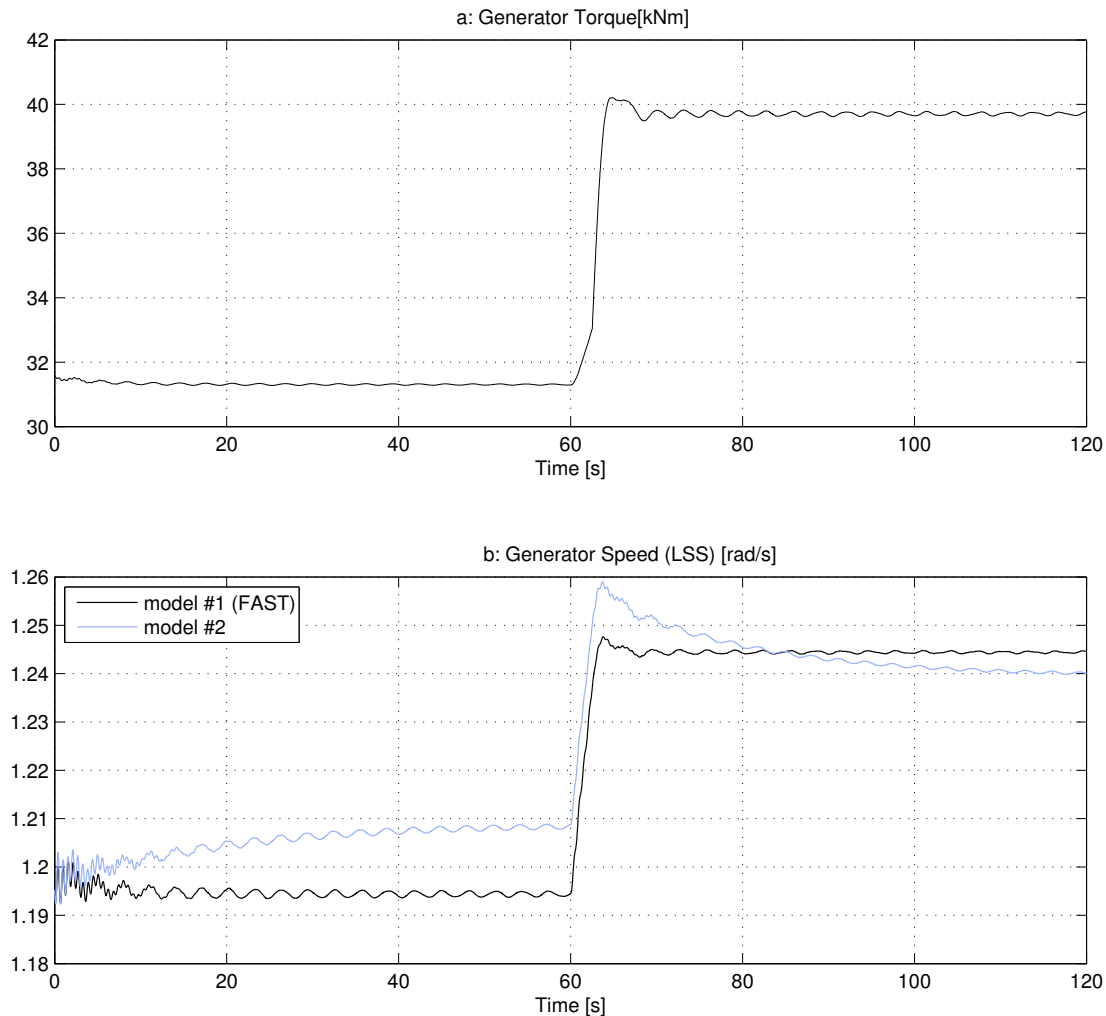


Figure 10.4. Generator torque and generator speed (#1 vs. #2).

In Figure 10.5 the drivetrain displacement and displacement velocity for model #1 and model #2 are seen. Figure 10.6 shows 2 different close-up intervals of the drivetrain displacement, Figure 10.5(a). The first interval Figure 10.6(a) shows the displacement before the step on the wind speed, and Figure 10.6(b) after the step. Both cases seem to have some of the same effects as were noticed for the displacement in side-side displacement of the tower, regarding amplitude deviation and a little delay, which both worsen after the step as expected.

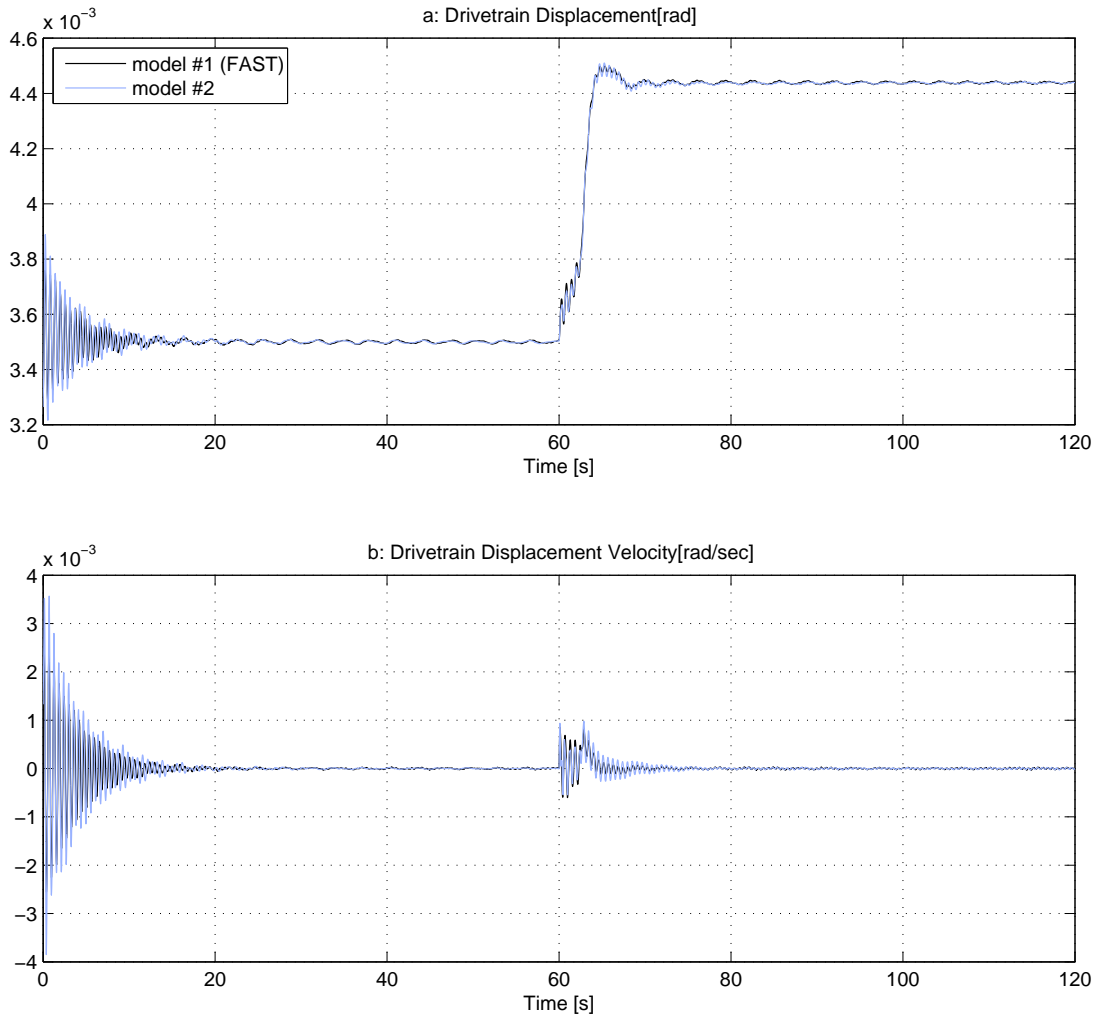


Figure 10.5. Drivetrain displacements (#1 vs. #2).

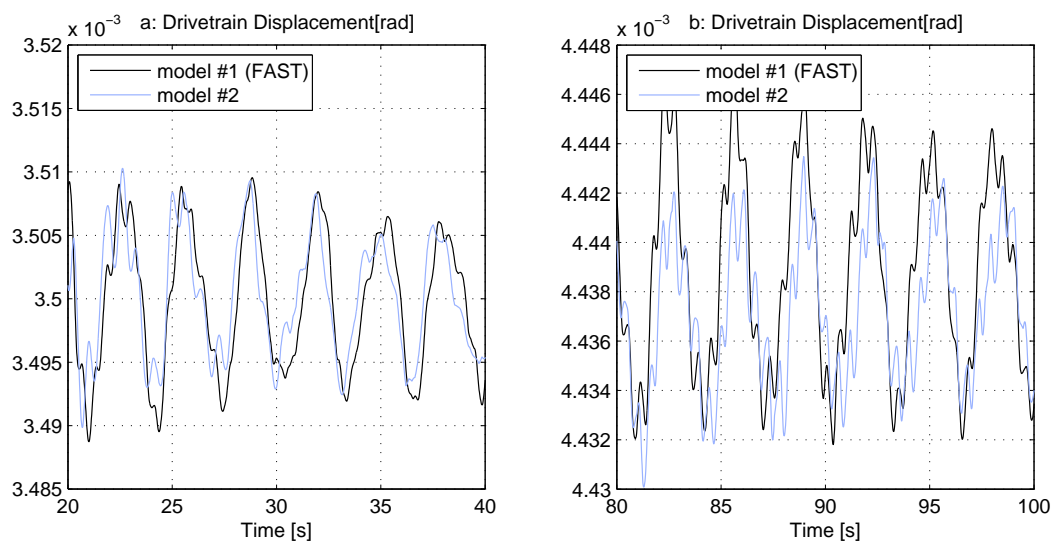


Figure 10.6. Drivetrain displacements (#1 vs. #2).

Figure 10.7(a) and (b) show respectively the flapwise and edgewise displacement of the 3 blades of model #2. It is not possible to conclude anything on this plot alone other than the 3 blades seem to behave as intended compared to each other. Figure 10.8(a) on the other hand shows an offset regarding the flapwise displacement of blade 1 from model #2 compared to model #1 of approximately 0.25 m and an amplitude deviation of approximately 0.25 m as well. The flapwise displacement velocity (see Figure 10.8(c)) deviates as well, as a result of the deviation in the flapwise displacement. It is noticed, that the flapwise displacement and the tower fore-aft displacement both suffer an offset in model #2 compared to model #1, which is assumed to be caused mainly by the exclusion of rotor overhang.

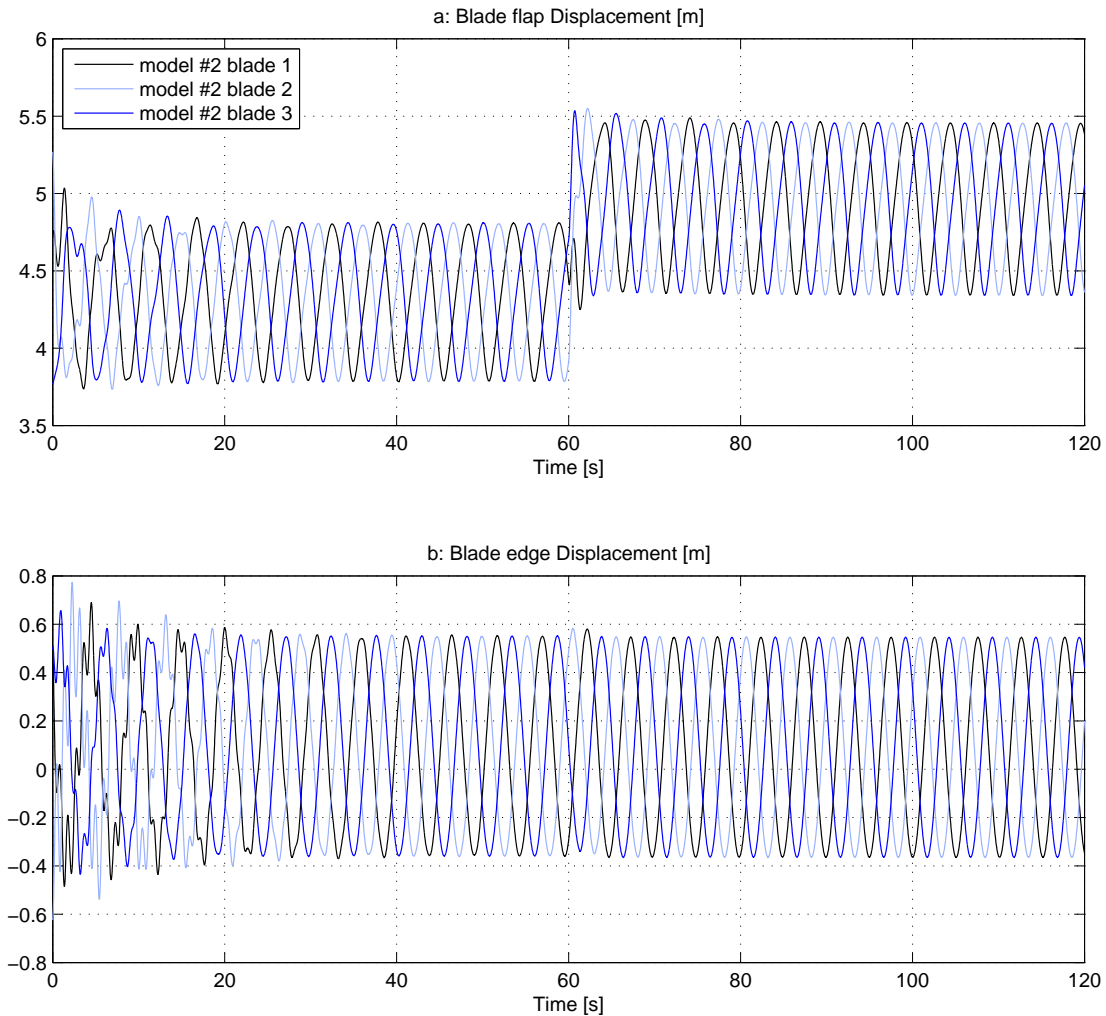


Figure 10.7. Blade displacements (#2).

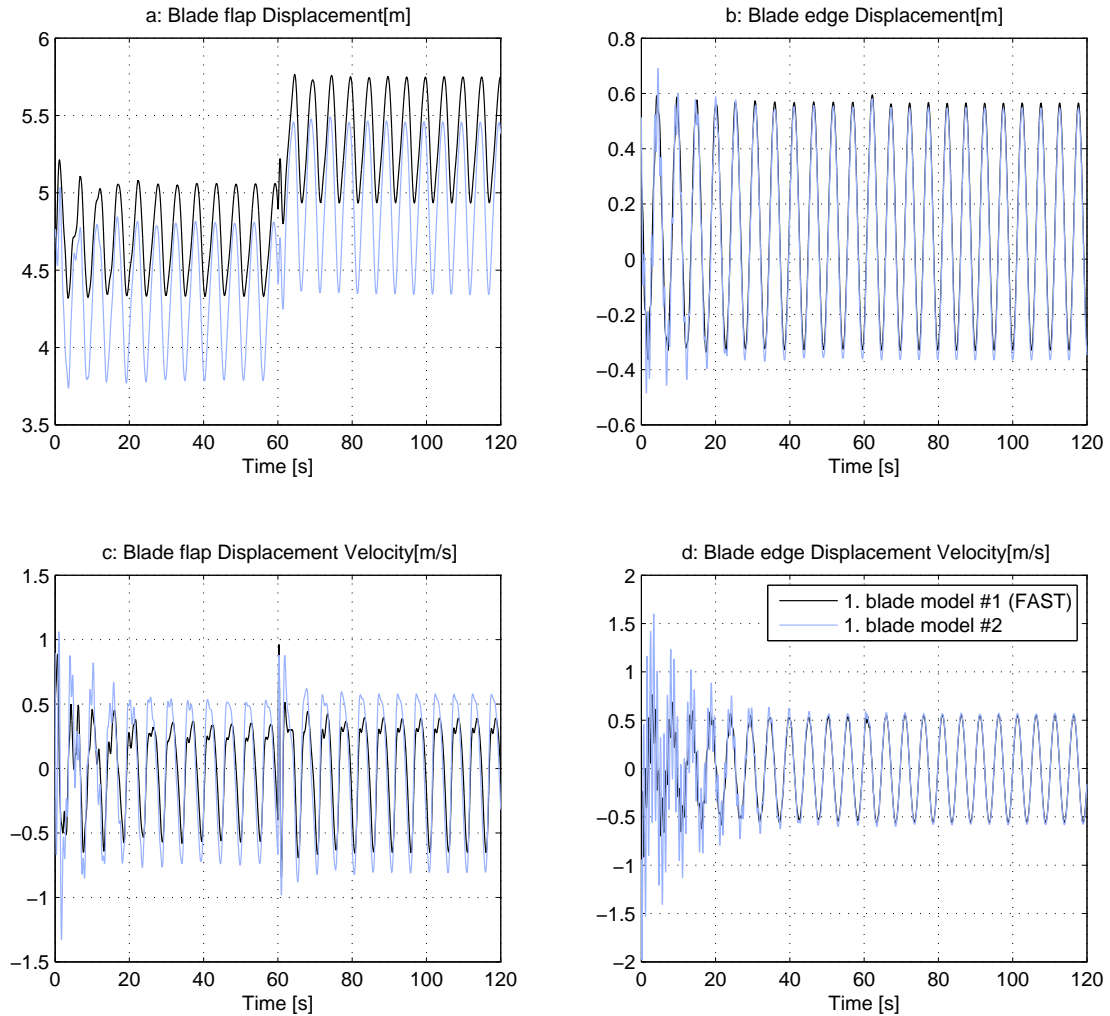


Figure 10.8. Blade displacements (#1 vs. #2).

10.1.2 Model #1 vs. Model #3

Following are the test results from the test of model #3 compared to the benchmark model, i.e. model #1. The idea of this is to determine whether it shows any effect from including the dynamics of; blade pre-coning, rotor shaft tilting, and rotor overhang on the linear model. The plots and close-ups presented are for the same intervals as for the test between model #1 and model #2 such that it is possible to justify the results one model over the other.

Figure 10.9 shows the tower displacement for model #1 and model #3. It is seen in Figure 10.9(a) that the offset of approximately 0.075 m, in the interval before the step, is now gone, and in the close up (Figure 10.10) around and after the step, great improvements are seen as well, both regarding following of amplitude and frequency. It must be concluded that including the dynamics that were excluded in model #2 have a great impact on the behaviour of both the tower fore-aft and side-side displacement.

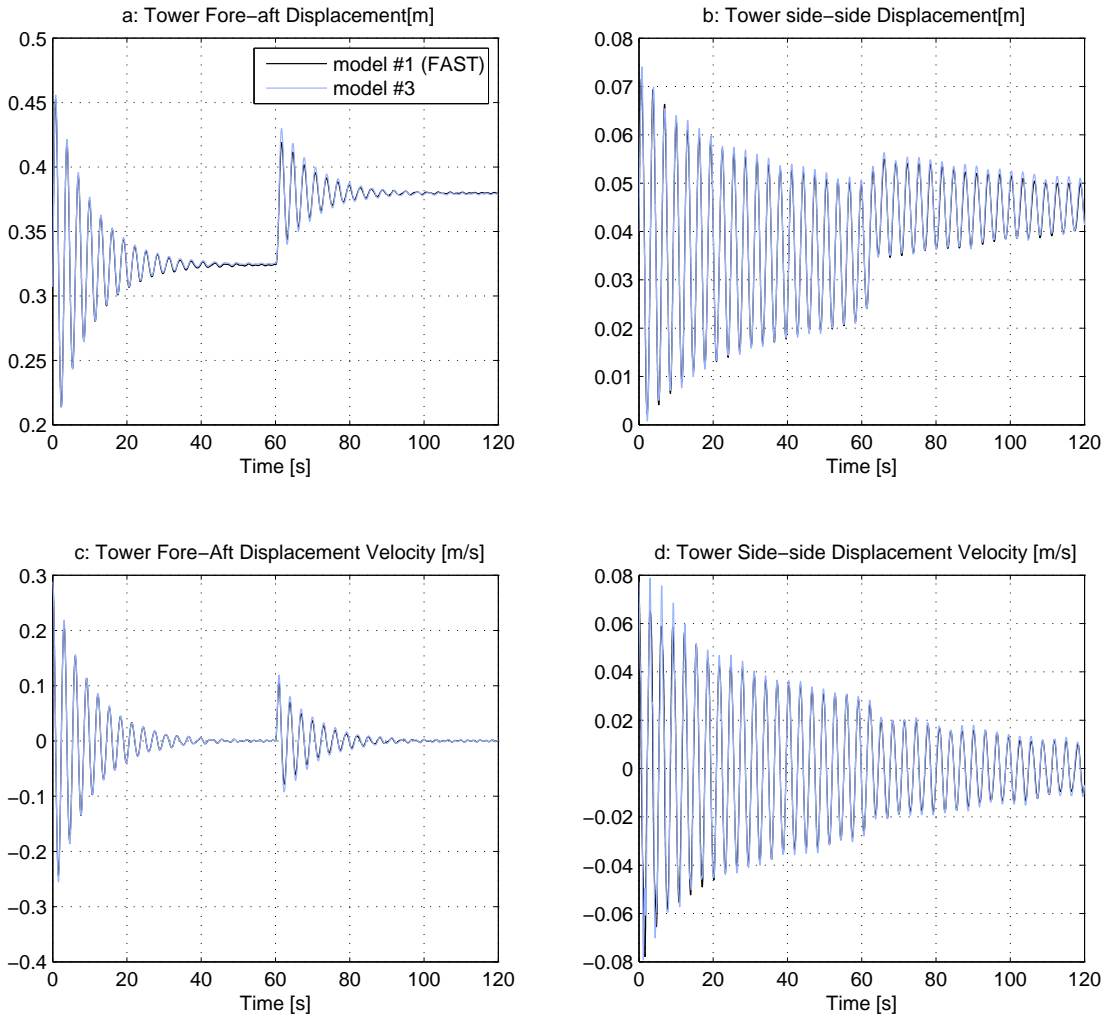


Figure 10.9. Tower displacements (#1 vs. #3).

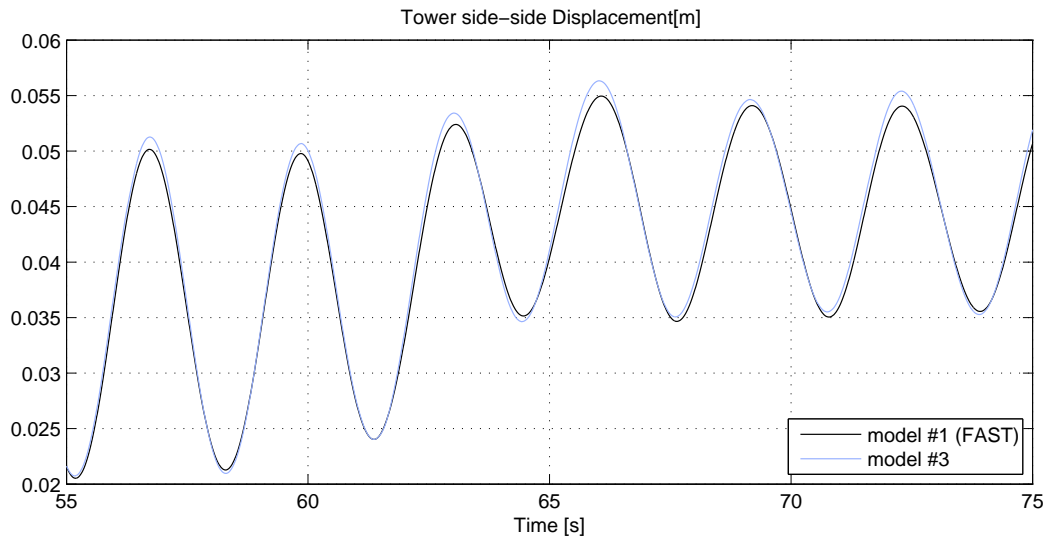


Figure 10.10. Tower displacements (#1 vs. #3) close-up.

For the generator speed, it can be seen in Figure 10.11(b), that the amplitude is now followed until the step on the wind speed, and then deviates after, which was not the case for model #2; hence it can be concluded that also here, the inclusion of the 3 excluded dynamics have a positive effect.

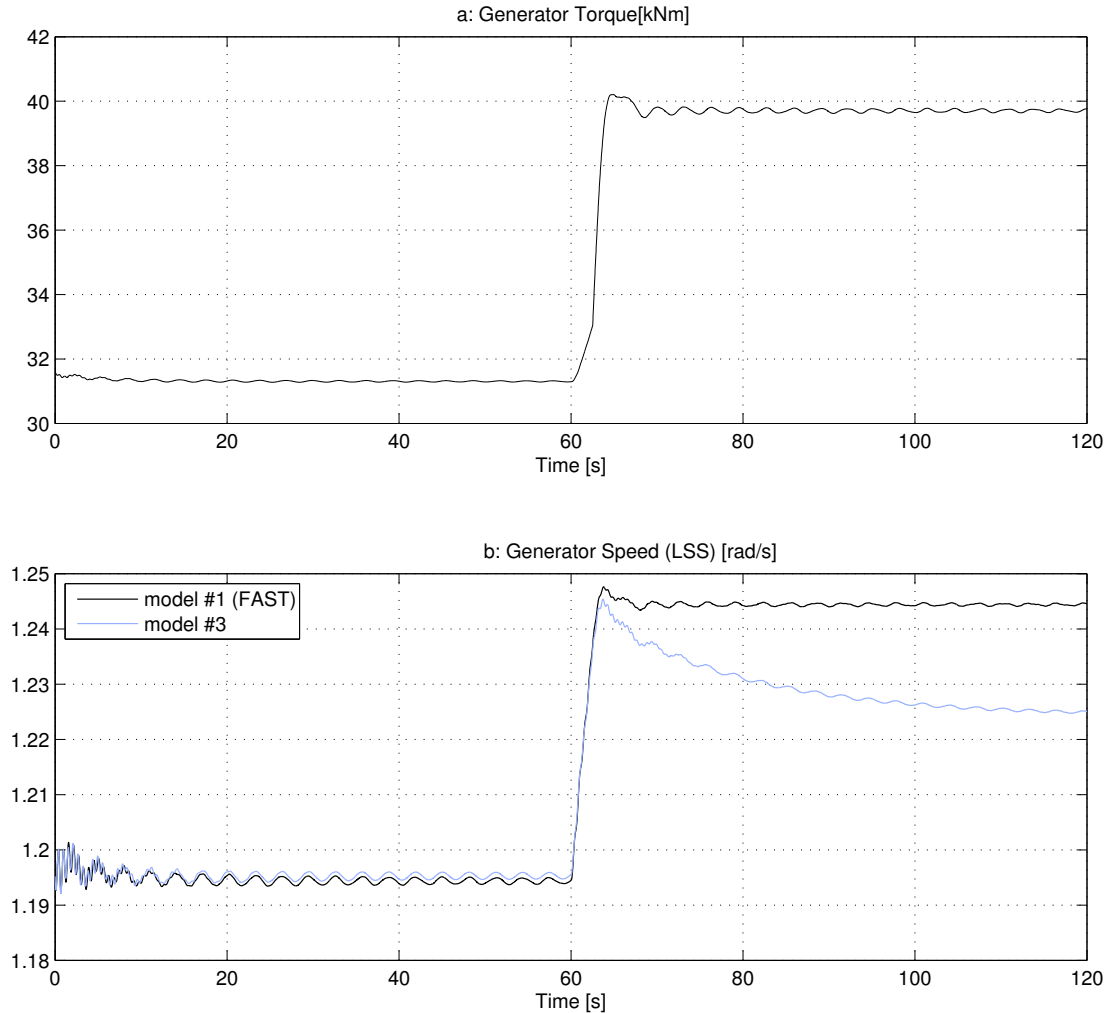


Figure 10.11. Generator torque and generator speed (#1 vs. #3).

For the drivetrain (Figure 10.12) improvements from including the excluded dynamics are seen as well regarding frequency and amplitude both in the interval before the step and after, which can be seen in the close-up plot in Figure 10.13.

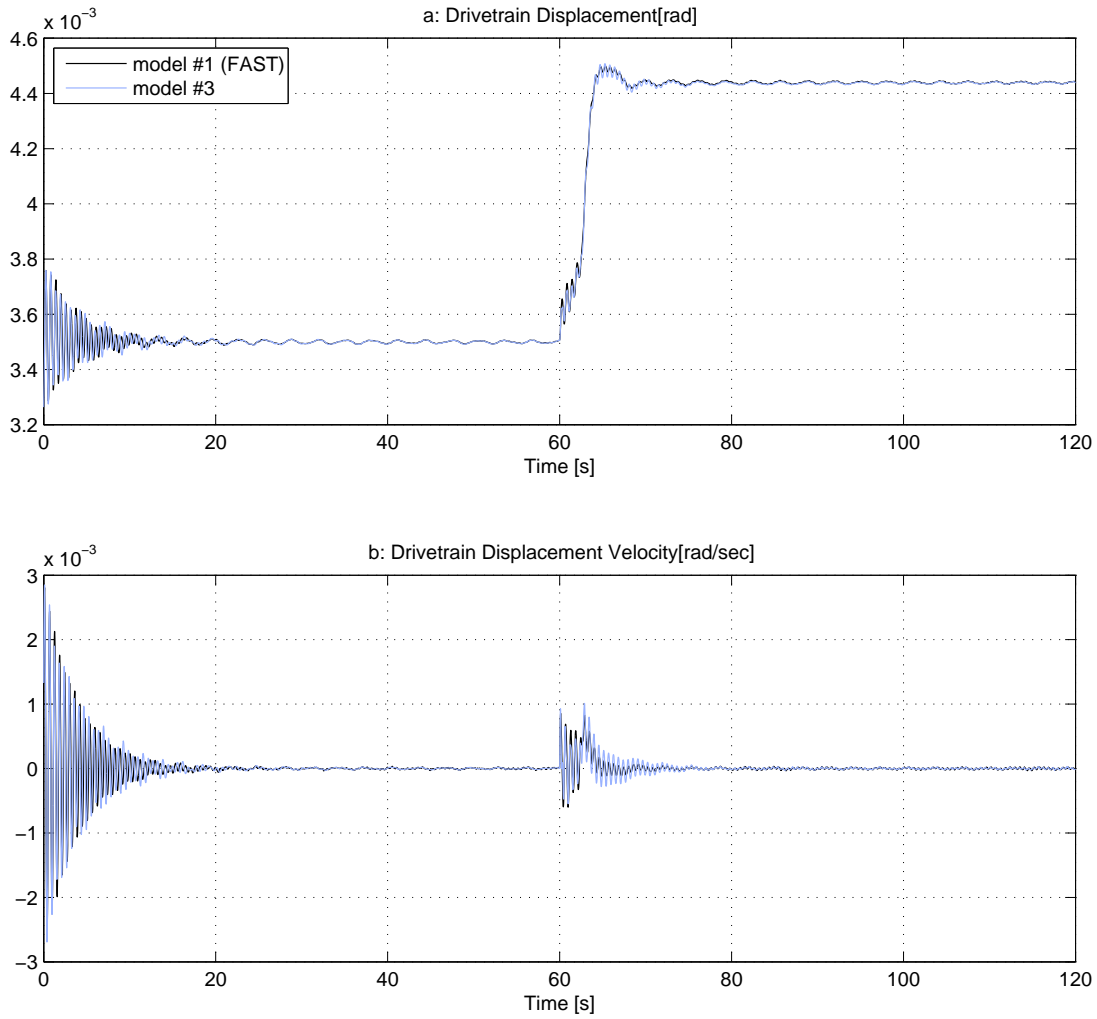


Figure 10.12. Drivetrain displacements (#1 vs. #3).

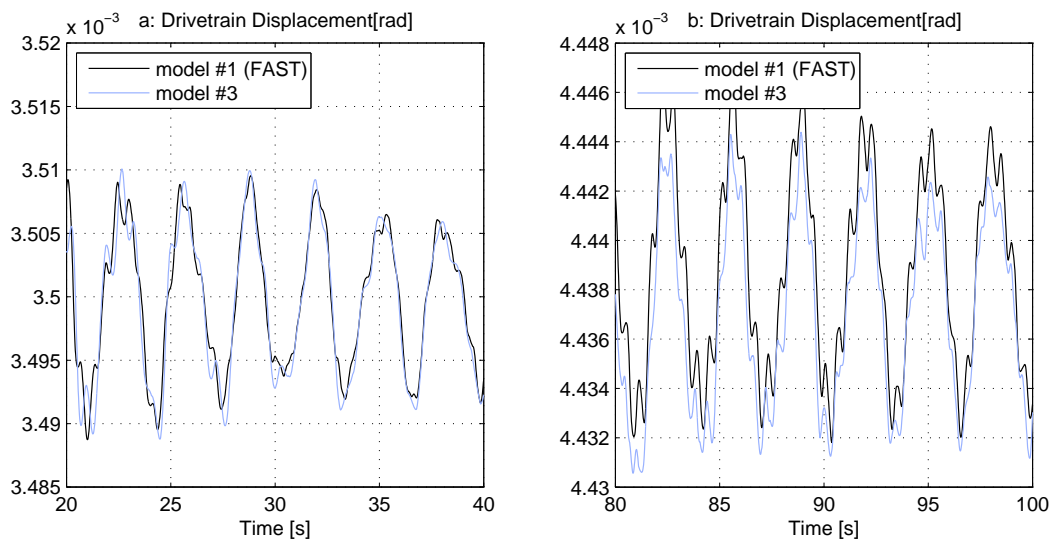


Figure 10.13. Drivetrain displacement (#1 vs. #3) close-up.

The blade edge- and flapwise displacements show great improvements as well, especially seen in Figure 10.15(a) if compared to the results from the test of model #2 against model #1, where the amplitude was off by approximately 0.25 m.

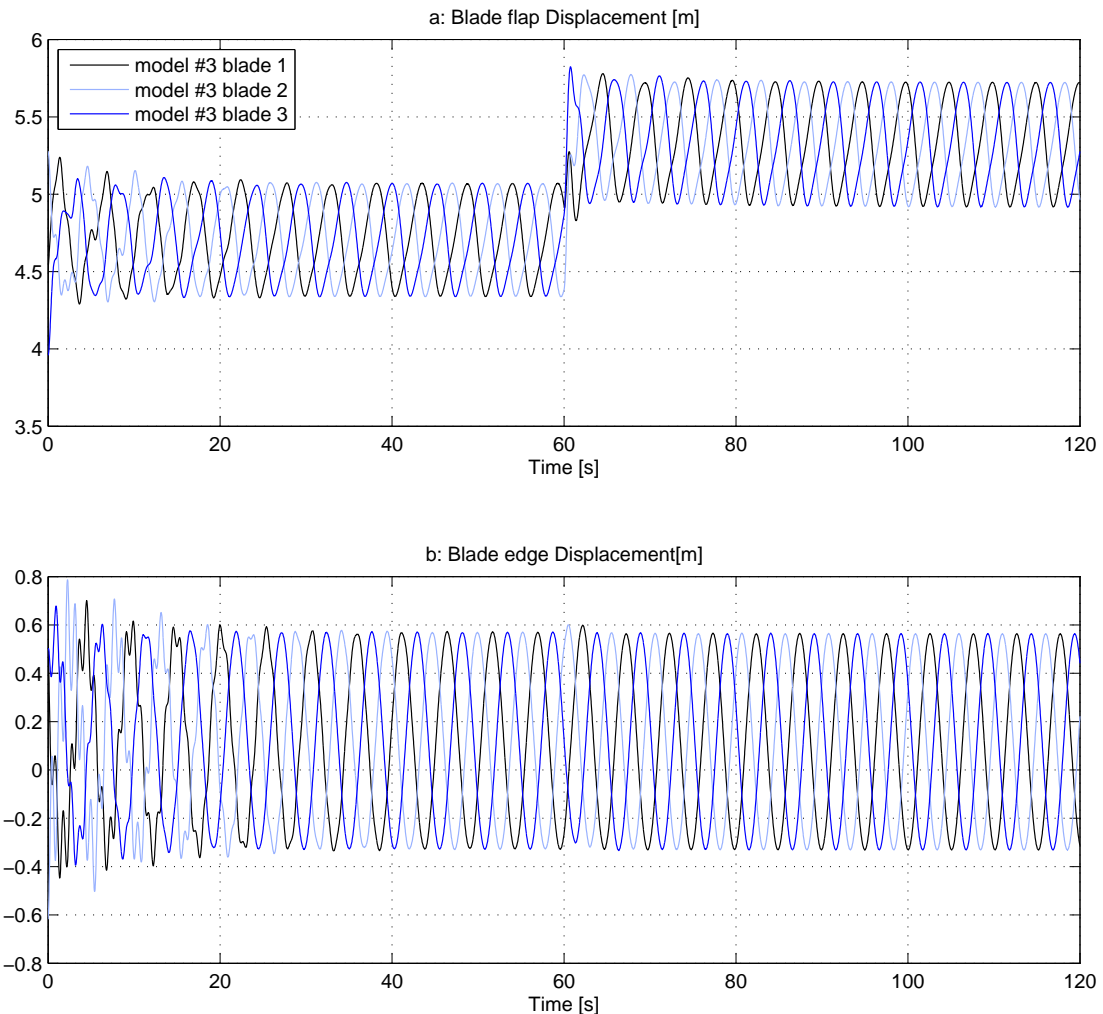


Figure 10.14. Blade displacements (#3).

10.1.3 Conclusion

Since the results from comparing model #1 to respectively model #2 and #3, shows much better results from model #3 than model #2, it must be concluded that the dynamics of blade preconing, rotor shaft tilting and rotor overhang can not be ignored, why the model developed in this project, in further work must include these.

In accordance to requirement **r.1** page 25, a model describing blade and tower deflections and vibrations caused by wind perturbation should be developed. Developing the model based on the model described in chapter 7, did not fully succeed due to time limitations. However, as described in section 9.1, linearised parts of the developed model was comparable to the linearised model from FAST. It was therefore, as an alternative

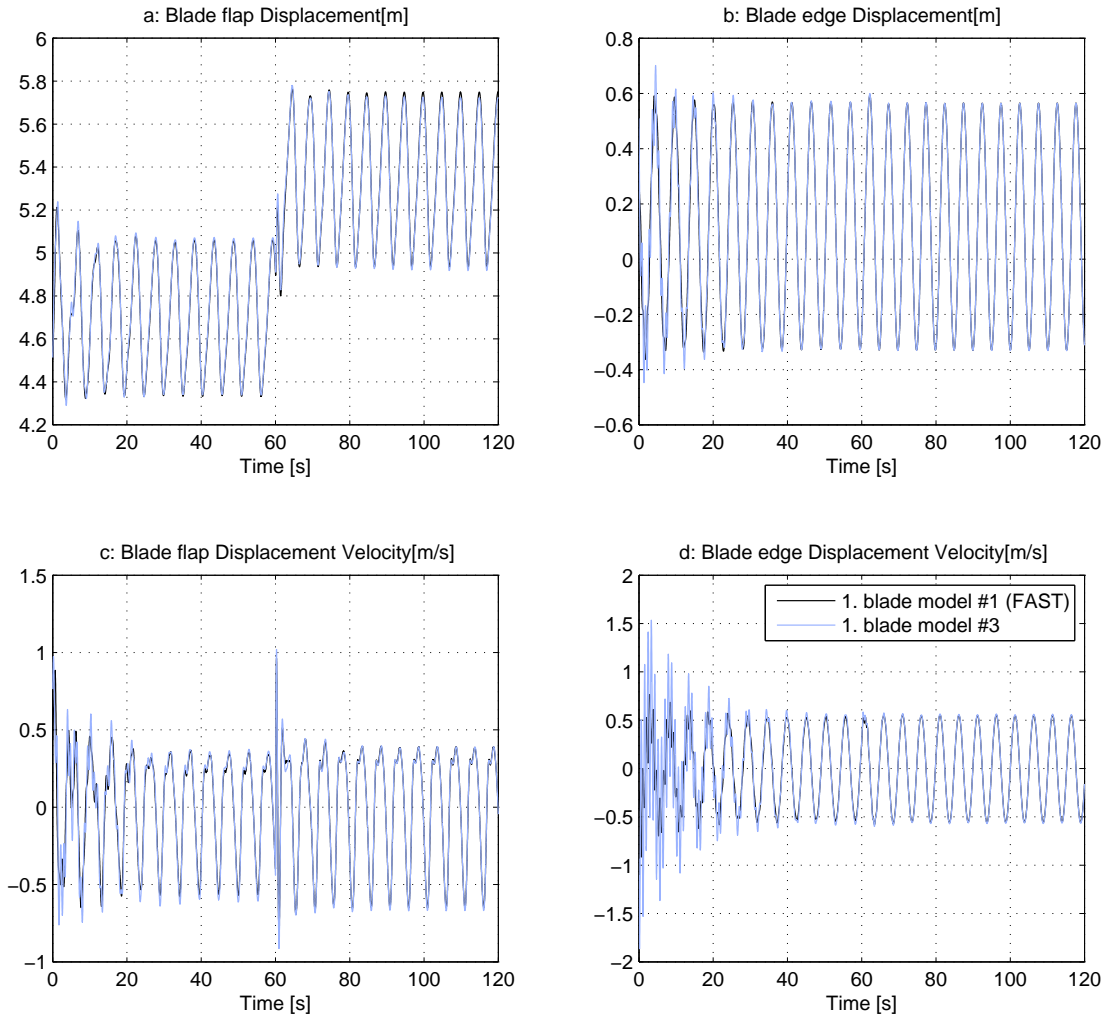


Figure 10.15. Blade displacements (#1 vs. #3).

approach and in order to have a model for usage in the estimator, chosen to use a FAST linearised model, since they showed potential as described in this section. The requirement is therefore considered partially fulfilled, since some of the system matrices in the developed model were consistent with the matrices from FAST, as seen in 9.1.

10.2 Test of Estimator

The test of the estimator is carried out by first simulating the FAST non-linear turbine model, creating a sequence of simulation data. The data sequence contains control inputs in terms of pitch and torque inputs alongside with corresponding state measurements in terms of the states described in appendix D. The simulation of the non-linear turbine is carried out with a wind field equal to the one used for validating the model in the previous chapter, meaning a vertical shear exponent of 0.1 and for the hub height wind speed a step from 10 m/s to 11 m/s.

The estimator described in section 9.2 is then used in attempt of estimating the shear exponent and the wind speed in hub height. First attempt is carried out by directly using

the simulated state measurements for the non-linear turbine simulation without adding noise. In second attempt, sensor noise is added in terms of white Gaussian noise. The procedure and results from the attempts are described in the following.

10.2.1 Estimation without sensor noise

For the first attempt no sensor noise is added. Initially the covariance for the process noise is set equally for all states to 0.01 and for the wind 0.001 and shear 0.00005. These values are, when designing Kalman filters considered tuning parameters, why they are arbitrarily set at the first estimation attempt. The reason for setting these values is that the shear is assumed to change slower than the wind speed. It is observed from the test, that the estimates of wind speed, generator speed, and drivetrain torsion adapts too slowly, why the covariances for those are increased.

This yields the estimation of the wind parameters shown in Figure 10.16, where the simulated wind is plotted alongside with the estimation of it. The deviation in the estimate from the simulated wind speed is 0.22 % and for shear it is 1.14 %, when looking at the last 40 seconds of the estimation data.

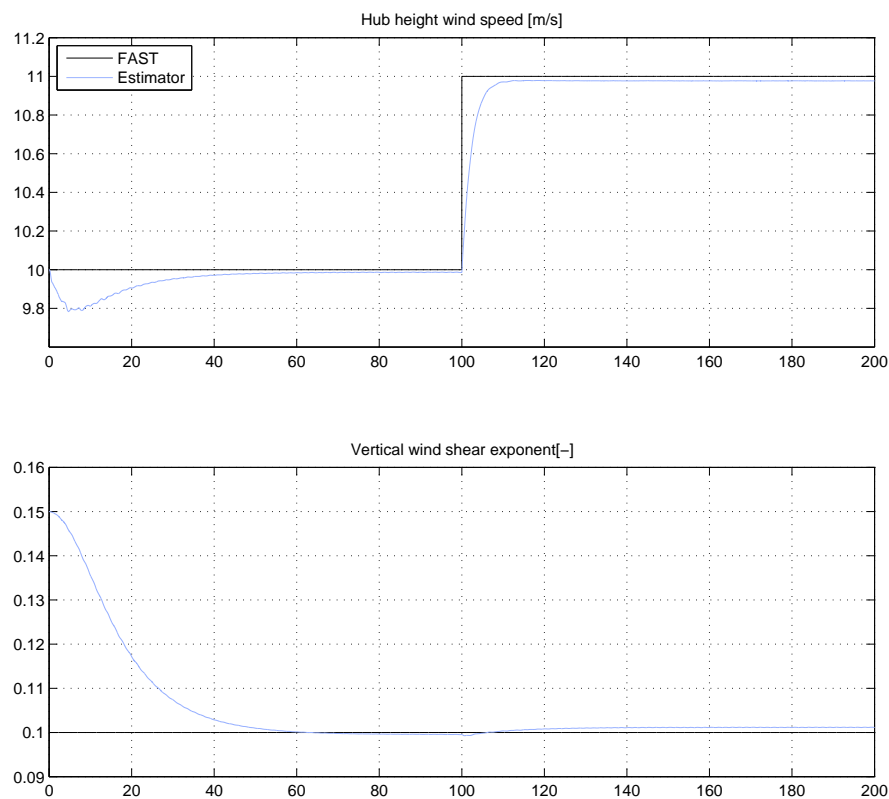


Figure 10.16. Estimation of wind speed and shear.

In Figure 10.17, 10.18 and 10.19 the estimation of respectively tower, drivetrain, generator and blade related states is shown.

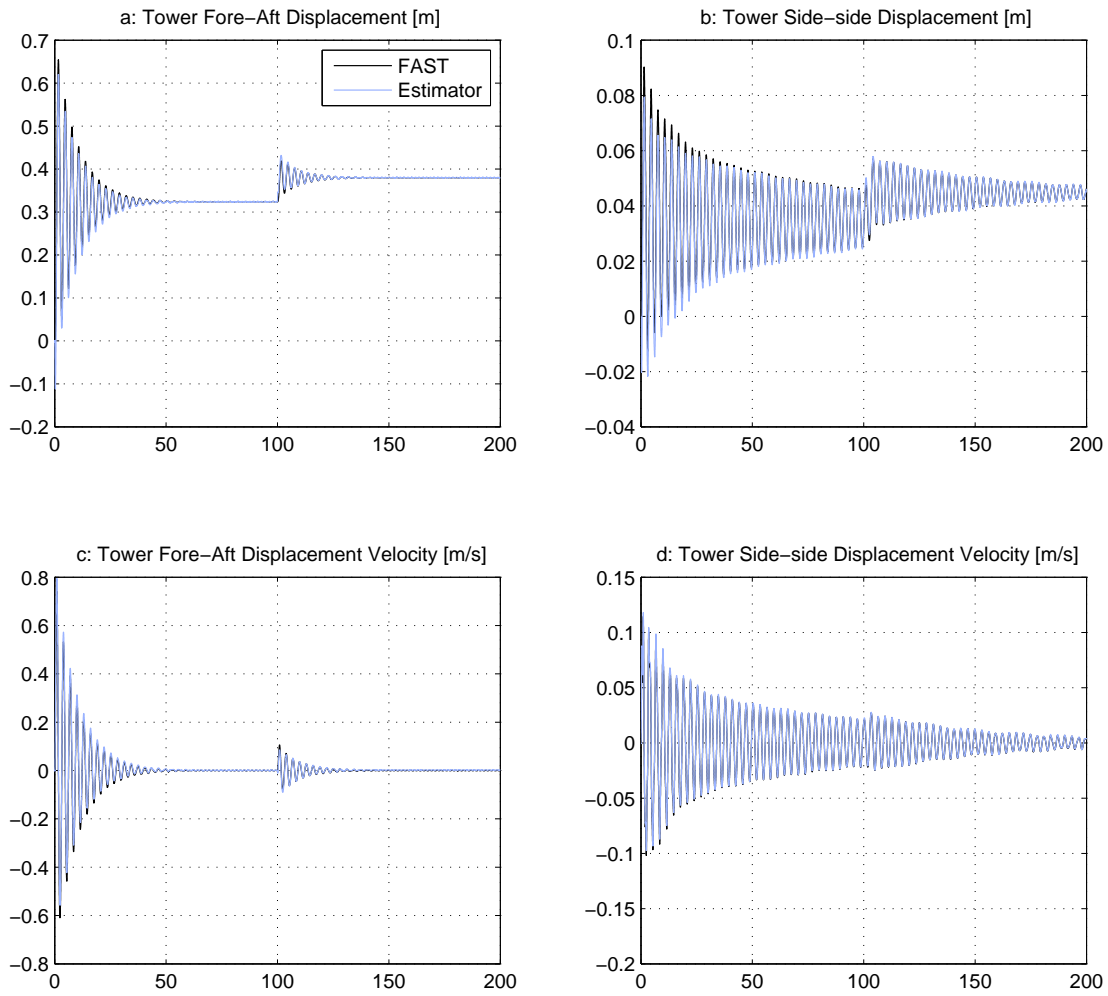


Figure 10.17. Estimation of tower related states.

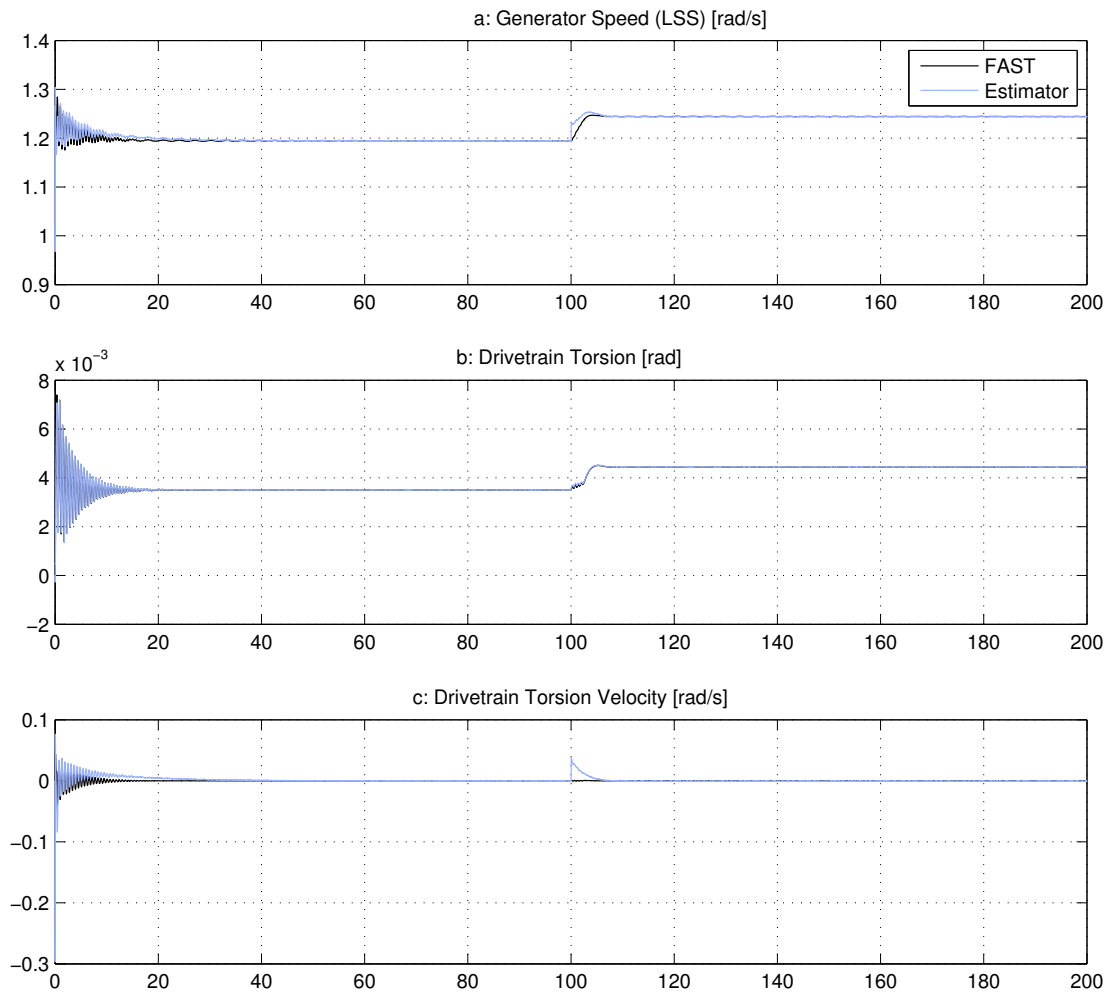


Figure 10.18. Estimation of drivetrain and generator related states.

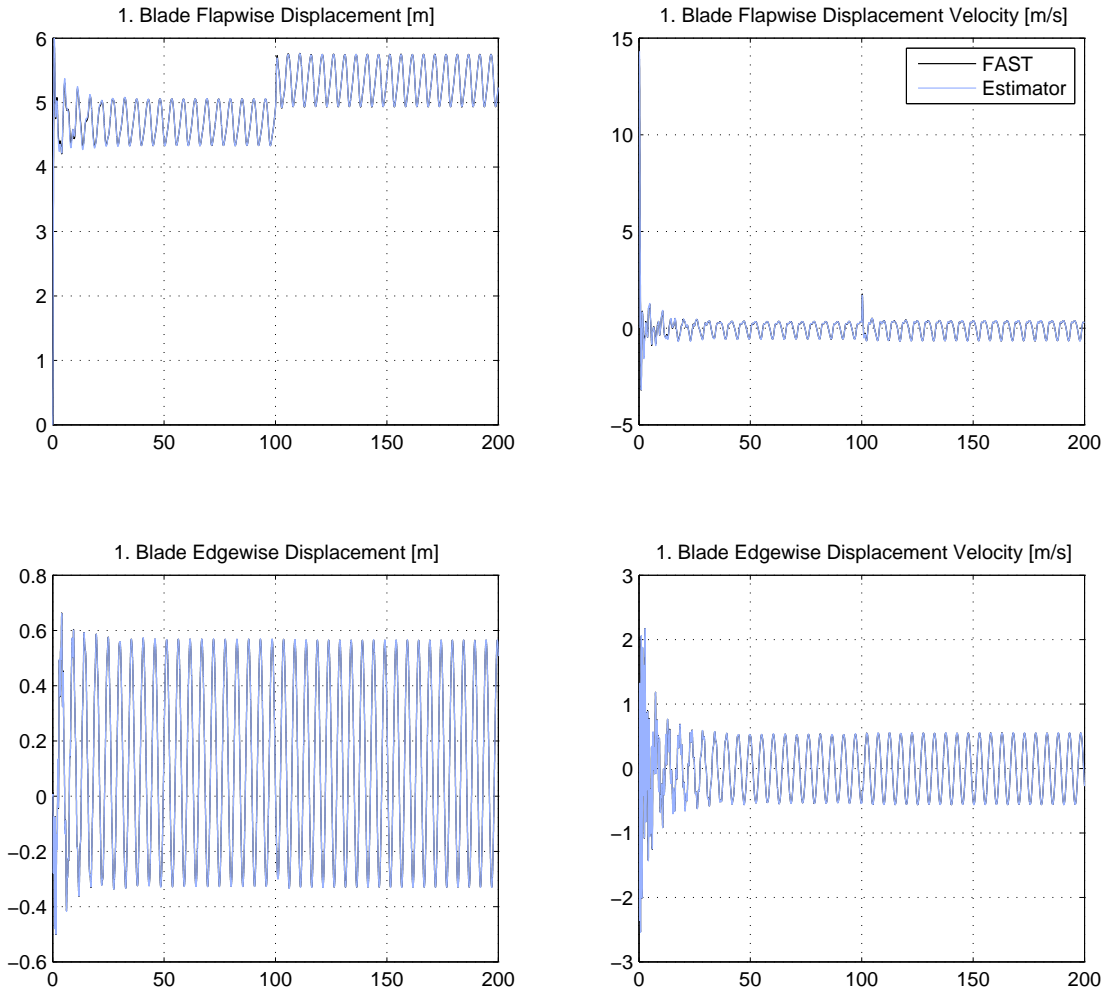


Figure 10.19. Estimation of blade related states. Note that only blade 1 is shown since the results where equal for blade 2 and 3, with the only difference that the oscillations are time shifted.

The deviations, at 100 seconds, in the two states illustrated in Figure 10.18(a) and Figure 10.18(c) are assumed to be caused by the estimation of wind speed. After the step on the wind speed is imposed, it takes some time for the filter to adapt to the sudden change in wind speed, why these two states deviate until the wind speed is estimated.

10.2.2 Estimation with noise

An estimation attempt with noise added to the measurements is carried out as well. The following standard deviations are used for generation of the noise added to the state measurements and torque input.

- Generator Torque: 45 Nm
- Generator speed: 0.025 rad/s
- Drivetrain torsion displacement: 0.025 rad
- Drivetrain torsion velocity: 0.025 rad/s

- Accelerometers in blades and tower: 0.01 m/s^2

These values are based on the standard deviations used in [4]. Note that for the standard deviations on the states describing blade and tower deflections and velocities, the standard deviations for an accelerometer are used. The squared of the standard deviations (variances) are used to define the measurement covariance. The generated noise sequence is added to the state measurements and torque inputs from the data also used in the estimation test without the presence of noise. The estimation is run and the the estimation of the wind parameters is shown in Figure 10.20, where the simulated wind is plotted alongside with the estimation of it. The mean deviation in the estimate from the simulated wind speed it is 0.33 % and 1.22 % for the wind shear and when looking at the last 40 seconds of the estimation data.

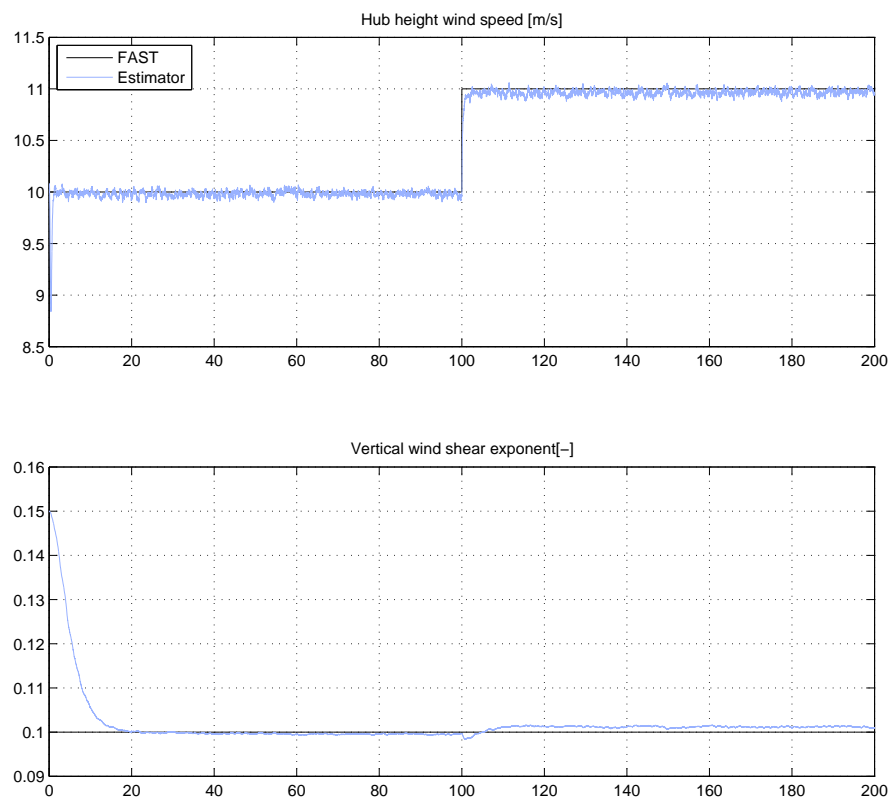


Figure 10.20. Estimation of wind speed and shear with the presence of sensor noise.

In order to check if all information from the simulated measurement data is utilised, the autocorrelation for all measurable states was investigated. An example of the autocorrelation, obtained using MATLAB, is shown in Figure 10.21. The autocorrelation for the remaining states behaved equally.

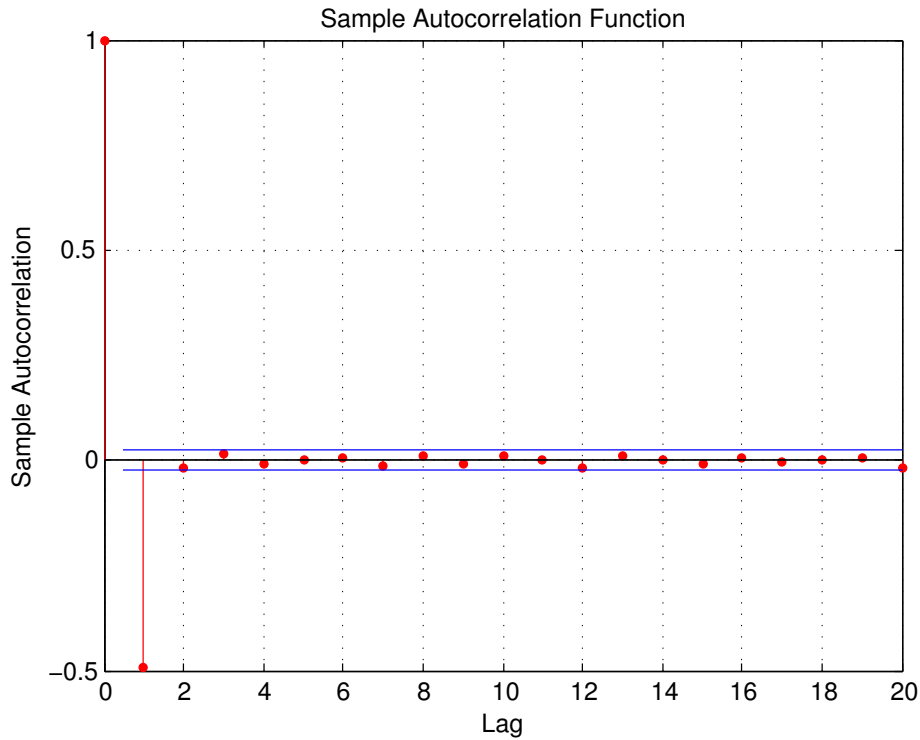


Figure 10.21. Autocorrelation for error between measured and estimated tower fore-aft displacement.

In order to have obtained all information from the measurements the estimation error should be white noise. The autocorrelation shows that all lags except for the 1st are within the 95 % confidence interval and therefore the estimation error is equal to zero-mean white noise. The correlation at the 1st lag is due to the discretisation, which causes the current state of the filter to be dependent on the previous state.

10.2.3 Conclusion

In accordance to requirement **r.2** on page 25 an estimation scheme should be designed in order to determine wind field characteristics in terms of vertical shear and wind speed. Since the estimation of the wind shear and speed in the presence of sensor noise estimated the simulated wind speed and -shear with respectively 1.22 % and 0.33 % deviation, the requirement is considered fulfilled.

Part III

Conclusion and Perspectives

11 Conclusion

The scope of this project was to develop a model and estimator for a wind turbine. The model should describe the structural deflections and vibrations of a wind turbine and account for how wind perturbation affects those. Based on this model an estimator for determining wind field characteristics should be designed.

A preliminary analysis was carried out to determine the structure of a wind turbine and how the wind is used in it as an energy source. Furthermore it was concluded that the wind measurements currently used in modern wind turbines are only used for safety shut down and periodically yaw misalignment correction. The low quality of the wind measurements makes them unsuitable for use in a control strategy. However due to the wind turbines' increase in size it would be beneficial to make use of measurements and estimations of the wind field for control purposes.

A problem description was carried out, concluding that it would be beneficial to make use of alternative sensors to estimate wind field parameters for usage in a control algorithm. This control algorithm's purpose should be to compensate for asymmetrical loading, due to wind perturbation, by usage of individual pitch control and knowledge of the wind field.

Afterwards a requirement specification was set, stating that a model and estimator should be designed in order to solve the described problem. Based on this, a design strategy was defined stating that by usage of sensors in blades and tower, a model and estimator should be used to determine wind field parameters.

An attempt of deriving a model describing the behaviour of a wind turbine was done. The turbine chosen was the National Renewable Energy Laboratory (NREL) 5 MW turbine, which is possible to simulate by usage of the non-linear turbine simulator FAST for MATLAB. The distributed structural parameters of the wind turbine were used in the model. The model was derived using an approach of Lagrangian mechanics. The model was due to time limitations not fully developed but showed some consistency when matched against the system matrices from the turbine in FAST. In order to have a model for usage when designing the wind estimator, a linearised model was obtained by using linearisation capabilities in FAST. The linearised model performs close to the non-linear turbine model, when operating around the operating points, that the model is linearised about.

An attempt of designing an estimator for estimating wind parameters was carried out. A Kalman filter was designed, and in order to actively account for non-linearities it would have been preferable to implement an Unscented Kalman Filter (UKF) or an EKF. However since the model extracted from FAST is not possible to use in such filters, a linear Kalman filter was used. The NREL 5 MW turbine was simulated with a specified wind field, yielding data sets of control inputs and model state measurements. The Kalman filter

was then used in attempt of estimating the wind field parameters used in the simulation of the wind. Attempts was carried out both with and without the presence of measurement noise. The wind field parameters attempted estimated was wind speed and vertical wind shear. The result was that in the presence of sensor noise a deviation of respectively 1.22 % and 0.33 % was obtained.

This means that for the requirements specified in this work the following can be concluded. A model was developed, however this was by usage of the capabilities in FAST and not based on the derived model, why the requirement regarding developing a model was only partially fulfilled. An estimator was developed, showing capabilities of estimating wind speed and vertical shear, why the requirement regarding estimation is considered fulfilled.

12 Perspectives

The estimator for wind speed and shear designed in this project used a pre defined linearised model and a linear Kalman filter. Meaning it is only suitable for operation around the chosen operating points, and in order to use it for other operating points it must be linearised around those again.

This process should be automated by finishing the development of the model attempted derived in this work. This model could then be used with an Unscented Kalman Filter (UKF) or Extended Kalman Filter (EKF) in order to perform linearisation in runtime. By doing such the estimator could hopefully be used for all conditions of the states in the wind turbine system. Also more wind parameters such as wind direction, could be included in the estimation scheme, such that control inputs could be calculated for correcting yaw misalignment.

The wind model could be expanded, to include turbulence and wake model.

Further work should also include controller design using the estimated wind parameters for control in order to examine the effect of including those in an control algorithm. This could be done, as mentioned, by usage of individual pitch control taken the assymetrical wind field into account and compensating for it by cyclic individual pitch control.

Given more time, a more thorough research on different sensor types could have been carried out. For example, given a hollow wind turbine blade, one could imagine that installing lasers inside pointing upwards through the blade, could detect the deflections of the blade.

Acronyms

BEM Theory Blade Element Momentum Theory

CFD Computational Fluid Dynamics

DOF Degree of Freedom

EKF Extended Kalman Filter

FEM Finite Element Method

HAWT Horizontal Axis Wind Turbine

NREL National Renewable Energy Laboratory

UKF Unscented Kalman Filter

Bibliography

- [1] D. S. Tony Burton, Nick Jenkins and E. Bossanyi, *Wind Energy Handbook*, 2nd ed. John Wiley and Sons, 2011.
- [2] E. Kulunk, *Aerodynamics of Wind Turbines*. InTech, 2011, chapter 1 from the collection: Fundamental and Advanced Topics in Wind Power.
- [3] H. D. B. Fernando D. Bianchi and R. J. Mantz, *Wind Turbine Control Systems : Principles, Modelling and Gain Scheduling Design*. Springer, 2007.
- [4] T. Esbensen and C. Sloth, "Fault diagnosis and fault-tolerant control of wind turbines," Aalborg University,Aalborg,Denmark, Tech. Rep., 2009.
- [5] K. Z. Østergaard, P. Brath, and J. Stoustrup, "Estimation of effective wind speed," *Journal of Physics: Conference Series 75 012082*, 2007.
- [6] M. O. L. Hansen, *Aerodynamics of Wind Turbines*, 2nd ed. Earthscan, 2008.
- [7] S. Suryanarayanan and A. Dixit, "A procedure for the development of control-oriented linear models for horizontal-axis large wind turbines," *Journal of Dynamic Systems, Measurement, and Control*, 2007.
- [8] T. Esbensen, B. T. Jensen, M. O. Niss, and C. Sloth, "Joint power and speed control of wind turbines," Aalborg University,Aalborg,Denmark, Tech. Rep., 2008.
- [9] T. S. HRISTOV, S. D. MILLER, and C. A. FRIEHE, "Linear time-invariant compensation of cup anemometer and vane inertia," Department of Mechanical and Aerospace Engineering, University of California, Irvine, California 92697-3975, U.S.A., Tech. Rep., 2000.
- [10] T. Mikkelsen, K. Hansen, N. Angelou, M. S. M. Harris, P. Hadley, R. Scullion, G. Ellis, and G. Vives, "Lidar wind speed measurements from a rotating spinner," *ewec - Europe's premier wind energy event Warsaw, Poland*, 2010.
- [11] F. Dunne, E. Simley, and L. Pao, "Lidar wind speed measurement analysis and feed-forward blade pitch control for load mitigation in wind turbines," 2011.
- [12] C. Bottasso and A. Croce, "Cascading kalman observers of structural flexible and wind states for wind turbine control," Dipartimento di Ingegneria Aerospaziale,Milano,Italy, Tech. Rep., 2009.
- [13] J. Jonkman. (Certified 2005) Last visited: 13-05-2013. [Online]. Available: <http://wind.nrel.gov/designcodes/simulators/fast/>

- [14] J. Jonkman, S. Butterfield, W. Musial, and G. Scott. (2009) Definition of a 5-mw reference wind turbine for offshore system development. Last visited: 13-05-2013. [Online]. Available: <http://www.nrel.gov/docs/fy09osti/38060.pdf>
- [15] J. Jonkman and M. L. B. J. . (2005) Fast user's guide. Last visited: 13-05-2013. [Online]. Available: <http://wind.nrel.gov/designcodes/simulators/fast/FAST.pdf>
- [16] D. J. Laino and A. C. Hansen, "User's guide to the wind turbine aerodynamics computer software aerodyn," 2002.
- [17] L. Meirovitch, *Elements of Vibration Analysis*, 2nd ed. McGraw-Hill Book Company, 1986.
- [18] J.-N. Juang and M. Q. Phan, *Identification and Control of Mechanical Systems*. Cambridge University Press, 2001, available on books.google.dk.
- [19] H. Goldstein, *Classical mechanics*, 2nd ed. Addison-Wesley, 1980.
- [20] A. Dixit, "Development of lti/ltv model templates for control of large wind turbines," 2005, master's Thesis, Department of Mechanical Engineering, Indian Institute of Technology Bombay Powai.
- [21] D. S. L. Dolan and P. W. Lehn, "Simulation model of wind turbine 3p torque oscillations due to wind shear and tower shadow," *IEEE TRANSACTIONS ON ENERGY CONVERSION*, VOL. 21, NO. 3, 2006.
- [22] P. V. Vessem and D. Williams, "Rediscovering the strain gauge pressure sensor," 2009, last visited: 07-05-2013. [Online]. Available: http://archives.sensorsmag.com/articles/0499/0499_36/
- [23] M. S. Grewal and A. P. Andrews, *Kalman filtering : theory and practice using MATLAB*, 3rd ed. John Wiley & Sons, 2008.
- [24] K. B. Petersen and M. S. Pedersen. (2009) The matrix cookbook. Last visited: 13-05-2013. [Online]. Available: <http://orion.uwaterloo.ca/~hwoikowi/matrixcookbook.pdf>
- [25] A. B. Borchersen, "Fast installing," 2013, last visited: 07-05-2013. [Online]. Available: <http://kom.aau.dk/~anb/fast/fastinstall.html>

Appendix

A Parameter Distribution

In this appendix the parameter distribution for data used in the developed model is presented.

A.1 Tower Parameter Distributions

Tower Mass Distribution (Figure A.1)

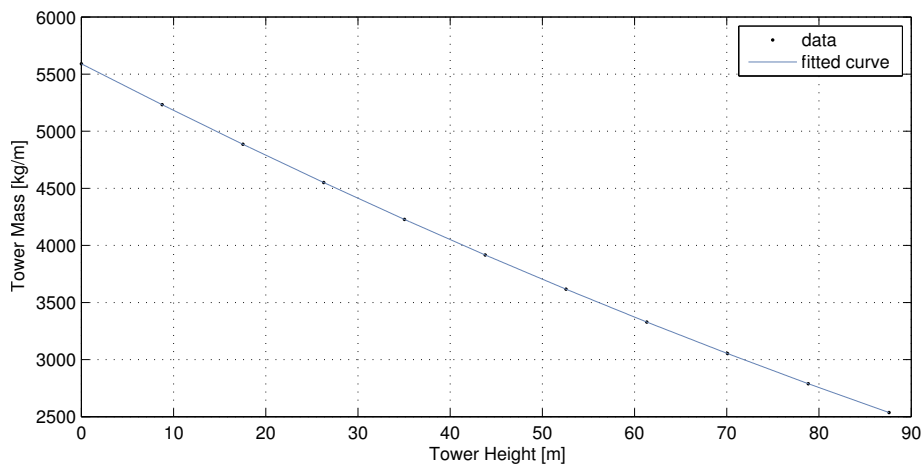


Figure A.1. Mass distribution of the tower.

Tower Fore-Aft Stiffness Distribution (Figure A.2)

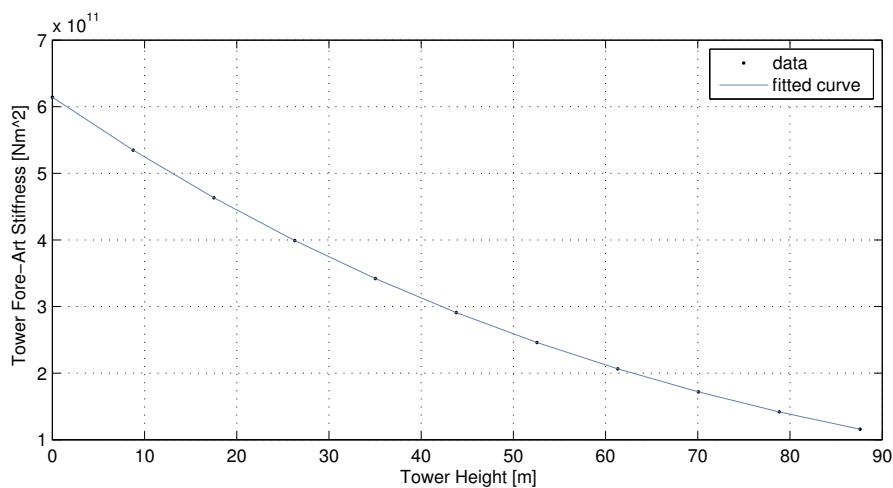


Figure A.2. Fore-aft stiffness distribution of the tower.

Tower Side-Side Stiffness Distribution (Figure A.3)

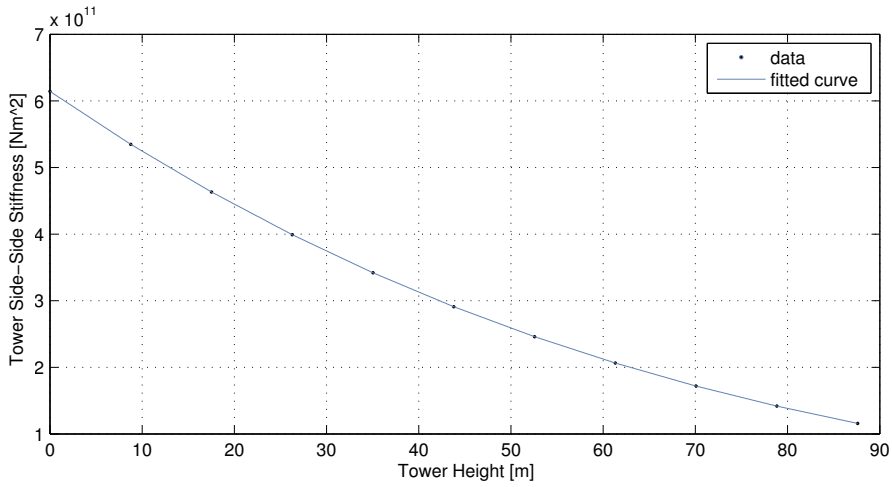


Figure A.3. Side-side stiffness distribution of the tower.

A.2 Blade Parameter Distribution

Blade Mass Distribution (Figure A.4)

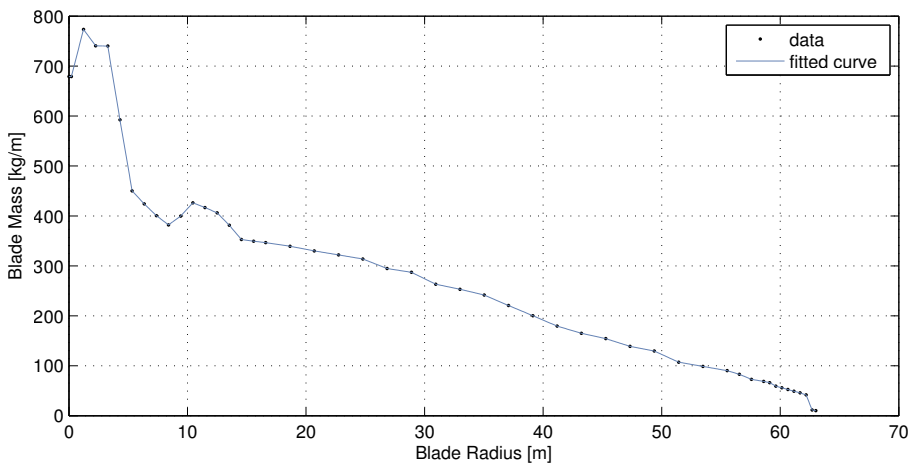


Figure A.4. Mass distribution of the blades.

Blade Flapwise Stiffness Distribution (Figure A.5)

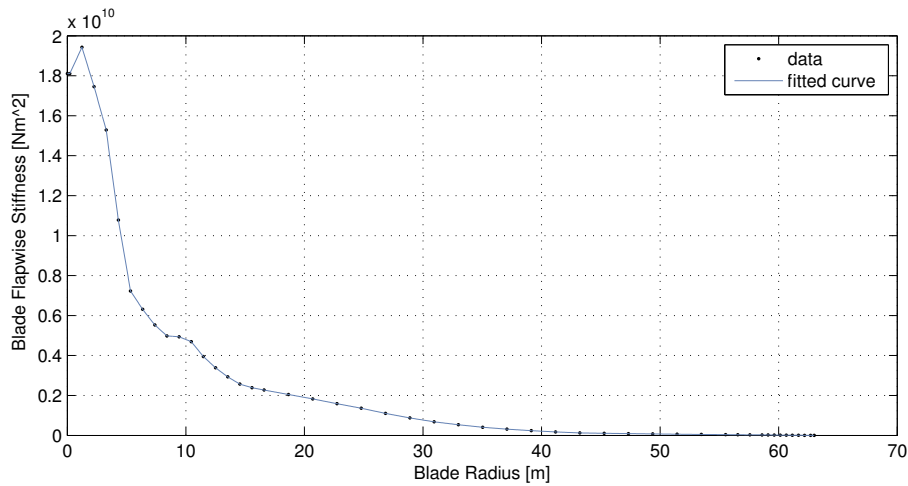


Figure A.5. Flapwise stiffness distribution of the blades.

Blade Edgewise Stiffness Distribution (Figure A.6)

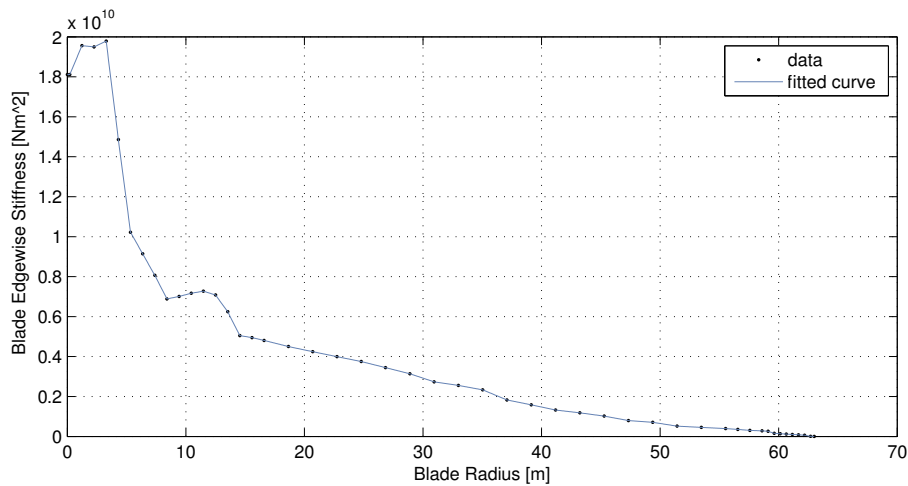


Figure A.6. Edgewise stiffness distribution of the blades.

A.3 Blade Lift and Drag Coefficients

In this appendix an example of calculation of the inflow angle, lift coefficients, drag coefficients and the derivatives of the lift and drag coefficients wrt. inflow angle is carried out. The calculation is carried out for the case where the rotor speed of the wind turbine is 12.1 rpm and the wind speed is 10 m/s.

The aerodynamic data, in terms of lift and drag coefficients, for the blades used in the NREL 5 MW wind turbine is specified by 8 airfoil tables, which are attached on the enclosed cd [/FAST_data/AeroData](#). The airfoil tables are used to describe the properties of 17 different sections of the blade, specified in [/FAST_data/NRELOffshrbaseline5MW_AeroDyn.ipt](#). The airfoil tables specifies the lift

and drag coefficients based on the wind inflow angle. In order to use inflow angle alongside with lift and drag coefficients for the developed model they must be calculated as distributed parameters depending on the radius of the blade.

This was done by using FAST to simulate the wind turbine and output a time series of data for the 17 blade sections used. The wind inflow angle alongside with lift and drag coefficients are included in the data file from the simulation `/lift_drag_coefficients/NRELOffshrBsline5MW_Onshore.elm`. The turbine was simulated until the coefficients reached steady state and the resulting coefficients are plotted in Figure A.7, Figure A.8 and Figure A.9

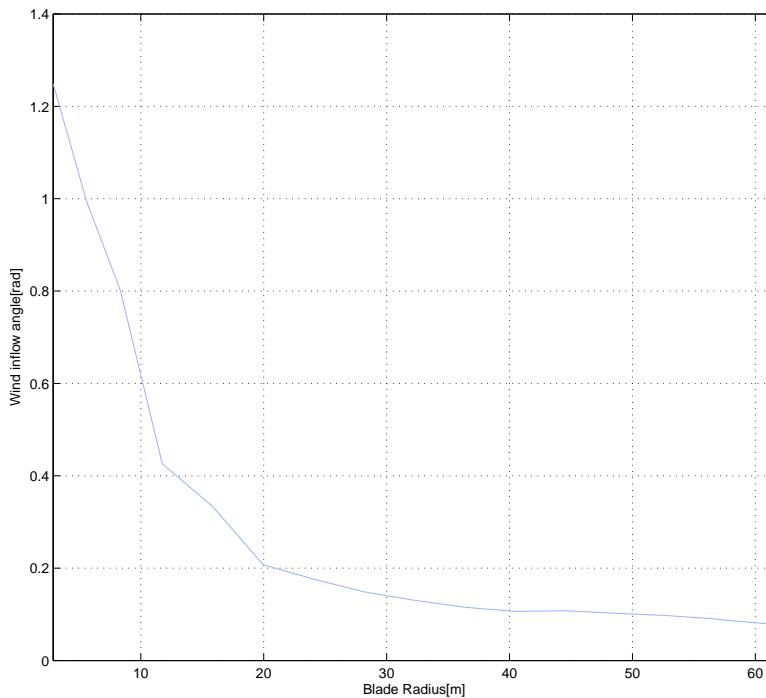


Figure A.7. Wind Inflow Angle plotted as function of the blade radius.

The developed model also requires derivatives of the lift and drag coefficients, wrt. inflow angle, as a function of radius on blade. These were calculated using Matlab and the m-file `/lift_drag_coefficients/calc_coef.m` and are plotted in Figure A.10.

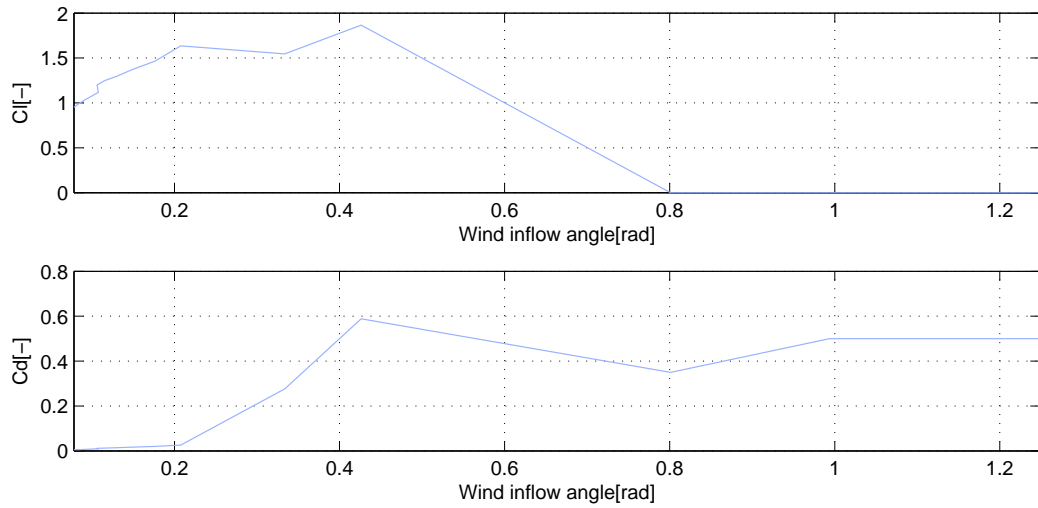


Figure A.8. Lift and drag coefficients plotted as function of the inflow angle.

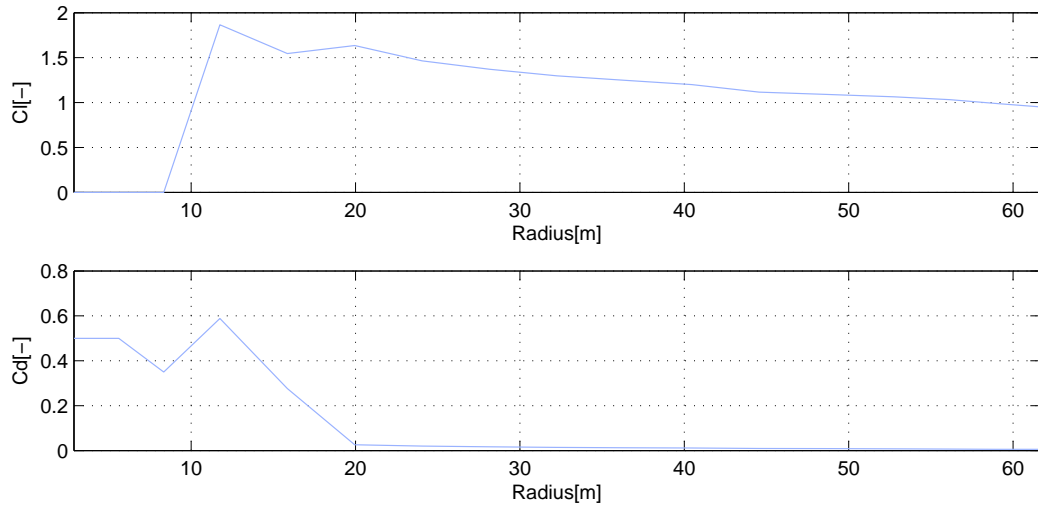


Figure A.9. Lift and drag coefficients plotted as function of the blade radius.

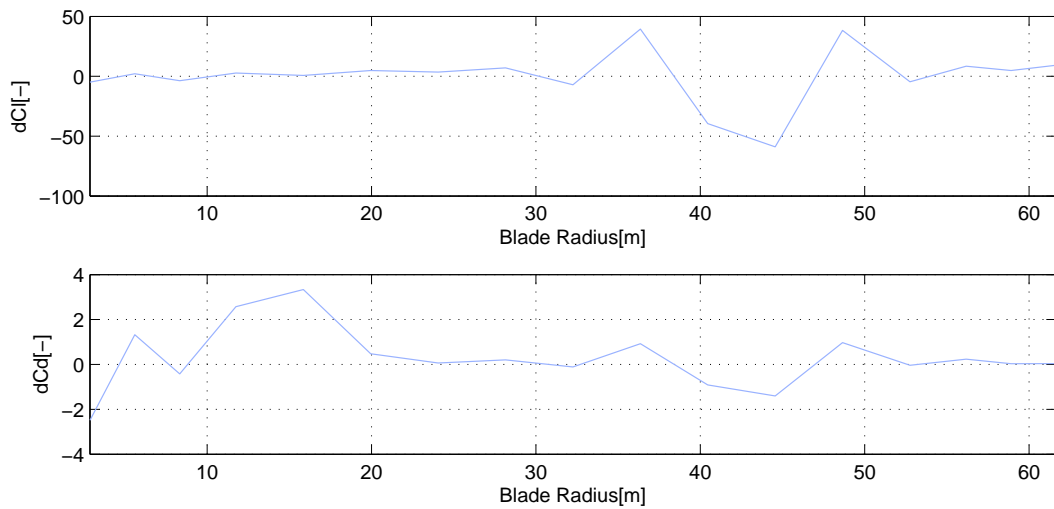


Figure A.10. Derivatives of lift and drag coefficients, wrt. inflow angle, plotted as function of the blade radius.

B System Matrices

In this appendix the equation for usage in the mass, stiffness and damping matrices are presented.

B.1 Mass Matrix, M

$$m_{11} = \int_0^H m_t(z) \mu_{\text{tfa}}(z)^2 dz + \sum_{i=1}^3 \int_0^R m_b(r) (1 + r \cos(\theta_i) \delta_{\text{tfa}})^2 dr + M \quad [\text{kg}]$$

$$m_{12} = 0$$

$$m_{13} = 0$$

$$m_{14} = 0$$

$$m_{15} = \int_0^R m_b(r) (1 + r \cos(\theta) \delta_{\text{tfa}}) \mu_{\text{bfop}}(r) dr$$

$$m_{16} = \int_0^R m_b(r) (1 + r \cos(\theta + \frac{2\pi}{3}) \delta_{\text{tfa}}) \mu_{\text{bfop}}(r) dr$$

$$m_{17} = \int_0^R m_b(r) (1 + r \cos(\theta - \frac{2\pi}{3}) \delta_{\text{tfa}}) \mu_{\text{bfop}}(r) dr$$

$$m_{18} = \int_0^R m_b(r) (1 + r \cos(\theta) \delta_{\text{tfa}}) \mu_{\text{beop}}(r) dr$$

$$m_{19} = \int_0^R m_b(r) (1 + r \cos(\theta + \frac{2\pi}{3}) \delta_{\text{tfa}}) \mu_{\text{beop}}(r) dr$$

$$m_{110} = \int_0^R m_b(r) (1 + r \cos(\theta - \frac{2\pi}{3}) \delta_{\text{tfa}}) \mu_{\text{beop}}(r) dr$$

$$m_{22} = \int_0^H m_t(z) [\mu_{\text{tss}}(z)]^2 dz + m_{\text{top}} + \delta_{\text{tss}} (J_r + nJ_g)$$

$$m_{23} = \delta_{\text{tss}} (J_r + J_g)$$

$$m_{24} = \delta_{\text{tss}} J_r$$

B.2 Stiffness Matrix, K

$$k_{11s} = \int_0^H EI_{\text{tfa}}(z) \left[\frac{\partial^2 \mu_{\text{tfa}}(z)}{\partial z^2} \right]^2 dz$$

$$k_{12s} = 0$$

$$k_{13s} = 0$$

$$k_{14s} = 0$$

$$k_{15s} = 0$$

$$k_{16s} = 0$$

$$k_{17s} = 0$$

$$k_{18s} = 0$$

$$k_{19s} = 0$$

$$k_{110s} = 0$$

B.3 Damping Matrix, C

Structural Damping Coefficients

$$c_{11s} = 2\zeta_1 \sqrt{k_{11} m_{11}}$$

$$c_{12s} = 0$$

$$c_{13s} = 0$$

$$c_{14s} = 0$$

$$c_{15s} = 0$$

$$c_{16s} = 0$$

$$c_{17s} = 0$$

$$c_{18s} = 0$$

$$c_{19s} = 0$$

$$c_{110s} = 0$$

Aerodynamic Damping Coefficients

$$\begin{aligned}
c_{11a} &= \int_0^R \sum_{k=1}^3 (1 + r \cos(\theta_k) \delta_{tfa})^2 f_{Nvxk}(r) dr \\
c_{12a} &= \int_0^R \sum_{k=1}^3 (1 + r \cos(\theta_k) \delta_{tfa}) f_{Nvyk}(r) \delta_{tss} r dr \\
c_{13a} &= \int_0^R \sum_{k=1}^3 (1 + r \cos(\theta_k) \delta_{tfa}) f_{Nvyk}(r) r dr \\
c_{14a} &= \int_0^R \sum_{k=1}^3 (1 + r \cos(\theta_k) \delta_{tfa}) f_{Nvyk}(r) r dr \\
c_{15a} &= \int_0^R (1 + r \cos(\theta) \delta_{tfa}) [f_{nvx1}(r) \mu_{bfop}(r) + f_{nvy1}(r) \mu_{bfip}(r)] dr \\
c_{16a} &= \int_0^R (1 + r \cos(\theta + \frac{2\pi}{3}) \delta_{tfa}) [f_{nvx2}(r) \mu_{bfop}(r) + f_{nvy2}(r) \mu_{bfip}(r)] dr \\
c_{17a} &= \int_0^R (1 + r \cos(\theta - \frac{2\pi}{3}) \delta_{tfa}) [f_{nvx3}(r) \mu_{bfop}(r) + f_{nvy3}(r) \mu_{bfip}(r)] dr \\
c_{18a} &= \int_0^R (1 + r \cos(\theta) \delta_{tfa}) [f_{nvx1}(r) \mu_{beop}(r) + f_{nvy1}(r) \mu_{beip}(r)] dr \\
c_{19a} &= \int_0^R (1 + r \cos(\theta + \frac{2\pi}{3}) \delta_{tfa}) [f_{nvx2}(r) \mu_{beop}(r) + f_{nvy2}(r) \mu_{beip}(r)] dr \\
c_{110a} &= \int_0^R (1 + r \cos(\theta - \frac{2\pi}{3}) \delta_{tfa}) [f_{nvx3}(r) \mu_{beop}(r) + f_{nvy3}(r) \mu_{beip}(r)] dr \\
c_{21a} &= \int_0^R \sum_{k=1}^3 \delta_{tss} r f_{tvxk}(r) (1 + r \cos(\theta) \delta_{tfa}) dr \\
c_{22a} &= \int_0^R \sum_{k=1}^3 (\delta_{tss} r)^2 f_{tvyk}(r) dr \\
c_{23a} &= \int_0^R \sum_{k=1}^3 \delta_{tss} r^2 f_{tvyk}(r) dr \\
c_{24a} &= \int_0^R \sum_{k=1}^3 \delta_{tss} r^2 f_{tvyk}(r) dr \\
c_{25a} &= \int_0^R \delta_{tss} r (f_{tvx1}(r) \mu_{bfop}(r) + f_{tvy1}(r) \mu_{bfip}(r)) dr \\
c_{26a} &= \int_0^R \delta_{tss} r (f_{tvx2}(r) \mu_{bfop}(r) + f_{tvy2}(r) \mu_{bfip}(r)) dr \\
c_{27a} &= \int_0^R \delta_{tss} r (f_{tvx3}(r) \mu_{bfop}(r) + f_{tvy3}(r) \mu_{bfip}(r)) dr \\
c_{28a} &= \int_0^R \delta_{tss} r (f_{tvx1}(r) \mu_{beop}(r) + f_{tvy1}(r) \mu_{beip}(r)) dr \\
c_{29a} &= \int_0^R \delta_{tss} r (f_{tvx2}(r) \mu_{beop}(r) + f_{tvy2}(r) \mu_{beip}(r)) dr \\
c_{210a} &= \int_0^R \delta_{tss} r (f_{tvx3}(r) \mu_{beop}(r) + f_{tvy3}(r) \mu_{beip}(r)) dr
\end{aligned}$$

$$\begin{aligned}
 c_{31a} &= \int_0^R \sum_{k=1}^3 r f_{tvxk}(r) (1 + r \cos(\theta_k) \delta_{tfa}) dr \\
 c_{32a} &= \int_0^R \sum_{k=1}^3 f_{tvyk}(r) \delta_{tss} r^2 dr \\
 c_{33a} &= \int_0^R \sum_{k=1}^3 f_{tvyk}(r) r^2 dr \\
 c_{34a} &= \int_0^R \sum_{k=1}^3 f_{tvyk}(r) r^2 dr \\
 c_{35a} &= \int_0^R r (f_{tvx1}(r) \mu_{bfop}(r) + f_{tvy1}(r) \mu_{bfip}(r)) dr \\
 c_{36a} &= \int_0^R r (f_{tvx2}(r) \mu_{bfop}(r) + f_{tvy2}(r) \mu_{bfip}(r)) dr \\
 c_{37a} &= \int_0^R r (f_{tvx3}(r) \mu_{bfop}(r) + f_{tvy3}(r) \mu_{bfip}(r)) dr \\
 c_{38a} &= \int_0^R r (f_{tvx1}(r) \mu_{beop}(r) + f_{tvy1}(r) \mu_{beip}(r)) dr \\
 c_{39a} &= \int_0^R r (f_{tvx2}(r) \mu_{beop}(r) + f_{tvy2}(r) \mu_{beip}(r)) dr \\
 c_{310a} &= \int_0^R r (f_{tvx3}(r) \mu_{beop}(r) + f_{tvy3}(r) \mu_{beip}(r)) dr \\
 c_{41a} &= \int_0^R \sum_{k=1}^3 r f_{tvxk}(r) (1 + r \cos(\theta_k) \delta_{tfa}) dr \\
 c_{42a} &= \int_0^R \sum_{k=1}^3 f_{tvyk}(r) \delta_{tss} r^2 dr \\
 c_{43a} &= \int_0^R \sum_{k=1}^3 f_{tvyk}(r) r^2 dr \\
 c_{44a} &= \int_0^R \sum_{k=1}^3 f_{tvyk}(r) r^2 dr \\
 c_{45a} &= \int_0^R r (f_{tvx1}(r) \mu_{bfop}(r) + f_{tvy1}(r) \mu_{bfip}(r)) dr \\
 c_{46a} &= \int_0^R r (f_{tvx2}(r) \mu_{bfop}(r) + f_{tvy2}(r) \mu_{bfip}(r)) dr \\
 c_{47a} &= \int_0^R r (f_{tvx3}(r) \mu_{bfop}(r) + f_{tvy3}(r) \mu_{bfip}(r)) dr \\
 c_{48a} &= \int_0^R r (f_{tvx1}(r) \mu_{beop}(r) + f_{tvy1}(r) \mu_{beip}(r)) dr \\
 c_{49a} &= \int_0^R r (f_{tvx2}(r) \mu_{beop}(r) + f_{tvy2}(r) \mu_{beip}(r)) dr \\
 c_{410a} &= \int_0^R r (f_{tvx3}(r) \mu_{beop}(r) + f_{tvy3}(r) \mu_{beip}(r)) dr
 \end{aligned}$$

$$\begin{aligned}
c_{51a} &= \int_0^R \sum_{k=1}^3 (1 + r \cos(\theta_k) \delta_{tfa}) (\mu_{bfop}(r) f_{nvxk}(r) + \mu_{bfip}(r) f_{tvxk}(r)) dr \\
c_{52a} &= \int_0^R \sum_{k=1}^3 \delta_{tss} r (\mu_{bfop}(r) f_{nvyk}(r) + \mu_{bfip}(r) f_{tvyk}(r)) dr \\
c_{53a} &= \int_0^R \sum_{k=1}^3 r (\mu_{bfop}(r) f_{nvyk}(r) + \mu_{bfip}(r) f_{tvyk}(r)) dr \\
c_{54a} &= \int_0^R \sum_{k=1}^3 r (\mu_{bfop}(r) f_{nvyk}(r) + \mu_{bfip}(r) f_{tvyk}(r)) dr \\
c_{55a} &= \int_0^R \mu_{bfop}^2(r) f_{nvx1}(r) + \mu_{bfop}(r) f_{nvy1}(r) \mu_{bfip}(r) + f_{tvx1}(r) \mu_{bfop}(r) + \mu_{bfip}^2(r) f_{tvy1}(r) dr \\
c_{56a} &= \int_0^R \mu_{bfop}^2(r) f_{nvx2}(r) + \mu_{bfop}(r) f_{nvy2}(r) \mu_{bfip}(r) + f_{tvx2}(r) \mu_{bfop}(r) + \mu_{bfip}^2(r) f_{tvy2}(r) dr \\
c_{57a} &= \int_0^R \mu_{bfop}^2(r) f_{nvx3}(r) + \mu_{bfop}(r) f_{nvy3}(r) \mu_{bfip}(r) + f_{tvx3}(r) \mu_{bfop}(r) + \mu_{bfip}^2(r) f_{tvy3}(r) dr \\
c_{58a} &= \int_0^R \mu_{bfop}(r) (f_{nvx1}(r) \mu_{beop}(r) + f_{nvy1}(r) \mu_{beip}(r)) \\
&\quad + \mu_{bfip}(r) (f_{tvx1}(r) \mu_{beop}(r) + f_{tvy1}(r) \mu_{beip}(r)) dr \\
c_{59a} &= \int_0^R \mu_{bfop}(r) (f_{nvx2}(r) \mu_{beop}(r) + f_{nvy2}(r) \mu_{beip}(r)) \\
&\quad + \mu_{bfip}(r) (f_{tvx2}(r) \mu_{beop}(r) + f_{tvy2}(r) \mu_{beip}(r)) dr \\
c_{510a} &= \int_0^R \mu_{bfop}(r) (f_{nvx3}(r) \mu_{beop}(r) + f_{nvy3}(r) \mu_{beip}(r)) \\
&\quad + \mu_{bfip}(r) (f_{tvx3}(r) \mu_{beop}(r) + f_{tvy3}(r) \mu_{beip}(r)) dr \\
c_{61a} &= \int_0^R \sum_{k=1}^3 (1 + r \cos(\theta_k) \delta_{tfa}) (\mu_{bfop}(r) f_{nvxk}(r) + \mu_{bfip}(r) f_{tvxk}(r)) dr \\
c_{62a} &= \int_0^R \sum_{k=1}^3 \delta_{tss} r (\mu_{bfop}(r) f_{nvyk}(r) + \mu_{bfip}(r) f_{tvyk}(r)) dr \\
c_{63a} &= \int_0^R \sum_{k=1}^3 r (\mu_{bfop}(r) f_{nvyk}(r) + \mu_{bfip}(r) f_{tvyk}(r)) dr \\
c_{64a} &= \int_0^R \sum_{k=1}^3 r (\mu_{bfop}(r) f_{nvyk}(r) + \mu_{bfip}(r) f_{tvyk}(r)) dr \\
c_{65a} &= \int_0^R \mu_{bfop}^2(r) f_{nvx1}(r) + \mu_{bfop}(r) f_{nvy1}(r) \mu_{bfip}(r) + f_{tvx1}(r) \mu_{bfop}(r) + \mu_{bfip}^2(r) f_{tvy1}(r) dr \\
c_{66a} &= \int_0^R \mu_{bfop}^2(r) f_{nvx2}(r) + \mu_{bfop}(r) f_{nvy2}(r) \mu_{bfip}(r) + f_{tvx2}(r) \mu_{bfop}(r) + \mu_{bfip}^2(r) f_{tvy2}(r) dr \\
c_{67a} &= \int_0^R \mu_{bfop}^2(r) f_{nvx3}(r) + \mu_{bfop}(r) f_{nvy3}(r) \mu_{bfip}(r) + f_{tvx3}(r) \mu_{bfop}(r) + \mu_{bfip}^2(r) f_{tvy3}(r) dr
\end{aligned}$$

$$\begin{aligned}
 c_{68a} &= \int_0^R \mu_{bfop}(r)(f_{nvx1}(r)\mu_{beop}(r) + f_{nvy1}(r)\mu_{beip}(r)) \\
 &\quad + \mu_{bfip}(r)(f_{tvx1}(r)\mu_{beop}(r) + f_{tvy1}(r)\mu_{beip}(r))dr \\
 c_{69a} &= \int_0^R \mu_{bfop}(r)(f_{nvx2}(r)\mu_{beop}(r) + f_{nvy2}(r)\mu_{beip}(r)) \\
 &\quad + \mu_{bfip}(r)(f_{tvx2}(r)\mu_{beop}(r) + f_{tvy2}(r)\mu_{beip}(r))dr \\
 c_{610a} &= \int_0^R \mu_{bfop}(r)(f_{nvx3}(r)\mu_{beop}(r) + f_{nvy3}(r)\mu_{beip}(r)) \\
 &\quad + \mu_{bfip}(r)(f_{tvx3}(r)\mu_{beop}(r) + f_{tvy3}(r)\mu_{beip}(r))dr \\
 c_{71a} &= \int_0^R \sum_{k=1}^3 (1 + r \cos(\theta_k)\delta_{tfa})(\mu_{bfop}(r)f_{nvxk}(r) + \mu_{bfip}(r)f_{tvxk}(r))dr \\
 c_{72a} &= \int_0^R \sum_{k=1}^3 \delta_{tss}r(\mu_{bfop}(r)f_{nvyk}(r) + \mu_{bfip}(r)f_{tvyk}(r))dr \\
 c_{73a} &= \int_0^R \sum_{k=1}^3 r(\mu_{bfop}(r)f_{nvyk}(r) + \mu_{bfip}(r)f_{tvyk}(r))dr \\
 c_{74a} &= \int_0^R \sum_{k=1}^3 r(\mu_{bfop}(r)f_{nvyk}(r) + \mu_{bfip}(r)f_{tvyk}(r))dr \\
 c_{75a} &= \int_0^R \mu_{bfop}^2(r)f_{nvx1}(r) + \mu_{bfop}(r)f_{nvy1}(r)\mu_{bfip}(r) + f_{tvx1}(r)\mu_{bfop}(r) + \mu_{bfip}^2(r)f_{tvy1}(r)dr \\
 c_{76a} &= \int_0^R \mu_{bfop}^2(r)f_{nvx2}(r) + \mu_{bfop}(r)f_{nvy2}(r)\mu_{bfip}(r) + f_{tvx2}(r)\mu_{bfop}(r) + \mu_{bfip}^2(r)f_{tvy2}(r)dr \\
 c_{77a} &= \int_0^R \mu_{bfop}^2(r)f_{nvx3}(r) + \mu_{bfop}(r)f_{nvy3}(r)\mu_{bfip}(r) + f_{tvx3}(r)\mu_{bfop}(r) + \mu_{bfip}^2(r)f_{tvy3}(r)dr \\
 c_{78a} &= \int_0^R \mu_{bfop}(r)(f_{nvx1}(r)\mu_{beop}(r) + f_{nvy1}(r)\mu_{beip}(r)) \\
 &\quad + \mu_{bfip}(r)(f_{tvx1}(r)\mu_{beop}(r) + f_{tvy1}(r)\mu_{beip}(r))dr \\
 c_{79a} &= \int_0^R \mu_{bfop}(r)(f_{nvx2}(r)\mu_{beop}(r) + f_{nvy2}(r)\mu_{beip}(r)) \\
 &\quad + \mu_{bfip}(r)(f_{tvx2}(r)\mu_{beop}(r) + f_{tvy2}(r)\mu_{beip}(r))dr \\
 c_{710a} &= \int_0^R \mu_{bfop}(r)(f_{nvx3}(r)\mu_{beop}(r) + f_{nvy3}(r)\mu_{beip}(r)) \\
 &\quad + \mu_{bfip}(r)(f_{tvx3}(r)\mu_{beop}(r) + f_{tvy3}(r)\mu_{beip}(r))dr \\
 c_{81a} &= \int_0^R \sum_{k=1}^3 (1 + r \cos(\theta_k)\delta_{tfa})(\mu_{beop}(r)f_{nvxk}(r) + \mu_{bfip}(r)f_{tvxk}(r))dr \\
 c_{82a} &= \int_0^R \sum_{k=1}^3 \delta_{tss}r(\mu_{beop}(r)f_{nvyk}(r) + \mu_{bfip}(r)f_{tvyk}(r))dr \\
 c_{83a} &= \int_0^R \sum_{k=1}^3 r(\mu_{beop}(r)f_{nvyk}(r) + \mu_{beip}(r)f_{tvyk}(r))dr \\
 c_{84a} &= \int_0^R \sum_{k=1}^3 r(\mu_{beop}(r)f_{nvyk}(r) + \mu_{beip}(r)f_{tvyk}(r))dr
 \end{aligned}$$

$$\begin{aligned}
c_{85a} &= \int_0^R \mu_{\text{beop}}(r)(f_{\text{nvx1}}(r)\mu_{\text{bfop}}(r) + f_{\text{nv1}}(r)\mu_{\text{bfip}}(r)) \\
&\quad + \mu_{\text{beip}}(r)(f_{\text{tvx1}}(r)\mu_{\text{beop}}(r) + f_{\text{tv1}}(r)\mu_{\text{bfip}}(r))dr \\
c_{86a} &= \int_0^R \mu_{\text{beop}}(r)(f_{\text{nvx2}}(r)\mu_{\text{bfop}}(r) + f_{\text{nv2}}(r)\mu_{\text{bfip}}(r)) \\
&\quad + \mu_{\text{beip}}(r)(f_{\text{tvx2}}(r)\mu_{\text{beop}}(r) + f_{\text{tv2}}(r)\mu_{\text{bfip}}(r))dr \\
c_{87a} &= \int_0^R \mu_{\text{beop}}(r)(f_{\text{nvx3}}(r)\mu_{\text{bfop}}(r) + f_{\text{nv3}}(r)\mu_{\text{bfip}}(r)) \\
&\quad + \mu_{\text{beip}}(r)(f_{\text{tvx3}}(r)\mu_{\text{beop}}(r) + f_{\text{tv3}}(r)\mu_{\text{bfip}}(r))dr \\
c_{88a} &= \int_0^R \mu_{\text{beop}}^2(r)f_{\text{nvx1}}(r) + \mu_{\text{beop}}(r)f_{\text{nv1}}(r)\mu_{\text{beip}}(r) + f_{\text{tvx1}}(r)\mu_{\text{beop}}(r) + \mu_{\text{bfip}}^2(r)f_{\text{tv1}}(r)dr \\
c_{89a} &= \int_0^R \mu_{\text{beop}}^2(r)f_{\text{nvx2}}(r) + \mu_{\text{beop}}(r)f_{\text{nv2}}(r)\mu_{\text{beip}}(r) + f_{\text{tvx2}}(r)\mu_{\text{beop}}(r) + \mu_{\text{bfip}}^2(r)f_{\text{tv2}}(r)dr \\
c_{810a} &= \int_0^R \mu_{\text{beop}}^2(r)f_{\text{nvx3}}(r) + \mu_{\text{beop}}(r)f_{\text{nv3}}(r)\mu_{\text{beip}}(r) + f_{\text{tvx3}}(r)\mu_{\text{beop}}(r) + \mu_{\text{bfip}}^2(r)f_{\text{tv3}}(r)dr \\
c_{91a} &= \int_0^R \sum_{k=1}^3 (1 + r \cos(\theta_k)\delta_{\text{tfa}})(\mu_{\text{beop}}(r)f_{\text{nvxk}}(r) + \mu_{\text{bfip}}(r)f_{\text{tvxk}}(r))dr \\
c_{92a} &= \int_0^R \sum_{k=1}^3 \delta_{\text{tss}}r(\mu_{\text{beop}}(r)f_{\text{nvky}}(r) + \mu_{\text{bfip}}(r)f_{\text{tvky}}(r))dr \\
c_{93a} &= \int_0^R \sum_{k=1}^3 r(\mu_{\text{beop}}(r)f_{\text{nvky}}(r) + \mu_{\text{beip}}(r)f_{\text{tvky}}(r))dr \\
c_{94a} &= \int_0^R \sum_{k=1}^3 r(\mu_{\text{beop}}(r)f_{\text{nvky}}(r) + \mu_{\text{beip}}(r)f_{\text{tvky}}(r))dr \\
c_{95a} &= \int_0^R \mu_{\text{beop}}(r)(f_{\text{nvx1}}(r)\mu_{\text{bfop}}(r) + f_{\text{nv1}}(r)\mu_{\text{bfip}}(r)) \\
&\quad + \mu_{\text{beip}}(r)(f_{\text{tvx1}}(r)\mu_{\text{beop}}(r) + f_{\text{tv1}}(r)\mu_{\text{bfip}}(r))dr \\
c_{96a} &= \int_0^R \mu_{\text{beop}}(r)(f_{\text{nvx2}}(r)\mu_{\text{bfop}}(r) + f_{\text{nv2}}(r)\mu_{\text{bfip}}(r)) \\
&\quad + \mu_{\text{beip}}(r)(f_{\text{tvx2}}(r)\mu_{\text{beop}}(r) + f_{\text{tv2}}(r)\mu_{\text{bfip}}(r))dr \\
c_{97a} &= \int_0^R \mu_{\text{beop}}(r)(f_{\text{nvx3}}(r)\mu_{\text{bfop}}(r) + f_{\text{nv3}}(r)\mu_{\text{bfip}}(r)) \\
&\quad + \mu_{\text{beip}}(r)(f_{\text{tvx3}}(r)\mu_{\text{beop}}(r) + f_{\text{tv3}}(r)\mu_{\text{bfip}}(r))dr \\
c_{98a} &= \int_0^R \mu_{\text{beop}}^2(r)f_{\text{nvx1}}(r) + \mu_{\text{beop}}(r)f_{\text{nv1}}(r)\mu_{\text{beip}}(r) + f_{\text{tvx1}}(r)\mu_{\text{beop}}(r) + \mu_{\text{bfip}}^2(r)f_{\text{tv1}}(r)dr \\
c_{99a} &= \int_0^R \mu_{\text{beop}}^2(r)f_{\text{nvx2}}(r) + \mu_{\text{beop}}(r)f_{\text{nv2}}(r)\mu_{\text{beip}}(r) + f_{\text{tvx2}}(r)\mu_{\text{beop}}(r) + \mu_{\text{bfip}}^2(r)f_{\text{tv2}}(r)dr \\
c_{910a} &= \int_0^R \mu_{\text{beop}}^2(r)f_{\text{nvx3}}(r) + \mu_{\text{beop}}(r)f_{\text{nv3}}(r)\mu_{\text{beip}}(r) + f_{\text{tvx3}}(r)\mu_{\text{beop}}(r) + \mu_{\text{bfip}}^2(r)f_{\text{tv3}}(r)dr
\end{aligned}$$

$$\begin{aligned}
 c_{101a} &= \int_0^R \sum_{k=1}^3 (1 + r \cos(\theta_k) \delta_{tfa}) (\mu_{beop}(r) f_{nvxk}(r) + \mu_{bfip}(r) f_{tvxk}(r)) dr \\
 c_{102a} &= \int_0^R \sum_{k=1}^3 \delta_{tss} r (\mu_{beop}(r) f_{nvyk}(r) + \mu_{bfip}(r) f_{tvyk}(r)) dr \\
 c_{103a} &= \int_0^R \sum_{k=1}^3 r (\mu_{beop}(r) f_{nvyk}(r) + \mu_{beip}(r) f_{tvyk}(r)) dr \\
 c_{104a} &= \int_0^R \sum_{k=1}^3 r (\mu_{beop}(r) f_{nvyk}(r) + \mu_{beip}(r) f_{tvyk}(r)) dr \\
 c_{105a} &= \int_0^R \mu_{beop}(r) (f_{nvx1}(r) \mu_{bfop}(r) + f_{nvy1}(r) \mu_{bfip}(r)) \\
 &\quad + \mu_{beip}(r) (f_{tvx1}(r) \mu_{beop}(r) + f_{tvy1}(r) \mu_{bfip}(r)) dr \\
 c_{106a} &= \int_0^R \mu_{beop}(r) (f_{nvx2}(r) \mu_{bfop}(r) + f_{nvy2}(r) \mu_{bfip}(r)) \\
 &\quad + \mu_{beip}(r) (f_{tvx2}(r) \mu_{beop}(r) + f_{tvy2}(r) \mu_{bfip}(r)) dr \\
 c_{107a} &= \int_0^R \mu_{beop}(r) (f_{nvx3}(r) \mu_{bfop}(r) + f_{nvy3}(r) \mu_{bfip}(r)) \\
 &\quad + \mu_{beip}(r) (f_{tvx3}(r) \mu_{beop}(r) + f_{tvy3}(r) \mu_{bfip}(r)) dr \\
 c_{108a} &= \int_0^R \mu_{beop}^2(r) f_{nvx1}(r) + \mu_{beop}(r) f_{nvy1}(r) \mu_{beip}(r) + f_{tvx1}(r) \mu_{beop}(r) + \mu_{bfip}^2(r) f_{tvy1}(r) dr \\
 c_{109a} &= \int_0^R \mu_{beop}^2(r) f_{nvx2}(r) + \mu_{beop}(r) f_{nvy2}(r) \mu_{beip}(r) + f_{tvx2}(r) \mu_{beop}(r) + \mu_{bfip}^2(r) f_{tvy2}(r) dr \\
 c_{1010a} &= \int_0^R \mu_{beop}^2(r) f_{nvx3}(r) + \mu_{beop}(r) f_{nvy3}(r) \mu_{beip}(r) + f_{tvx3}(r) \mu_{beop}(r) + \mu_{bfip}^2(r) f_{tvy3}(r) dr
 \end{aligned}$$

C Calculated Matrices

In this appendix the model based calculated system matrices alongside with the ones obtained from FAST linearisation is listed. The matrices are evaluated for an rotor angular position of 0. The subscript "model" indicates that the matrices are calculated by usage of the developed model, while the subscript "fast" indicates that the matrices are calculated by usage of the fast linearisation tool.

C.1 Mass Matrix, M

$$\begin{aligned}
 M_{\text{model}} = & \begin{bmatrix}
 4.0398e^5 & 0 & 0 & 0 & 3855.5 & 1276.9 & 1276.9 & 0 & 0 & 0 \\
 0 & 4.2068e^5 & 8.0967e^5 & 8.0967e^5 & 0 & 0 & 0 & -5634.6 & -1061.2 & -1061.2 \\
 0 & 8.0967e^5 & 4.3785e^7 & 3.876e^7 & 0 & 0 & 0 & -1.2378e^5 & -1.2378e^5 & -1.2378e^5 \\
 0 & 8.0967e^5 & 3.876e^7 & 3.876e^7 & 0 & 0 & 0 & -1.2378e^5 & -1.2378e^5 & -1.2378e^5 \\
 3855.5 & 0 & 0 & 0 & 906.48 & 0 & 0 & 0 & 0 & 0 \\
 1276.9 & 0 & 0 & 0 & 0 & 906.48 & 0 & 0 & 0 & 0 \\
 1276.9 & 0 & 0 & 0 & 0 & 0 & 906.48 & 0 & 0 & 0 \\
 0 & -5634.6 & -1.2378e^5 & -1.2378e^5 & 0 & 0 & 0 & 1411.4 & 0 & 0 \\
 0 & -1061.2 & -1.2378e^5 & -1.2378e^5 & 0 & 0 & 0 & 0 & 1411.4 & 0 \\
 0 & -1061.2 & -1.2378e^5 & -1.2378e^5 & 0 & 0 & 0 & 0 & 0 & 1411.4
 \end{bmatrix} \\
 M_{\text{fast}} = & \begin{bmatrix}
 4.348e^5 & 0 & 0 & 0 & 4056 & 1378 & 1378 & 0 & 0 & 0 \\
 0 & 4.477e^5 & 8.123e^5 & 8.112e^5 & 0 & 0 & 0 & -5898 & -1055 & -1055 \\
 0 & 8.123e^5 & 4.386e^7 & 3.883e^7 & 0 & 0 & 0 & -1.278e^5 & -1.278e^5 & -1.278e^5 \\
 0 & 8.112e^5 & 3.883e^7 & 3.883e^7 & 0 & 0 & 0 & -1.278e^5 & -1.278e^5 & -1.278e^5 \\
 4056 & 0 & 0 & 0 & 943.3 & 0 & 0 & 0 & 0 & 0 \\
 1378 & 0 & 0 & 0 & 0 & 943.3 & 0 & 0 & 0 & 0 \\
 1378 & 0 & 0 & 0 & 0 & 0 & 943.3 & 0 & 0 & 0 \\
 0 & -5898 & -1.278e^5 & -1.278e^5 & 0 & 0 & 0 & 1449 & 0 & 0 \\
 0 & -1055 & -1.278e^5 & -1.278e^5 & 0 & 0 & 0 & 0 & 1449 & 0 \\
 0 & -1055 & -1.278e^5 & -1.278e^5 & 0 & 0 & 0 & 0 & 0 & 1449
 \end{bmatrix}
 \end{aligned}$$

C.2 Stifness Matrix, K

$$K_{\text{model}} = \begin{bmatrix} 1.9127e+06 & 0 & 0 & 0 & 0 & 0 & 0 & 0 & 0 & 0 \\ 0 & 1.8442e+06 & 0 & 0 & 0 & 0 & 0 & 0 & 0 & 0 \\ 0 & 0 & 0 & 0 & 0 & 0 & 29900 & -14950 & -14950 & 0 \\ 0 & 0 & 0 & 8.6764e+08 & 0 & 0 & 29900 & -14950 & -14950 & 0 \\ 0 & 0 & 0 & 0 & 17409 & 0 & 0 & 0 & 0 & 0 \\ 0 & 0 & 0 & 0 & 0 & 17409 & 0 & 0 & 0 & 0 \\ 0 & 0 & 0 & 0 & 0 & 0 & 17409 & 0 & 0 & 0 \\ 0 & 0 & 29900 & 29900 & 0 & 0 & 0 & 67739 & 0 & 0 \\ 0 & 0 & -14950 & -14950 & 0 & 0 & 0 & 0 & 67739 & 0 \\ 0 & 0 & -14950 & -14950 & 0 & 0 & 0 & 0 & 0 & 0 \end{bmatrix}$$

$$K_{\text{fast}} = \begin{bmatrix} 1.849e+06 & -0.2912 & 1.26 & 0.5971 & 2467 & -1496 & -1494 & -24.66 & -8.35 & -8.685 \\ 918.7 & 1.773e+06 & -1.016e+05 & -1.019e+05 & -0.4864 & 2022 & -2023 & 5814 & -2310 & -1994 \\ -78.31 & -3.383 & 13.37 & 14.46 & -21.07 & 580.3 & -631 & 30330 & -15300 & -15300 \\ -78.31 & -3.383 & 13.37 & 8.676e+08 & -21.07 & 580.3 & -631 & 30330 & -15300 & -15300 \\ 620.2 & -0.06143 & 0.3914 & 0.06563 & 19220 & 0.09431 & -0.1555 & -3.753 & 0.0375 & 0.1647 \\ -1119 & -12.73 & -607.5 & -607.3 & 0.1983 & 19720 & 0.2197 & -0.1262 & 3.516 & 0.03751 \\ -697.1 & 12.65 & 608.1 & 608.3 & -0.02662 & -0.2188 & 19720 & 0.1364 & -0.1066 & -11.02 \\ -285.9 & 635.4 & 30410 & 30500 & -0.2024 & -0.01897 & 0.0339 & 67490 & -0.009075 & -0.03614 \\ 106.5 & -317.7 & -15210 & -15250 & -0.04299 & -7.455 & -0.04525 & 0.02747 & 68170 & -0.009079 \\ 180 & -317.7 & -15210 & -15250 & 0.005717 & 0.05037 & 7.07 & -0.02757 & 0.02314 & 68170 \end{bmatrix}$$

C.3 Damping Matrix, C

$$C_{\text{model}} = \begin{bmatrix} 1.4371e+06 & 21903 & 1.6089e+05 & 1.6089e+05 & 3476.9 & -74.096 & -74.096 & -8463 & -2681.5 & -2681.5 \\ -11118 & 7154.7 & -99665 & -99665 & -3594.4 & -1004.5 & -1004.5 & 759.66 & 153.26 & 153.26 \\ -5.6774e+05 & 1.8408e+06 & -4.7711e+06 & -4.7711e+06 & -89413 & -89413 & -89413 & 17013 & 17013 & 17013 \\ -5.6774e+05 & 1.848e+06 & -4.7711e+06 & 1.4439e+06 & -89413 & -89413 & -89413 & 17013 & 17013 & 17013 \\ 3476.9 & 6874.8 & 1.6264e+05 & 1.6264e+05 & 3084.1 & 0 & 0 & -2034.7 & 0 & 0 \\ -3847 & 1658.8 & 1.6264e+05 & 1.6264e+05 & 0 & 3084.1 & 0 & 0 & -2034.7 & 0 \\ 3698.8 & 1658.8 & 1.6264e+05 & 1.6264e+05 & 0 & 0 & 3084.1 & 0 & 0 & -2034.7 \\ 4031.1 & 759.66 & 17013 & 17013 & 0 & 0 & 0 & -99.713 & 0 & 0 \\ 1151.4 & 153.26 & 17013 & 17013 & 0 & 0 & 0 & 0 & -99.713 & 0 \\ 1151.4 & 153.26 & 17013 & 17013 & 0 & 0 & -193.08 & 0 & 0 & -99.713 \end{bmatrix}$$

$$C_{\text{fast}} = \begin{bmatrix} 61870 & -14240 & -4.735e+05 & -4.735e+05 & 8970 & 2634 & 2674 & 3161 & 985.8 & 962 \\ 11820 & 9065 & 64550 & 64550 & 2121 & 508.4 & 508.5 & -497.7 & 6986 & -7187 \\ 3.914e+05 & 64760 & 3.09e+06 & 3.09e+06 & 50090 & 50070 & 50070 & -11140 & -11140 & -11140 \\ 3.914e+05 & 64760 & 3.09e+06 & 9.305e+06 & 50090 & 50070 & 50070 & -11140 & -11140 & -11140 \\ 8945 & -2732 & -65720 & -65720 & 2599 & -0.1197 & 0.09532 & 867.2 & -0.01013 & 0.1003 \\ -1266 & -685.3 & -65720 & -65720 & 0.1349 & 2599 & -0.1197 & 0.06996 & 867.2 & -0.01013 \\ 6568 & -685.3 & -65720 & -65720 & 0.1349 & 0.1861 & 2599 & -0.08787 & 0.06996 & 867.2 \\ -2525 & -496.3 & -11070 & -11070 & -645.2 & 0.03925 & -0.01789 & 225.3 & 0.009027 & -0.01979 \\ -807.5 & -99.96 & -11070 & -11070 & -0.03319 & -645.1 & 0.03925 & -0.01313 & 225.3 & 0.009027 \\ -807.5 & -99.96 & -11070 & -11070 & -0.03319 & -0.0457 & -645.1 & 0.02881 & -0.01313 & 225.3 \end{bmatrix}$$

D Simulation and Linearisation by usage of FAST

*This appendix covers a description of how **FAST** was used for computing linearised wind turbine model and how they were simulated and validated up against the non-linear **FAST** wind turbine simulator.*

D.1 Linearisation

FAST is capable of linearising in two different ways. The one method linearises the model around initial conditions, while the other by using an iterative approach determines operating points for all states and inputs followed by a linearisation around those also.

In order to use the linearised matrices for simulation of the wind turbine it is advantageous to evaluate the matrices for a set of operating points for all the states and inputs used in the model. Operating points for rotor speed is specified in the main fast input file `© /FAST_data/NRELOffshrBslime5MW_Onshore.fst`, and a static wind field is specified in the **Aerodyn** wind input file `© /FAST_data/wind/steady15_shear_step.wnd`. **FAST** is then configured to run in linear analysis mode and run from command line[15].

After an amount of iterations, until a steady state solution is obtained, a set of operating points alongside with matrices linearised around them is calculated. The **FAST** linearisation yields a set of mass, stiffness, damping, forcing matrices and state space representation of the system. The linear matrices are dependent on different angular rotor positions, which is an amount of equally spaced positions yielding 36 different matrices if the spacing for instance is 10 degree, alongside with them a set of operating point is supplied which are also dependent on the angular rotor position. For usage in simulation the state space representation is used, note that the generator position is removed in order to avoid computational problems. The linearised state space representation used for simulation and in the filter has the following states, inputs and wind disturbances:

States:

$x_1 \in \mathbb{R}$	is the tower fore-aft displacement	[m]
$x_2 \in \mathbb{R}$	is the tower side-side displacement	[m]
$x_3 \in \mathbb{R}$	is the torsion of the low speed shaft in the drivetrain	[rad]
$x_4 \in \mathbb{R}$	is the flap-wise displacement of blade 1	[m]
$x_5 \in \mathbb{R}$	is the flap-wise displacement of blade 2	[m]
$x_6 \in \mathbb{R}$	is the flap-wise displacement of blade 3	[m]
$x_7 \in \mathbb{R}$	is the edge-wise displacement of blade 1	[m]
$x_8 \in \mathbb{R}$	is the edge-wise displacement of blade 2	[m]
$x_9 \in \mathbb{R}$	is the edge-wise displacement of blade 3	[m]
$x_{10} \in \mathbb{R}$	is the tower fore-aft displacement velocity	[m/s]
$x_{11} \in \mathbb{R}$	is the tower side-side displacement velocity	[m/s]
$x_{12} \in \mathbb{R}$	is the angular displacement velocity of the generator (low speed side)	[rad/s]
$x_{13} \in \mathbb{R}$	is the torsion velocity of the low speed shaft in the drivetrain	[rad/s]
$x_{14} \in \mathbb{R}$	is the flap-wise displacement velocity of blade 1	[m/s]
$x_{15} \in \mathbb{R}$	is the flap-wise displacement velocity of blade 2	[m/s]
$x_{16} \in \mathbb{R}$	is the flap-wise displacement velocity of blade 3	[m/s]
$x_{17} \in \mathbb{R}$	is the edge-wise displacement velocity of blade 1	[m/s]
$x_{18} \in \mathbb{R}$	is the edge-wise displacement velocity of blade 2	[m/s]
$x_{19} \in \mathbb{R}$	is the edge-wise displacement velocity of blade 3	[m/s]

Inputs:

$u_1(t) \in \mathbb{R}$	is the applied generator torque	[Nm]
$u_2(t) \in \mathbb{R}$	is the pitch of blade 1	[rad]
$u_3(t) \in \mathbb{R}$	is the pitch of blade 2	[rad]
$u_4(t) \in \mathbb{R}$	is the pitch of blade 3	[rad]

Wind disturbances:

$d_1(t) \in \mathbb{R}$	is the hub height wind speed	[m/s]
$d_2(t) \in \mathbb{R}$	is vertical power law shear exponent	[-]

The simulation of the states space system will now be described.

D.2 Simulation

In order to validate the linearised model a simulation of the model was carried out where the National Renewable Energy Laboratory (NREL) 5 MW non-linear wind turbine simulator was used as benchmark.

The non-linear simulation of the NREL 5MW turbine is done by using **FAST** simulator. Where the possibility of using **MATLAB** for configuring the turbine in terms of structural parameters and a specified wind field, from inputs files `Ⓞ/FAST_data` was used alongside with **Simulink** for simulation of the turbine. The configuration of **FAST** was done by following the guide [25].

The turbine is then simulated by usage of an from **FAST** given internal torque and pitch controller, the pitch controller used will only be activated at above rated speeds[15].

The simulations results in a data set containing inputs in terms of wind disturbances and control inputs alongside with the resulting outputs in terms of state measurements of the chosen states. The inputs from the data sets can then be used to simulate the developed model by simulating its response.

The simulation of the linearised model is carried out in **MATLAB** and to validate it the outputs from it is compared to the outputs from **FAST**. The linearised matrices alongside with corresponding operating point from **FAST** is as mentioned linearised for 36 different angular rotor positions, therefore in order to simulate them a combination of them was used. This was done by usage of output data from the non-linear simulation of the NREL 5MW turbine, here the angular position for the rotor is amongst others given. This angular rotor position was used to calculate a weighted sum of the two matrices around the current angular rotor position.

The matlab files used for simulation is attached on the enclosed cd `Ⓞ/simulator`.